Development of calibration techniques for ultrasonic hydrophone probes in the frequency range from 1 to 100 MHz

A Thesis

Submitted to the Faculty

of

Drexel University

by

Sumet Umchid

in partial fulfillment of the

requirements for the degree

of

Doctor of Philosophy

November 2007

Dedication

to my parents

Acknowledgments

I would like to express my sincere acknowledgement to the following people for their contributions to the completion of this dissertation. Before anyone else, I would like to whole-heartedly thank my advisor, Dr. Peter A. Lewin for his guidance. The accomplishment of this study would not be possible without his advice and encouragement. The opportunities and learning experience he has given me are gratefully appreciated.

I thank Drs. Afshin S. Daryoush, Mahmoud A. El-Sherif and Lalit Bansal, for their support and direction on the fiber optic part. Their contribution has made all of this possible and has enhanced the quality of the work.

Also, I would like to thank Drs. Philip E. Bloomfield, Afshin S. Daryoush, Elisabeth S. Papazoglou, Ryszard Lec and Steven Wrenn for serving on my committee and for all their advice and support.

My research and study would not be feasible without financial support from the Ministry of Science and Technology, the Royal Thai Government, and the National Institutes of Health (NIH, grant #5 RO1 EB007117-02).

Early introduction to the topics discussed in this dissertation given by Dr. Emil G. Radulescu are also acknowledged.

I wish to thank all my fellow students in Acousto-optic teams (Karthik Srinivasan, Rupa Gopinath, Piyush Arora and Gaurav Gandhi) for an ideal atmosphere. Our friendship made the most difficult time more enjoyable.

I also would like to give special thanks to the Thai community in Philadelphia for consistently supporting me and making my Drexel life more entertaining.

Last but not least, I would like to thank my parents, sister, brother and my girlfriend for giving me unconditional love and support from the other side of the world.

Table of contents

List of tables

List of figures

Abstract

Development of calibration techniques for ultrasonic hydrophone probes
in the frequency range from 1 to 100 MHz
Sumet Umchid
Peter A. Lewin, Ph.D.

The primary objective of this research was to develop and optimize the calibration techniques for ultrasonic hydrophone probes used in acoustic field measurements up to 100 MHz. A dependable, 100 MHz calibration method was necessary to examine the behavior of a sub-millimeter spatial resolution fiber optic (FO) sensor and assess the need for such a sensor as an alternative tool for high frequency characterization of ultrasound fields. Also, it was of interest to investigate the feasibility of using FO probes in high intensity fields such as those employed in HIFU (High Intensity Focused Ultrasound) applications. In addition to the development of a novel, 100 MHz calibration technique the innovative elements of this research include implementation of a prototype FO sensor with an active diameter of about 10 μm that exhibits uniform sensitivity over the considered frequency range and does not require any spatial averaging corrections up to about 75 MHz. The calibration technique provided the sensitivity of conventional, finite aperture piezoelectric hydrophone probes as a virtually continuous function of frequency and allowed the verification of the uniformity of the FO sensor frequency response. As anticipated, the overall uncertainty of the calibration was dependent on frequency and determined to be about ±12% (±1 dB) up to 40 MHz, ±20% (±1.5 dB) from 40 to 60 MHz and ±25% (±2 dB) from 60 to 100 MHz. The outcome of this research indicates that

once fully developed and calibrated, the combined acousto-optic system will constitute a universal reference tool in the wide, 100 MHz bandwidth.

CHAPTER 1: Introduction

This dissertation deals with the specific aspects of ultrasound metrology and is organized in the following way. Below the specific aims of this work are summarized.

The specific aims of this project were:

1. Development of a calibration technique suitable for characterization of ultrasonic hydrophone probes in the frequency range up to 100 MHz.

2. Preliminary testing of a fiber optic (FO) prototype hydrophone probe operating as a quasi-point receiver in the frequency range considered.

The next chapter (2) presents the background and the motivation for this work. In Chapter 3, the experimental setup and methodology is described. Chapter 4 describes the results of the piezoelectric and fiber optic hydrophone calibrations. Chapter 5 contains the discussion of the results and conclusions of the work. The suggestions for the future work are outlined in Chapter 6.

CHAPTER 2: Background and significance

This chapter provides background and motivation for this research. To facilitate interpretation of the results given in Chapter 4, the basic properties and characteristics of both piezoelectric and fiber optic (FO) ultrasonic hydrophone probes are briefly discussed. Also, the hydrophone calibration techniques and their associated instrumentation such as hydrophone preamplifiers are described. In addition, the principle of nonlinear wave propagation and its application to obtain hydrophone's sensitivity at discrete frequencies is introduced.

2.1 Significance

In the past few decades, medical diagnostic ultrasound has become the primary noninvasive imaging modality because it does not employ ionizing radiation such as X-rays and also provides real-time information of the anatomical structures. However, under certain conditions ultrasound exposure in general may introduce undesirable biological effects [1]. Therefore, the acoustic output of the diagnostic ultrasound devices is regulated and cannot exceed prescribed limits. In the USA, these prescribed limits are established by the Food and Drug Administration, Center for Devices and Radiological Health, which requires the safety indicators such as Mechanical Index (MI) and Thermal Index (TI) to be displayed on the ultrasound imaging systems [2-4]. Determination of these two indices requires a faithful recording of the acoustic pressure-time waveforms produced by an imaging transducer or a scan head.

According to AIUM/NEMA standards and FDA guidelines [2-4] such recording requires the use of ultrasound hydrophone probes calibrated up to eight times the center frequency of the imaging transducer. This frequency limit has been introduced to take into account nonlinear propagation phenomena (to be discussed in the following), which lead to presence of harmonics in the pressure-time waveform launched into the examined tissue. Although the majority of clinically relevant ultrasound imaging devices operate in the frequency range from 1-15 MHz, recently, many new applications of ultrasound imaging at frequencies greater than 15-20 MHz have been introduced. Catheter based systems often use frequencies beyond 20 MHz. 50 MHz ultrasound transducers were used to determine osteoarthritic changes in articular cartilage [5]. Similarly, high frequency of tens of megahertz was employed to investigate image enhancement properties of contrast agents in-vivo in rabbit eye [6]. The newly researched methods for early cancer detection by monitoring the developing vascularity indicate the growing need for sub-millimeter image resolution and hence the use of frequencies well beyond 20 MHz [7]. In the past years, several research groups published data obtained using new generation transducers operating in the frequency range of 40-100 MHz and reported significantly improved sub-millimeter spatial resolution which allows such structures as discrete layers of the carotid wall, corneal thickness and skin layers to be resolved [7-11]. Imaging frequencies well beyond 20 MHz are also widely used in basic science and pre-clinical applications [8-15]. The results of research presented in [16] indicated that the image resolution achieved at frequencies on the order of 40 MHz was adequate to examine structural and functional properties of small animals and provided an alternative to more complex and expensive methods such as Magnetic Resonance Imaging. In addition to estimation of

blood flow in discrete vessels and the microvasculature, ultrasound has great potential to efficiently detect and monitor defects in genetically engineered animal models [17, 18].

As noted above, for presently used medical diagnostic ultrasound devices, their -3 dB frequency of operational bandwidth usually begins in the low megahertz range (1-2 MHz) and rarely exceeds 15 MHz [19]. However, the optimization of harmonic imaging techniques generated by transducer arrays in the 12-15 MHz range requires field parameters to be measured in the 100 MHz bandwidth [2-4, 20, 21]. In this context it is worth noting that, despite the fact that the characterization of ultrasound hydrophone probes at frequencies beyond 20 MHz appears to be necessary to ensure adequate characterization of clinically applicable devices, the sensitivity of the probes used in ultrasound exposimetry measurements is typically available in the frequency range from 1-20 MHz, only. This is partly due to the fact that the calibration procedures available beyond 20 MHz are very time consuming and relatively difficult to implement.

Bacon [22, 23] first suggested to predict the hydrophone frequency response by observing the differences between experimentally measured and computer modeled nonlinear propagation of plane waves. However, his method required large flat sources to be available and measurements to be performed at large distances, so that ideal “N” shock plane waves could be achieved. This created limitations due to transducer availability and test tank dimensions. His model assumed that the hydrophone spatial averaging and source diffraction effects were negligible. Also, the calibration was not verified using a primary or secondary calibration technique beyond 20 MHz. Other

researchers [24, 25] have also proposed similar methods to determine the hydrophone frequency response. Filipczynski et al. [24] combined the hydrophone frequency response and spatial averaging effects and introduced "effective" frequency response of the hydrophone. Baker et al. [25] assumed plane wave conditions and neglected spatial averaging corrections. In these two studies the hydrophone frequency response has not been verified and the data were limited to about 40 MHz.

The concept of using a focusing source for hydrophone calibration has been suggested in [21, 26-30]. Lum et al. [26, 27] described a nonlinear procedure carried out at discrete frequencies based on producing a distorted pressure-time waveform with high harmonic content. This method was used to estimate frequency response, bandwidth, and angular response of high frequency, spot poled, 4 μm thick PVDF membrane hydrophones. However, the authors themselves concluded that their calibration required additional work to evaluate the absolute hydrophone response in the frequency range beyond 20 MHz [27].

The applications of ultrasound energy for therapeutic treatment purpose have also grown significantly in the past few years. High Intensity Focused Ultrasound (HIFU) [31, 32] treatment of tissue has gained attention as a tool for thermal tissue ablation by producing highly localized lesions and elevating tissue temperature to about 55 deg C or above. However, HIFU procedures seldom use transducers with center frequencies beyond 10 MHz. On the other hand, the spatial peak, temporal average intensities produced in the focal volume range between 1000 and 10,000 W/cm^2 [33]. Although the detailed

characterization of the HIFU produced fields is indispensable to optimize tissue ablation and minimize collateral damage, this characterization of HIFU fields is challenging as in general, the widely used piezopolymer hydrophone probes cannot withstand the temperatures and/or cavitation effects produced by HIFU transducers in the focal region [34].

At present, to avoid damaging of the expensive hydrophone probes (a bilaminar PVDF polymer probe's price may exceed 15,000 USD) the characterization of the HIFU transducer is carried out at low (diagnostic rather than therapeutic) excitation levels. Such characterization includes delineation of the focal volume and measurement of pressure amplitudes. It is assumed that the acoustic output is proportional to the excitation voltage driving the HIFU source and hence, that the pressure amplitudes at the actual HIFU treatment site can be determined by linear scaling or extrapolation. It is further assumed that the distribution of the acoustic field is independent on the excitation level. These assumptions are questionable because it is most likely that the pressure wave developed at the HIFU excitation levels is highly distorted and contains a significant number of harmonics. The existence of these harmonics is associated with excessive attenuation that will influence the actual energy levels at the HIFU treatment [35]. The solution proposed here and based on the use of the fiber optic (FO) probe would be useful in verification of whether the field extrapolation assumption is valid. Also, the FO probe would be helpful in determining the possible errors in the calculation of extrapolated intensity levels. This is proposed to be done by a direct measurement of the pressure-time (p-t) waveform in the HIFU field. The eventual damage to the fiber tip [36, 37] can easily be repaired by re-

cleaving, which regenerates a similar endface. As already noted the HIFU field measurements are not possible at the present time using the polymer hydrophones without risking their damage due to elevated temperatures and cavitation. Although it might be argued that an appropriate protection of the polymer probe could be adopted to make them useable in HIFU applications, any protective stand-off material would affect both the frequency content of the measured HIFU waveform and the probe's sensitivity. Therefore, in practice, such material, if available, would have to be comprehensively studied so the field distortions that are caused by the stand-off material and the finite aperture of the PVDF polymer sensitive element could be accounted for. Other solutions such as utilization of acoustoelectric phenomenon [38] to construct disposable probes were suggested; however, the methods of the absolute calibration of such probes are yet to be developed and their frequency response is practically unknown. The FO probe described in the following is able to provide the HIFU field data in the full frequency bandwidth and without the need for spatial averaging corrections.

As mentioned earlier, for all applications in biomedical ultrasound it is necessary to know the pressure-time waveform interacting with tissue. However, characterization and measurements of the acoustic fields (especially in the high frequency range) are challenging due to the finite aperture of existing hydrophone probes. A majority of the commercially available probes has a nominal active element diameter or aperture on the order of 500 μm. Although accepted for acoustic output measurements [2-4], such an aperture is too large for measurements in the fields beyond 3 MHz. This is because in order to eliminate the effects of spatial averaging, the hydrophones should be able to

sample the field with at least half-wavelength resolution. At 100 MHz such resolution in water medium would require an active aperture on the order of 7 μm. The hydrophones available have the smallest nominal diameter of 40 μm; however, their sensitivity exhibits rapid variations (approximately 10 dB) against frequency [21]. Also, the details of such response are often unknown as the calibration data are usually provided at discrete frequencies and intervals that are too large (typically 1 or 2 MHz) to detect the peaks and valleys in the frequency response. From the above, it is evident that the piezoelectric hydrophone probes have diameters that are on the order of magnitude too large to comply with 100 MHz, point-receiver behavior and as a result an alternative fiber optic (FO) hydrophone design began to gain attention.

A fiber optic sensor was proposed for lithotripter field measurement almost two decades ago. The probe described in [39] uses 100/140 micron (total cross-section diameter 240 μm) step-index silica material and was developed specifically for measurements of shock waves. The sensitivity of the silica sensor is relatively low (about -300 dB re 1V/μPa) in comparison with that of the polymer hydrophone probes used at present (about -266 dB re 1V/μPa) and thus makes it unsuitable for acoustic output measurements. Also, as already noted, at 100 MHz the wavelength of the acoustic wave in water is approximately 15 μm. Therefore, the lithotripter sensor of [39] is inadequate for sampling at this frequency. In fact, such thick fiber would introduce a spatial averaging error already at frequencies beyond 3 MHz (wavelength at 3 MHz is 500 μm). In contrast, the FO probe developed here and described in Chapter 3 uses an active aperture of about 10 μm that is

identical with its physical dimensions and hence eliminates the need for spatial averaging correction up to about 75 MHz.

Beard et al. [40] examined the possibility of using optic hydrophone in the 1-20 MHz range as an alternative to the PVDF polymer probes. Their goal was to reach sensitivity numbers comparable to those currently available with PVDF polymer hydrophones by employing optical resonator approach. However, their work is not immediately applicable to achieve the desirable, uniform (say ±1 dB) frequency response with concurrent elimination of the need for spatial averaging corrections in the whole 100 MHz bandwidth. Indeed, the Beard et. al. results show that the relative sensitivity of their probes is not flat and varies considerably between the four "nominally identical optical fiber hydrophones", exhibiting several peaks and valleys in the limited, 20 MHz bandwidth. This is because their design is based on the use of the resonator. Moreover, even their very best probe shows a difference on the order of 6 dB (a factor of 2) in the sensitivity (between the maximum at around 10 MHz and the minimum at about 14 MHz). In fact, this difference may be as large as 10-12 dB (a factor of 3-4) as shown for other probes.

A few comments on the existing optic methods used in ultrasound field measurements may be appropriate here. Schneider and Shung [41] used a commercially available Schlieren system to characterize high frequency ultrasonic fields and reported a good correlation with data obtained using a commercially available hydrophone calibrated up to 20 MHz. It is important to realize that a Schlieren system alone is not adequate to

characterize devices to FDA requirements [3] and calibrated hydrophones are needed to record pressure-time waveforms produced by the imaging transducers.

Also, optical interferometry has been used in the past to provide sensitivity of hydrophone probes at discrete frequencies up to 20 MHz. However, only recently has this calibration method been reported to be capable of providing the sensitivity data up to 60 MHz [29]. In the optical interferometry method, described in [29] a 5 MHz focused transducer was used to generate a highly shocked field containing 12 harmonics, and a 9 micron, PVDF coplanar membrane hydrophone (this film thickness corresponds to fundamental resonance frequency in water of about 110 MHz) was calibrated at discrete frequencies at 5 MHz intervals. In their conclusion, the authors pointed out the need to provide independent validation of their interferometer technique. Another group of researchers working with an interferometric principle improved the membrane hydrophone model and used it to corroborate experimentally determined data at discrete frequencies between 20-50 MHz [29]. However, the results presented in [39] indicate that a conventional or single mode fiber may be of limited use beyond 10 MHz due to its effective cross-section.

The primary hydrophone calibration up to 70 MHz based on an optical interferometry technique was introduced by Koch et al. [42] and then Wilkens et al. [43, 44], who extended the frequency range of the piezoelectric hydrophone characterization up to 140 MHz with a substitution calibration technique using an optical multilayer hydrophone presented in [42] as the reference receiver. However, their calibrations are time

consuming and require a fairly complex and expensive interferometric approach in comparison with the fiber optic system developed in the course of this work.

From the above, it is clear that there is a well defined need for a novel, rugged hydrophone probe and associated measurement system that not only would be able to perform characterization of diagnostic ultrasound fields in the frequency range beyond 20 MHz but also suitable to measure acoustic fields generated by HIFU transducers.

The next section describes the basic characteristics of both piezoelectric and fiber optic hydrophone probes used in this work and introduces the fundamentals of nonlinear wave propagation.

2.2 Ultrasound hydrophone probes and their properties

In the following, the piezoelectric and optic hydrophone design used in this work are briefly described and the fundamentals of the nonlinear wave propagation utilized to obtain calibration data up to 100 MHz are presented.

2.2.1 Piezoelectric hydrophone probes

Hydrophones are the universal instruments used to characterize the acoustic output of medical diagnostic ultrasound devices. Hydrophones generate an electrical output when subjected to acoustic pressure. Their voltage output is directly proportional to the

acceleration of the acoustic pressure. The performance of hydrophones is related to their physical characteristics; therefore many designs have emerged that vary in dimensions and in the piezoelectric material used as the sensitive element. The materials that have been used for ultrasonic hydrophones include solid piezoelectric ceramics (e.g. lead zirconate titanate, PZT), single crystals (e.g. quartz or tourmaline), and polymers (e.g. polyvinylidene fluoride, PVDF). Ceramic and crystal-based hydrophones have a tendency not to meet the important criteria necessary for high performance hydrophones because of their bandwidth, dynamic range, and directivity. They also suffer from radial resonances and a non-uniform frequency response. For these reasons, most commercial ultrasonic hydrophone probes used presently are constructed with PVDF as the sensitive element [45].

There are two basic PVDF hydrophone designs [22, 45-48]: the spot-poled membrane and the Lewin or needle-type hydrophone [45]. Both types employ an active element on the order of or less than 0.5 mm. The sensitive element thickness is typically in the range of 9 to 50 μm and, to a large extent, controls the bandwidth of the probe.

Since both membrane and needle hydrophones were used for calibration up to 100 MHz during this work, details in the design and fabrication of these hydrophones are explored in the next two sections.

2.2.1.1 Membrane hydrophones

A typical membrane hydrophone design is shown in Figure 2.1. It uses a thin film (4 – 50 μm) of the piezoelectric polymer material (PVDF), which is stretched over a supporting hoop. The diameter of the hoop is about 100 mm to allow the acoustic beam from an acoustic source to pass through its aperture [22]. The small circular region (typically about 0.5-1 mm in diameter) in the center of the hydrophones, referred to as the active element, is poled and electroded [47].

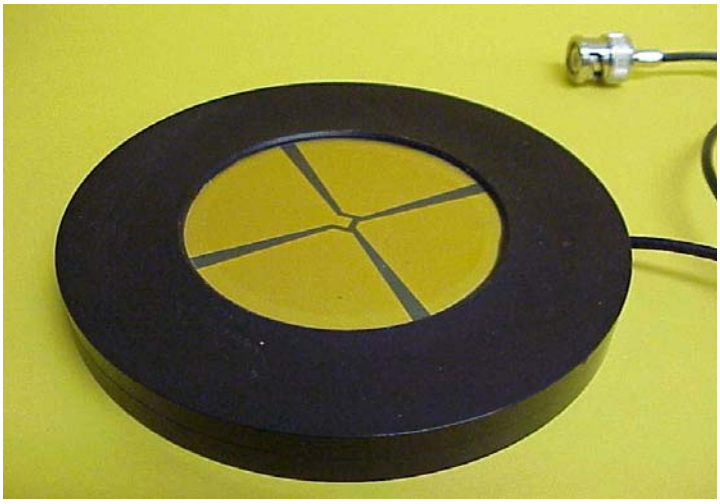

Figure 2.1: Photograph of a bilaminar membrane hydrophone (courtesy of Sonora Medical Systems, Longmont, Colorado).

The membrane hydrophones have been found to be acoustically transparent to waves in the typical imaging frequency range (between 1 and 15 MHz). These hydrophones resonate in the fundamental thickness mode at 1/2 ultrasonic wavelength (λ/2). As the speed of sound in PVDF material is about 2 mm/μs, a 25 μm thick PVDF membrane will have a resonance at about 40 MHz. For the bilaminar membrane hydrophone (shown in

Figure 2.1), which is immune to water conduction and radio frequency (RF) interference effects, since two layers are used, the center frequency is just half of one layer, which is about 20 MHz [33]. Radial resonance modes occur well below the frequency of interest and are highly damped as a result of a large diameter membrane with no backing [22]. Typically, the frequency response is relatively flat (about 0.3 dB/MHz) below the resonance and decays (about 0.6 dB/MHz) beyond the resonance.

In the past several years, the development has been made in extending the bandwidth of ultrasonic hydrophone probes. Lum et al [27] fabricated a membrane hydrophone from a 4 μm thick film of vinylidene fluoride trifluoroethylene copolymer, (PVDF-TrFE). Preliminary measurement results have shown that the VDF co-polymer hydrophone had an effective spot diameter of about 100 μm and a bandwidth that extended to 150 MHz. The authors concluded that although their design needed further work to fully characterize the frequency response above 20 MHz and to examine the behavior of the effective diameter of the sensitive area, the 4 μm membrane hydrophone showed potential to faithfully determine the temporal and spatial parameters of ultrasonic diagnostic transducers in the 10-40 MHz range [27].

2.2.1.2 Needle-type (Lewin) hydrophones

The needle-type hydrophones have a coaxial construction of stainless steel and various insulating materials. Figure 2.2 shows a photograph of a needle-type hydrophone. This type of hydrophone behaves as a quarter wavelength (λ/4) resonator with an active

diameter on the order of 0.5-1 mm. A detailed description of the design and construction of the needle-type hydrophone can be found in [48].

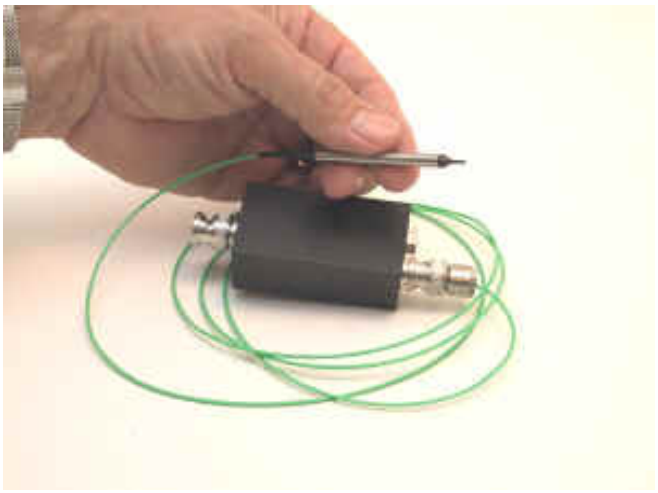

(a)

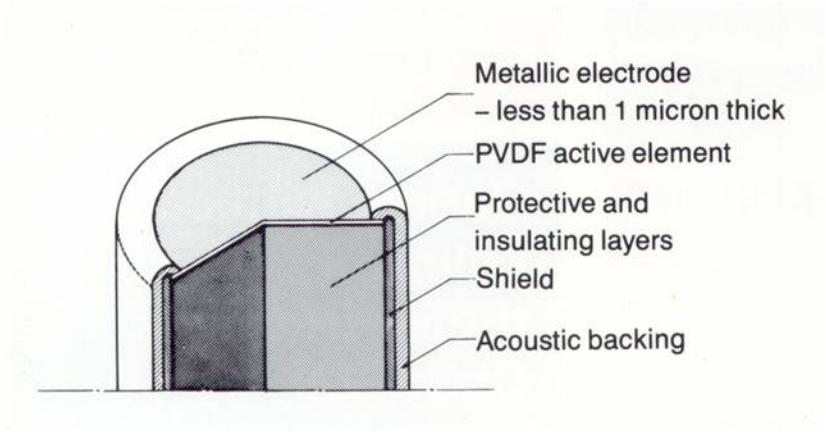

(b)

Figure 2.2: (a) Photograph of a needle PVDF hydrophone and (b) the details of the sensor element. (Courtesy of Force Institute, Copenhagen, Denmark).

The needle hydrophone has an advantage over the membrane hydrophone in that it can be used for in situ exposure measurements in the body and in many other applications where the physical size might cause a problem. Although needle hydrophones have become

primary hydrophones in many laboratories, membrane hydrophones have become more prevalent for acoustic output measurements because of their reliability and relatively flat frequency response over the range necessary for imaging transducers [33].

Table A1.1 (Appendix 1) enumerates both needle and membrane hydrophone probes used during this work whereas Table A1.2 describes the measurements carried out with each of these hydrophones.

The next subsection describes the key properties of electronic preamplifiers that are often used with the hydrophones and therefore have an influence on the overall characteristics, including the frequency response of the hydrophone probes.

2.2.1.3 Hydrophone Preamplifiers

In order to obtain faithfully reproduced acoustic pressure-time waveforms, it is desirable to incorporate a high quality voltage preamplifier between the piezoelectric sensor or hydrophone and the associated analyzing equipment. This is because the output voltage signal generated by the hydrophone is developed across an extremely high electrical impedance (on the order of hundreds kilo-Ohms or Mega-Ohms). In addition, the hydrophone's (circular) active element is usually on the order of 0.5 mm in diameter and therefore its capacitance is relatively low. For a typical sensor using PVDF film thickness of 50 μm this capacitance is about 0.3 pF.

Loading the hydrophone's output even by relatively high impedance loads, can still lead to reduction in its sensitivity (in μV/Pa or dB re 1μV/Pa) as well as severely limit its frequency response. To prevent or help minimize these effects it is essential that the signal from a hydrophone is fed through a preamplifier before applying it to measuring and recording instrumentation [49, 50]. Therefore, a preamplifier is necessary to convert the high output impedance (about 1 Mega-Ohms) of the hydrophone to a lower value typically 50 ohms that provides electrical matching where recording the acoustic pressure-time waveforms.

A preamplifier provides two basic functions. As already noted, the first one is to convert the high output impedance of the hydrophone to a lower value (typically 50 ohms) that is much less susceptible to loading by the relatively low input impedance of the measuring instrument used. The second one is to amplify, if needed, the relatively weak output signal from the hydrophone so as to obtain sufficient signal level (usually voltage) to drive the measuring instrumentation.

The analysis given below provides additional background describing the advantages and fundamental limitations when using a hydrophone probe with a preamplifier. All probes measured in this work were used with a voltage preamplifier. Accordingly, the discussion below considers a hydrophone to represent a voltage source, which is terminated with a voltage preamplifier. To minimize hydrophone's loading, the preamplifier input impedance should be on the order of Mega-Ohms. In practice, loading is unavoidable as even with voltage preamplifiers that have the highest practically achievable input

impedance (on the order of 100 MΩ) the parallel capacitance of the hydrophone output connection cable (C_c) has to be considered [51]. This capacitance varies as it depends on the cable length between the preamplifier and the active element. The severity of the loading may be estimated by knowing the capacitance of the sensitive element and the cable length (typical coaxial (or equivalent) cable capacitance is about 100 pF/m). It is clear that even built-in preamplifier with a very short cable length, say 5 cm, will reduce the input signal by about 25 dB (or about 19 times) assuming the sensitive element capacitance C_a to be about 0.3 pF. The reasons for this can be explained with reference to the simplified voltage preamplifier equivalent circuit shown in Figure 2.3, where it can be seen that the charge Q_a produced by a hydrophone when exposed to acoustic pressure appears as a voltage V_a. This voltage is developed across the internal capacitance C_a of the hydrophone and the parallel capacitance C_c of the output connection cable (Noted that the internal resistance R_a of the hydrophone and the inductance L_c of the output connection cable are negligible). Together C_a and C_c act as a frequency independent voltage divider network which attenuates V_a to produce the output voltage V_{ao}.

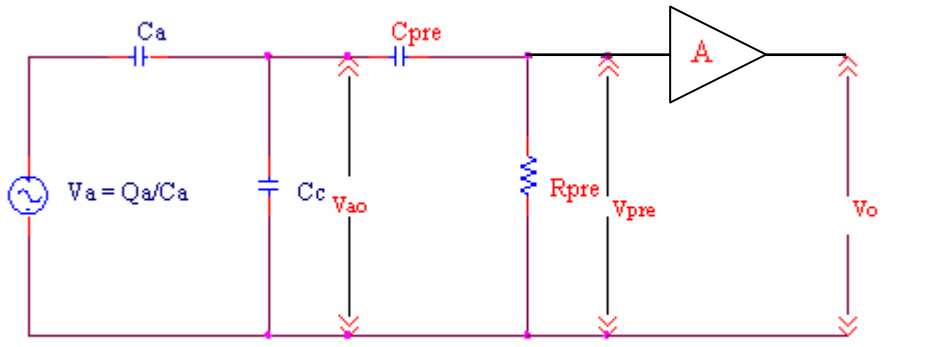

Figure 2.3: Equivalent circuit of voltage preamplifier using a hydrophone as a voltage source.

Thus a hydrophone's voltage sensitivity S_v depends not only on its charge sensitivity S_q and capacitance C_a, but also on the parallel capacitance C_c of its output connection cable and follows the relation:

$$S_v = \frac{S_q}{C_a + C_c} \tag{2.1}$$

Unlike S_q and C_a, which are hydrophone constants, C_c is dependent on cable length. When the connection cable length increases the voltage sensitivity of a hydrophone will be reduced as the attenuation due to C_a and C_c increase. Consequently, if the length of the cable is changed, the attenuation will be altered meaning that new voltage sensitivity for the hydrophone has to be determined. The use of a voltage preamplifier is therefore only recommended with fixed, minimal length of cable connecting the hydrophone and preamplifier. To optimize the sensitivity of the hydrophone and its frequency response, the preamplifier can be built into the hydrophone probe housing. A detailed discussion of advantages and limitation when using a preamplifier is given in [51].

The input impedance of voltage preamplifiers influences the voltage sensitivity characteristics of hydrophone primarily at low frequencies. At these frequencies the combined reactance of C_a and C_c with C_{pre}, the AC input coupling capacitance of the preamplifier, starts to become comparable with the input resistance R_{pre} of the preamplifier. Together, these components form a frequency dependent voltage divider network which attenuates the hydrophone voltage V_{ao} and determines the lower limiting

frequency (f_L) of the hydrophone and preamplifier. The frequency at which V_{pre} = $0.707V_{ao}$ is termed the -3dB lower limiting frequency and is given by:

$$f_L = \frac{C_a + C_c + C_{pre}}{2\pi R_{pre}(C_a + C_c)C_{pre}} \tag{2.2}$$

By using a direct coupled voltage preamplifier, an input coupling capacitor C_{pre} can be omitted and -3dB lower limiting frequency can be determined as:

$$f_L = \frac{1}{2\pi R_{pre}(C_a + C_c)} \tag{2.3}$$

For the previously discussed example, if the cable length between the preamplifier and the active hydrophone element is 5 cm, C_c is 0.5 pF, C_a is 0.3 pF and R_{pre} is about 1 Mega-Ohms, the low frequency roll-off (f_L) of the hydrophone and preamplifier would be approximately 30 kHz. This frequency cut-off is fully adequate for measurements of diagnostic ultrasound fields.

As already mentioned, incorporating a preamplifier into the hydrophone assembly has also been shown to overcome the loading effects introduced by the cable [51]. The preamplifier is also helpful in minimizing the measured waveform distortions when a significant finite amplitude distortion in the pressure wave is present [49, 50]. Some trade-off to using a preamplifier is that it would add to the complexity and the cost of the hydrophone and it could limit the dynamic range [51]. Also, the bandwidth of the

preamplifier must be considered in order to minimize the errors introduced by non-ideal frequency responses [52]. Moreover, accessory electronic components could have an impact on hydrophones performance. Carefully implemented radio frequency (RF) shielding is required to reduce the noisy environment created by the medical ultrasonic equipment.

The hydrophone probes used in biomedical ultrasound measurements have to meet several requirements [2]. These requirements include linearity, frequency response, hydrophone sensitivity and hydrophones' effective aperture and are briefly discussed below:

Linearity

Linearity is an important parameter in the characterization of an ultrasonic hydrophone. The ultrasonic diagnostic imaging equipment can generate instantaneous pressure amplitudes on the order of 10 MPa [45]. Therefore, the hydrophone sensitivity must be linear over that range.

Meeks and Ting [53] provided evidence that PVDF polymer is linear to about 65 MPa. They acquired the linearity response as a function of dynamic pressure pulses with a rise time of 1-3 ms and peak amplitudes up to 75 MPa. Such pressure amplitudes are beyond those used in imaging and are typical of therapeutic lithotripters [54]. The deviations of linearity at 65 MPa for the different types of PVDF polymers tested were less than 7% when compared to ideal linearity response [53].

Frequency response

Theoretically, a hydrophone should convert the acoustic pressure waveform into a corresponding voltage waveform. The frequency response of hydrophones is the hydrophone sensitivity as a function of frequency. Ideally, the frequency response of the hydrophone and associated electronics should be uniform over the whole range of frequencies, which are contained in the waveform in order to reproduce the pressure-time waveform correctly. Smith [50] has shown that the thickness of the active hydrophone element and the cable length influence the frequency response. A relatively thick element gives rise to a lower resonance frequency, which reduces the -3 dB frequency bandwidth of the hydrophone. For example, compared to a 50 μm thick membrane, a 9 μm thick membrane hydrophone has a flat frequency response over a frequency range approximately 5 times greater. The results of Smith's work suggest that the cable resonance has a greater impact on the frequency response than the thickness-mode resonance and suggests limiting cable length to about 15 cm [50].

Voltage sensitivity

One of the goals in the ultrasound metrology is to determine the voltage sensitivity by measuring the voltage at the hydrophone terminals. The end-of-cable loaded sensitivity of a hydrophone, $M_L(f)$, is calculated from Equation 2.4**,** when used in a continuous single-frequency sound field of frequency *f*:

$$M_L(f) = \frac{v}{p} \tag{2.4}$$

where v is the voltage generated by the acoustic pressure incident on the sensitive element of the hydrophone and p represents the free-field acoustic pressure at the hydrophone. $M_L(f)$ should be expressed as a function of f when it is important to emphasize that the hydrophone sensitivity may vary with frequency.

The end-of-cable open-circuit sensitivity $M_c(f)$, is a convenient way to specify sensitivity independent of the loading conditions; however, it is difficult to measure as it assumes that at the time of calibration, the measured hydrophone voltage was loaded with an infinite resistance (open-circuit) [51]. Once the end-of-cable loaded sensitivity has been measured, the open-circuit sensitivity can simply be calculated using the following relationship [45]:

$$M_L = M_C \sqrt{\frac{\{\mathrm{Re}(Z_{el})\}^2 + \{\mathrm{Im}(Z_{el})\}^2}{\{\mathrm{Re}(Z_{el}) + \mathrm{Re}(Z)\}^2 + \{\mathrm{Im}(Z_{el}) + \mathrm{Im}(Z)\}^2}} \tag{2.5}$$

where $\mathrm{Re}(Z_{el})$ and $\mathrm{Im}(Z_{el})$ are, respectively, the real and imaginary components of the complex impedance of the measuring device and Re(Z) and Im(Z) represent, respectively, the real and imaginary portions of the hydrophone's complex impedance. Assuming the loading of the measurement system is a parallel circuit of resistance R_L and capacitance C_L, the complex impedance components can be calculated as,

$$\mathrm{Re}(Z_{el}) = \frac{R_{el}}{1 + \omega^2 {R_{el}}^2 {C_{el}}^2} \tag{2.6}$$

and

$$\mathrm{Im}(Z_{el}) = \frac{-\omega {R_{el}}^2 C_{el}}{1+\omega^2 {R_{el}}^2 {C_{el}}^2} \tag{2.7}$$

where ω is the angular frequency ($2\pi f$) and f is the frequency at the specified $M_c(f)$

If the impedance of the hydrophone and the load of the system are assumed to be capacitive, the end-of-cable sensitivity can be reduced to

$$M_L = M_C \frac{C_a}{C_a + C_c + C_s} \tag{2.8}$$

where C_a, C_c, and C_s are the capacitance of the sensitive element, the coaxial cable, and the stray capacitance, respectively. Figure 2.4 shows a schematic representation of this loading situation described in Equation 2.8. The major loading on C comes from the cable capacitance C_c (typically 90-100 pF/m), which is much larger than the sensor capacitance, often on the order of 0.3 pF-3pF. Reducing the length of the cable is one way to decrease the impact of the cable capacitance on the hydrophone sensitivity.

The (excessive) cable length can also lead to distortions in the measured pressure-time waveform due to transmission line phenomenon. The use of a low pass filter suggested in [55] can effectively alleviate this problem.

The end-of-cable voltage sensitivity determined is terms of V/Pa is often expressed in decibels,

$$G_L(dB) = 20\log(M_L / M_{ref}) \tag{2.9}$$

where M_{ref} = 1V/Pa or 1 V/μPa [56].

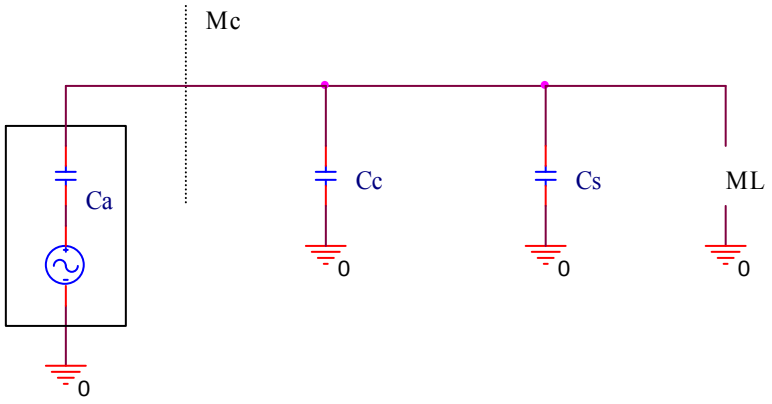

Figure 2.4: Schematic of line capacitance effect on the end-of-cable sensitivity.

Effective aperture

Since a hydrophone's effective diameter was used as one of the input parameters to perform the semi-empirical nonlinear calibration described in section 3.2.3, this section discusses the importance of the effective diameter and the theory behind its determination. As noted in Table A1.1, all hydrophone probes used in this work had circular active elements.

The active element size is presented in two different ways; "effective size" and "nominal or geometrical size". The nominal or geometrical hydrophone diameter is the physical

measurement of the active electrode area but the effective diameter of the hydrophone is determined from the hydrophone's directional response [2]. The effective diameter must be smaller than the acoustic wavelength and the ultrasound beam dimensions; if not, the measured acoustic pressure amplitude would not be correct. The reason for the discrepancy in the measured and actual pressure is that the hydrophone responds to the space integral of pressure over its active surface. Therefore, when the effective aperture of the hydrophone is greater than the incident acoustic beam dimensions, the net effect would be a reduced spatially averaged pressure [49]. To minimize the spatial averaging, the effective hydrophone d_e must comply with the inequality requirements shown in Equation 2.10.

$$d_e < \frac{\lambda z}{2d_s} \quad \text{if} \quad \frac{z}{d_s} \geq 1$$
$$d_e < \frac{\lambda}{2} \quad \text{if} \quad \frac{z}{d_s} < 1 \tag{2.10}$$

where z is the distance between the hydrophone and the acoustic source, d_s is the diameter of the source, and λ is the acoustic wavelength. The calculation of the effective diameter involves a careful measurement of the hydrophone's directivity pattern. It is assumed that this pattern can be described as:

$$p(\theta) = \frac{2J_1(ka\sin\theta)}{ka\sin\theta} \tag{2.11}$$

where $p(\theta)$ is the directivity corresponding to angle θ, a is the radius of the active element of the hydrophone, J_1 is the Bessel function of the first order and k is the wave number given in Equation 2.12:

$$k = \frac{2\pi f}{c} = \frac{\omega}{c} \tag{2.12}$$

where f is the frequency, ω is the angular frequency and c is the speed of sound in water.

The hydrophone effective radius is suggested in [4] to be calculated from the arithmetic mean of a_3 and a_6:

$$a_3 = \frac{1.62}{k \cdot \sin(\theta_3)}$$
$$a_6 = \frac{2.22}{k \cdot \sin(\theta_6)} \tag{2.13}$$

where a_3 and a_6 are the effective radii calculated for the -3 dB and -6 dB drop levels from the peak, and θ_3 and θ_6 are the corresponding half angles.

Equation 2.13 is valid under the assumption that the effective diameter is constant with the frequency. However, there is evidence that the effective diameter of a hydrophone decreases with increasing frequency [57]. The analytical relationship between frequency

and the effective diameter is shown in Equation 2.14 [57].

$$a \approx \sqrt{a_g^2 + \frac{1}{4f^2}} \tag{2.14}$$

where a is the effective radius in mm, f is the frequency in MHz and a_g is the geometrical radius of the hydrophone in mm.

The spatial averaging correction (used during this work) is also dependent on the effective aperture of the hydrophone probes. The details of the spatial averaging correction are given in Section 3.1. This correction was necessary to obtain valid calibration results using both swept frequency techniques such as Time Delay Spectrometry (TDS) and Time Gating Signal Analysis (TGFA) described in Chapter 3. The spatial averaging correction was also implemented in the nonlinear propagation model, which was indispensable in achieving the calibration range of 100 MHz. Prior to introducing the model it is worth noting that attempts were made to obtain hydrophone calibration at the frequencies of tens of Megahertz using optical methods, such as interferometry [58]. However, the maximum frequency at which the reliable data were reported was well below the 100 MHz mark considered here [58].

The fundamental principles of the nonlinear wave propagation along with a brief introduction of the nonlinear propagation model used in this work are given below.

2.2.1.4 Nonlinear wave propagation and its modeling.

Nonlinear wave propagation is caused by the (nonlinear) properties of a medium through which the wave travels. The nonlinearity of the medium causes the compressional peak amplitude to travel faster than the rarefactional dip [2]. As a result the original sinusoidal wave is being distorted, so its frequency spectrum broadens due to the content of harmonics. The ultrasonic waveform distortions depend upon the attenuation in the medium. The attenuation of a wave is determined by scattering and absorption. Since scattering and absorption are frequency and distance dependent, the ultrasonic wave distortions increase with increasing propagation distance from the radiating acoustic source, increasing strength of electronic or mechanic focusing gain and increasing frequency.

The level of the nonlinearity of the pressure-time waveform can be estimated by considering the nonlinearity propagation parameter σ_m. Equation 2.15 shows the equation of σ_m for unfocused transducers in the far field [2, 59].

$$\sigma_m = \frac{\beta \omega r_O p_O}{\rho c^3} \sinh^{-1}\left(\frac{z}{r_O}\right) \tag{2.15}$$

where β is the nonlinearity parameter that is equal to 3.5 for pure water at 20 degrees Celsius, z is the distance from the transducer, ω is the angular frequency, $\omega = 2\pi f_c$, ρ is the water density and c is the speed of sound in water. p_o is the acoustic pressure at the

surface of the transducer and r_o is the transition distance or Rayleigh length given by $r_O = \frac{\pi d^2}{4\lambda} = \frac{\omega d^2}{8c}$ (d is the diameter of the transducer and λ is the wavelength in water for the center frequency, f_c).

For focused transducers, σ_m can be calculated from [2, 59]:

$$\sigma_m = \frac{\beta \omega z p_m}{\rho c^3} \frac{1}{\sqrt{F_g - 1}} \ln\left(\sqrt{F_g - 1} + \sqrt{F_g}\right) \tag{2.16}$$

where p_m is the mean peak cycle acoustic pressure at the point in the acoustic field corresponding to the spatial peak temporal peak acoustic pressure at the axial distance, z. F_g is 0.69 times the ratio of the geometrical area of the ultrasonic transducer to the -6 dB beam area at z. In the case of circular focused transducers, $F_g = G^2$, where G is the linear focusing gain designated by $G = \frac{r_O}{z}$, and σ_m is defined by Equation 2.17.

$$\sigma_m = \frac{\beta \omega z p_m}{\rho c^3} \frac{1}{\sqrt{G^2 - 1}} \ln\left(\sqrt{G^2 - 1} + \sqrt{G}\right) \tag{2.17}$$

There are three levels of nonlinearity, depending on the value of σ_m [2]. For $\sigma_m < 0.5$, there is little or no nonlinearity and the amplitude at the center frequency differs by less than 5% from the value without the nonlinear effects. For $0.5 < \sigma_m < 1.5$, the wave is

characterized as having medium nonlinear distortion. Here, the amplitude measured in a ½ octave band centered at the center frequency may differ from its value without the nonlinear effects by between 5 and 25%. For σ_m > 1.5, there is also loss in energy associated with the considerable nonlinear distortion of the pressure-time waveform. The amplitude in this case may differ by more than 25% from its value in the absence of nonlinear effects.

The nonlinear propagation acoustic model used here is referred to as the JW model to honor Dr. Janusz Wójcik, who originally developed it [60]. This model can be used both with circular spherically focused transducers and, rectangular mechanically and electronically focused transducers. It can predict the pressure-time waveforms at any point in the acoustic field in front of the acoustic source. A detailed description of the JW model is given in [60, 61].

Briefly, the JW model is based on the modified Kuznetsov equation describing the propagation of the acoustic disturbance in the nonlinear and lossy medium as shown in Equations 2.18 and 2.19 [62].

$$\Delta\Phi - \partial_{tt}\Phi - 2\partial_t \mathrm{A}\Phi = q\partial_t(\partial_t\Phi)^2 + 2q_1 L[\Phi] \tag{2.18}$$

$$L[\Phi] \equiv \frac{1}{2}\left[(\nabla\Phi)^2 - (\partial_t \Phi)^2\right]$$

$$q \equiv \frac{P_O(\gamma+1)}{2\rho_O c_O^2}, q_1 \equiv \frac{P_O}{\rho_O c_O^2} \tag{2.19}$$

$$A\Phi = A(x) \underset{\times}{\otimes} \Phi(x,t)$$

$$A(x) = \hat{(F)}^{-1}\left[a(e \cdot K)\right]$$

where $\Delta \equiv \nabla \cdot \nabla$ is the Laplace operator, $\nabla \cdot$ is the divergence operation and ∇ is the gradient operator. Φ is the normalized acoustic potential, P_o is the characteristic absolute peak pressure value at the source surface, ρ_o is the equilibrium density, c_o is equilibrium sound velocity and *(x,t)* are the normalized space and time coordinates. $\gamma = c_p c_v$ is the exponent of the adiabate and c_p, c_v are the specific heats at constant pressure and volume, respectively. $\gamma = B/A+1$ where B/A is the nonlinear parameter [60]. Operator A can be described as in Equation 2.19, where *A(x)* is the kernel of the convolution $\underset{\times}{\otimes}$ with respect to the space variable; *e* is the unit vector in the direction of the real component of the complex wave vector *K*.

The JW model is suitable for predicting the characteristic of strongly nonlinear waveforms and uses the apodization function measured in the immediate vicinity of the transducer surface. This semi-empirically determined function provides a better prediction of the nonlinear field than other models that assume the Gaussian distribution of the transmitter surface displacement amplitude as one of the input boundary

conditions [30]. The solution of the JW model is presented in terms of Fourier Series of the acoustic pressure-time waveform [24].

As only the circular spherically focused sources were used during this work, the boundary conditions of the excitation pulses to the model could be described as the spectral components of time domain function:

$$C_n(0,r) = C_{bn} e^{-\frac{ink_0 r^2}{2F_g}} \tag{2.20}$$

$$C_{bn} = 0 \quad \text{for} \quad r \geq a, k_0 = \frac{\omega_0}{c_0}$$

Further, the pressure pulse on the transducer surface exhibits a pattern that can be described by:

$$f(t) = \left(1 - \left|\frac{t - t_C}{t_S - t_C}\right|^m\right) \sin\left[\omega(t - t_C)\right] \tag{2.21}$$

$$f(t) = 0 \quad \text{for} \quad t \notin (t_S, t_e)$$

where $m = 2$ and t_s, t_c, t_e are times of start, of the middle part and of the end of the pulse, respectively. These conditions were suitable for the boundary pulse at the surface of the spherical focused source, assuming a parabolic lens located at the boundary. The plane wave front was generated from the transducer source and then transformed into a sector

of the focused spherical wave with a focal length of F_g.

Microsoft FORTRAN Power station 4.0 was used to solve the nonlinear JW model (Equations 2.18 and 2.19) with the boundary conditions given by Equations 2.20 and 2.21. The FORTRAN program calculated the Fourier coefficients of the excitation pulse. The coefficients were then used to predict the pressure-time waveform in a selected point of the field. To graphically display the waveform a Mathcad 12 was used. The JW model was able to simulate both linear and nonlinear wave propagation conditions. For the linear propagation conditions, the numerical algorithm described by Equation 2.22 was used. In this case, the number of spectral components was equal to the number of components used to describe the boundary conditions.

$$C_n(z+\Delta z, r) = B^{-1}\left[H(n, k_r, \Delta z)\cdot B\left[C_n(z, r)\right]\right] \qquad n = 1, 2, 3, \ldots \text{N} \tag{2.22}$$

where $B[\cdot]$ is the Fourier-Bessel transform (Hankel transform of the order 0), $C_n(z+\Delta z, r) = B\left[C_n(z, r)\right]$, $B^{-1}[\cdot]$ is the inverse transform, k_r is the radial component of the wave vector. $k_n^2 \equiv n^2(\omega_0 / c_0)^2 = k_z^2 + k_r^2$. Hankel transformation (H) of the Green function of the propagation equation is given by:

$$H(n, k_r, \Delta z) = e^{i\Delta z\left(\sqrt{k_n^2 + k_r^2 + 2ik_n a(n\omega_0)} - k_n\right)} \tag{2.23}$$

Function H propagates the wave field from the plane located at z to the next plane located at $z+\Delta z$ axial distance. The absorption coefficient is given by $a(n\omega_0)=\alpha_l(\omega_0/2\pi)^l n^l$; (n, l = 1, 2, 3, … N), where α_l and l depend on the propagation medium.

Nonlinear propagation conditions were simulated using Equation 2.24:

$$C_n(z+\Delta z,r)=B^{-1}\left[H(n,k_r,\Delta z)\cdot B\left[C'_n(z,r)\right]\right]$$

$$C'_n(z,r)=NL^n\left(\{C_l(z,r)\}\right) \qquad (2.24)$$

$$n,\ l\ = 1, 2, 3, \ldots \text{N}$$

where the NL is the nonlinear operator representing the interaction between the spectral component $\{C_n\}$ and the generation of new components along the transmission path Δz. The details of NL were explained in [60]. To minimize the computer calculation time, the number of spectral components was not equal to the number of components used to describe the boundary condition; but it depended upon the degree of the nonlinearity and the interaction between the nonlinear components. Also, the numerical method used here was dynamically selectable from the second order Lagrange method to the fourth order Runge-Kutta method. The absorption coefficient used in Equation 2.24 was assumed to be dependent on temperature, and the polynomial approximation described in [63] was used.

The output of the JW model was presented as the spectra of the normalized pressure-time

waveforms at any location in the field in front of the acoustic source. The time waveforms were obtained from the spectra by applying the Inverse Fourier Transform. The four parameters used as input boundary conditions are briefly described in the following. The parameters included the normalized acoustic pressure-time waveform(s) described by its Fourier series [24], the apodization function, the focal distance and the peak pressure amplitude at the surface of the acoustic source.

Pressure-time waveform(s)

The normalized propagating acoustic pressure-time waveform used by the JW nonlinear model was defined by the following parameters: frequency, number of cycles, repetition frequency and the exponent coefficient of the envelope function (E_{window}):

$$E_{window}(x)=1-\left|\frac{2x}{np}-1\right|^{xx} \tag{2.25}$$

where x is the time index, np is the number of the points in the waveform where the signal is nonzero and xx is the exponent coefficient of the envelope.

Figure 2.5 shows the normalized acoustic pressure-time waveform with the following parameters: 10 MHz, 10 cycles pulse with an envelope coefficient of 25. These parameters were used to perform the experiments described in Section 3.2.3 (Nonlinear pressure-time waveform measurement, Chapter 3). The Y axis represents the normalized acoustic pressure amplitude and the X axis represents the retarded time normalized to 2π.

Figure 2.6 shows the corresponding spectrum of the pulse shown in Figure 2.5. This spectrum was used as one of the boundary conditions for the JW nonlinear model described in Section 3.2.3.

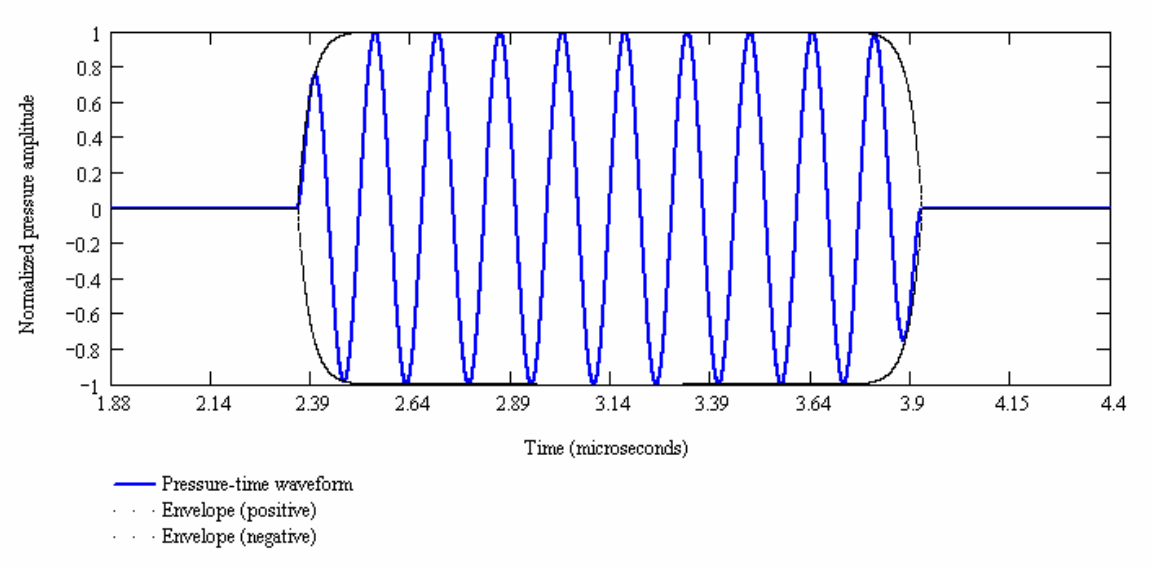

Figure 2.5: Normalized acoustic pressure-time waveform used as an input for the JW nonlinear model with the following parameters: fundamental frequency: 10 MHz, pulse length: 10 cycles and the envelope coefficient of 25. The Y axis represents the normalized acoustic pressure amplitude and the X axis represents the retarded time normalized to 2π.

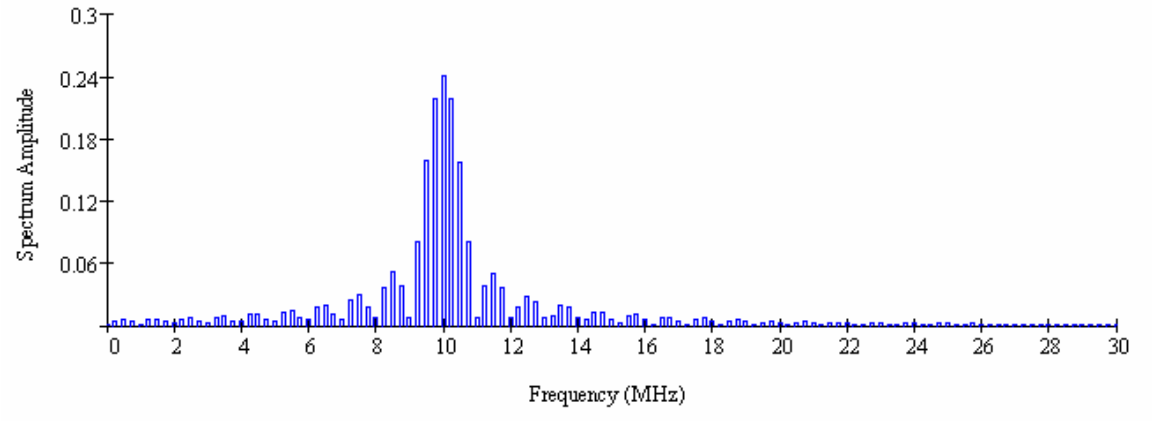

Figure 2.6: Spectrum of the normalized acoustic pressure-time waveform model with the following parameters: fundamental frequency: 10 MHz, pulse length: 10 cycles and the envelope coefficient of 25.

Surface apodization function

The FORTRAN programs used to implement the JW nonlinear model allow any function to be set as apodization for a given surface of acoustic sources. It should be noted that, although the JW model is capable of predicting the pressure-time waveforms for both circular spherically focused acoustic sources and, rectangular focused sources [61], the experiments described in Section 3.2.3 (Nonlinear pressure-time waveform measurement, Chapter 3) used circular spherically focused acoustic sources only. The apodization functions for the circular focused aperture were determined individually for each measurement condition as described in more detail in Chapter 3.

This chapter concludes with a brief description of a hydrophone that does not use piezopolymer material as its active element. This alternative hydrophone probe employs optical fiber and allows probe implementation that is close to that of an ideal, point receiver in the frequency range considered.

2.2.2 Fiber hydrophone probes

The principle of a fiber optic hydrophone operation is based on the measurement of Fresnel reflectance from the tip of the optical fiber and its dependence on the acoustic pressure. The Fresnel reflectance at the interface of glass water is given below (Equation 2.26) [39]:

$$R = \left[\left(n_c - n_w \right) / \left(n_c + n_w \right) \right]^2 \tag{2.26}$$

where, n_c and n_w are the indices of refraction of the fiber core and water, respectively.

In the presence of an acoustic pressure field in water, the relationship between the change of the index of refraction of water and the acoustic pressure amplitude can be described as [39]:

$$\Delta n_w / \Delta p \approx 1.4 \times 10^{-4} MPa^{-1} \tag{2.27}$$

The corresponding value for a silica fiber is given by [39]:

$$\Delta n_c / \Delta p \approx 5 \times 10^{-6} MPa^{-1} \tag{2.28}$$

where p is the acoustic pressure amplitude. As $\Delta n_c / \Delta p << \Delta n_w / \Delta p$, for simplicity, the compressibility of the fiber core with respect to water can be ignored (i.e. $\Delta n_c = 0$), at the expense of the minor and acceptable error of +3.6% [39]. Hence, the reflectance change (ΔR) is directly proportional to the acoustic pressure (see Figure 2.7); i.e.:

$$\Delta R \propto p \tag{2.29}$$

Thus, by detecting the reflected light signal, the acoustic pressure amplitude at the fiber tip can be measured. Also, according to Equation 2.29, output electrical power (P_{out}) has the following relationship with laser power (P_{laser}) and acoustic pressure (p):

$$P_{out} \propto P_{laser}^2 , \quad P_{out} \propto p^2 \tag{2.30}$$

As shown in Figure 2.7, the relationship between power reflectance and acoustic pressure is linear in the range of pressure amplitudes typical of those used in medical ultrasound imaging application. Yadav et al [64] has reported the threshold level for silica nonlinearity to be 380 MPa [65], which is well above the pressure amplitudes encountered in biomedical ultrasound applications.

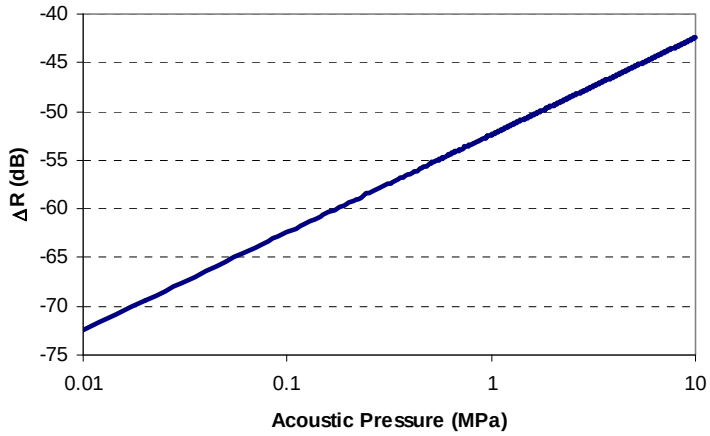

Figure 2.7: Reflectance change versus acoustic pressure (Linear relationship).

A prototype fiber optic (FO) ultrasound hydrophone probe similar to the one described in [66] was used. The initial measurements were performed using 10 μm diameter untapered fiber [66]. Such aperture is adequate for acoustic field measurements in the frequency

range up to about 75 MHz without the need for any spatial averaging correction. The details of the experimental method using the FO hydrophone probes are given in Section 3.3.

CHAPTER 3: Experimental setups and methodology

This Chapter describes the measurement arrangements and methodology applied to develop and optimize the calibration techniques for ultrasonic hydrophone probes in the frequency range up to 100 MHz. Three different acoustic methods (Time Delay Spectrometry (TDS), Time Gated Frequency Analysis (TGFA), and a semi-empirical nonlinear propagation model) have been combined to determine the frequency dependent sensitivity of the finite aperture hydrophone probes and the frequency response of the 10 μm diameter fiber optic (FO) prototype. All methods account for spatial averaging correction and two of them (TDS and TGFA) allow the hydrophones' sensitivities to be measured as a quasi-continuous function of frequency. The nonlinear approach yields sensitivity values at discrete frequency intervals depending on the fundamental working frequency of the source used. The results presented in Chapter 4 were obtained by employing TDS calibration from 1 to 40 MHz, TGFA method from 20-100 MHz and the nonlinear model from 10-100 MHz. This overlapping of frequency ranges provided the sensitivity of hydrophone probes as a virtually continuous function of frequency from 1-100 MHz, and allowed verification of the developed calibration approach and minimized the overall uncertainty.

This chapter is divided into three sections: the first section (3.1) describes the theoretical model used to determine the effect of spatial averaging in acoustic measurements performed with finite aperture ultrasonic hydrophone probes. The second section (3.2)

describes the hydrophone probe calibration techniques used in this work. The third section (3.3) presents the acousto-optic measurement setup.

3.1 Hydrophone spatial averaging correction

As already noted, hydrophone calibration procedures have to take into account spatial averaging correction due to the finite aperture of hydrophone probes [67]. This is because the receiver's (hydrophone's) finite dimensions are much larger than the half wavelength at the highest frequency considered (here 100 MHz). The spatial averaging correction model was used here to account for the space integral of pressure over its active surface since errors in the pressure amplitude measurements occur when the effective aperture of the hydrophone is greater than the cross section of the incident acoustic beam.

The source properties, pulsing conditions and hydrophone probe's characteristics such as hydrophone's frequency response and effective aperture were all used as input parameters to the spatial averaging model. The spatial correction procedure can be conveniently discussed referring to Figure 3.1.

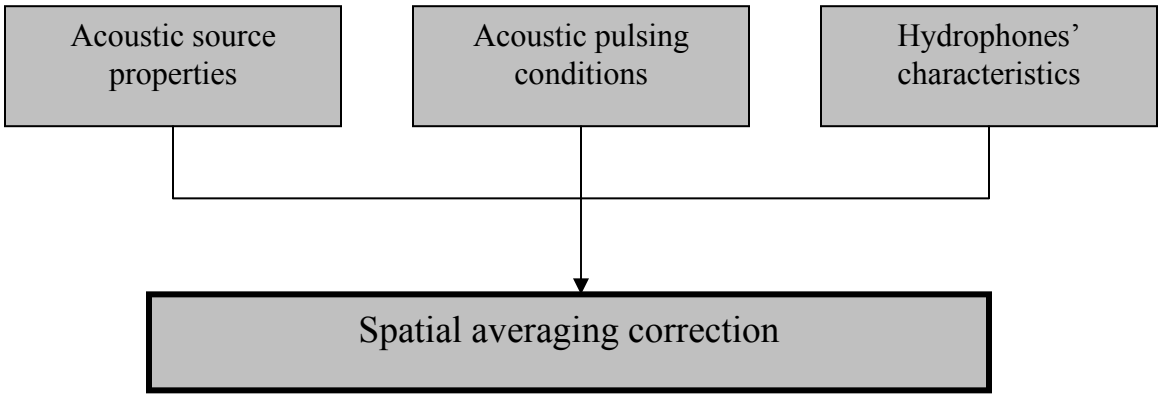

Figure 3.1: Flowchart showing the input parameters used in determining the spatial averaging correction.

The model used is applicable to focused sources of circular geometry, accounts for the effects of hydrophone probe finite aperture and allows the secondary calibration based on the absolute hydrophone calibration using substitution technique to be performed when the physical dimensions of the active elements of reference and tested hydrophone probes differ significantly. In describing the transmitter properties, it is convenient to use the focal number (F#) parameter, defined as the quotient of the focal distance to the diameter of the active transducer surface. Several broadband sources having different focal numbers (2, 3.84, 10.16 and 19.24) were used to produce ultrasound fields with frequencies up to 100 MHz (see Appendix 2). The effective diameters of the ultrasonic hydrophone probes calibrated in the focal plane of the sources ranged from 120–1200 μm (Table A1.1, Appendix 1). The hydrophones with diameters smaller than that of the reference hydrophone exhibited experimentally determined absolute sensitivity higher than the true one. This discrepancy increased with decreasing focal numbers and increasing frequency [67]. It was determined that the error was governed by the cross-section of the beam in the focal plane and the ratio of the effective diameters of the

reference and tested hydrophone probes (see Figure 3.2). In addition, the error was found to vary with the frequency dependent effective hydrophone radius [67].

In Figure 3.2 two conditions encountered during hydrophone calibrations performed here are shown. In the first one (Figure 3.2a), hydrophone aperture is fully immersed in the acoustic field which results in a faithful measurement of the pressure-time waveform. The second condition (Figure 3.2b) corresponds to the situation where the hydrophone's diameter is larger than the cross section of acoustic beam at the focal plane. In this case due to the spatial averaging error the pressure-time waveform is not faithfully reproduced.

The acoustic model used to predict spatial averaging correction is briefly described in the following. The cross-section of the beam profile of a circular focused source in its geometric focal plane can be described as a Jinc function [68, 69]:

$$\frac{p(r)}{p(0)} = \exp\left(\frac{ikr^2}{2D}\right)\frac{2J_1\left(\frac{kar}{D}\right)}{\left(\frac{kar}{D}\right)} \tag{3.1}$$

where *p(r)* is the acoustic pressure at a radial distance *r* from the acoustic axis in the focal plane, *p(0)* is the acoustic pressure on the acoustic axis in the focal plane, *k* is the wave number, J_1 is the Bessel function of the first order, *a* is the source radius and *D* is the radius of curvature of the source transducer.

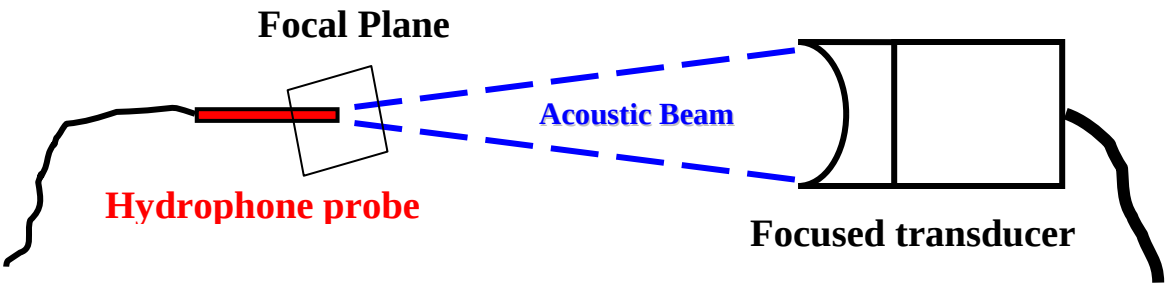

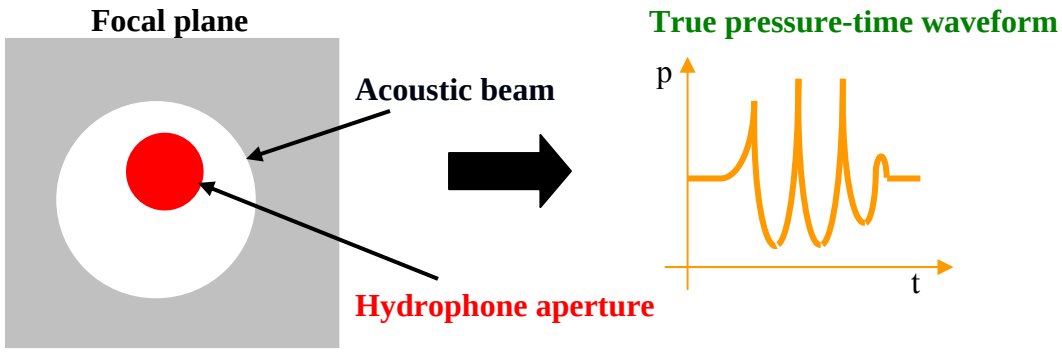

Figure 3.2a: At the focal plane, the hydrophone's aperture is smaller than the cross section of the acoustic beam.

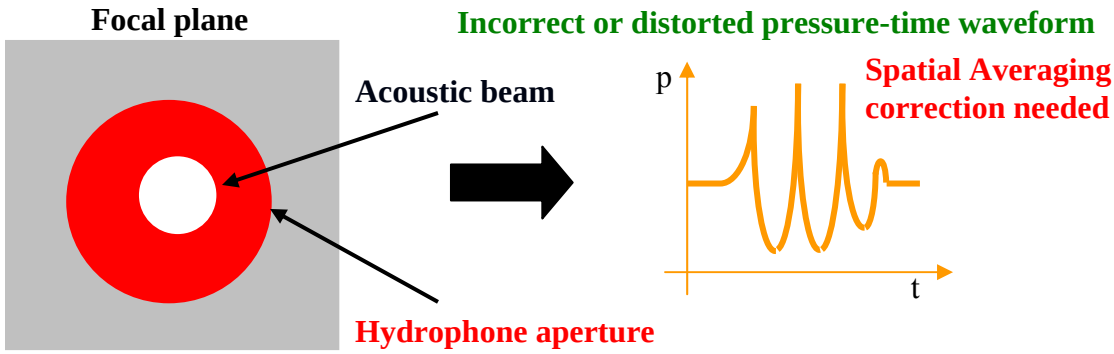

Figure 3.2b: At the focal plane, the hydrophone's aperture is greater than the cross section of the acoustic beam.

Figure 3.2: The influence of the effective aperture size and the incident acoustic beam dimensions on the measurements of the pressure-time waveform.

Equation 3.2 allows the pressure averaging on the active surface of the ultrasonic hydrophone probes at the focal plane to be predicted. The averaging effect was determined using the following expression [70]:

$$p_{average}(M,R) = \frac{\iint_{aperture} r \cdot p(M,r) \cdot dr \cdot d\varphi}{\iint_{aperture} r \cdot dr \cdot d\varphi} \quad (3.2)$$

where $p_{average(M,R)}$ represents the effective hydrophone response after the integration of the instantaneous acoustic pressure p over the hydrophone's active element area at the point M of the acoustic field; R represents the radius of the aperture of the hydrophone, and r and φ are the polar integration coordinates. Equation 3.2 was numerically evaluated using MATLAB 6.5 for a set of circular acoustic sources having focal numbers 3.84, 10.16 and 19.24 (see Table A2 in Appendix 2), and ultrasonic hydrophone probes including both needle and membrane types and having active element diameters of 150, 500 and 1200 μm (see Table A1.1 from Appendix 1).

Figure 3.3 shows the plots of the spatial averaging correction factors predicted by MATLAB 6.5 for a 150 μm diameter needle hydrophone probe. The correction factors are presented for three different focal number sources (3.84, 10.16 and 19.24) versus frequency. The reference hydrophone used was a 500 μm nominal diameter PVDF membrane hydrophone. Figure 3.4 illustrates the plots of the spatial averaging correction factors predicted for a 1200 μm nominal diameter PVDF membrane hydrophone using the same reference hydrophone. It is worth noting that the values of the corrections in Figure 3.3 are negative whereas the correction factors in Figure 3.4 are positive. The reason is that the 150 μm diameter is smaller than 500 μm diameter of the reference hydrophone probe, whereas the 1200 μm diameter is larger than the diameter of the reference probe.

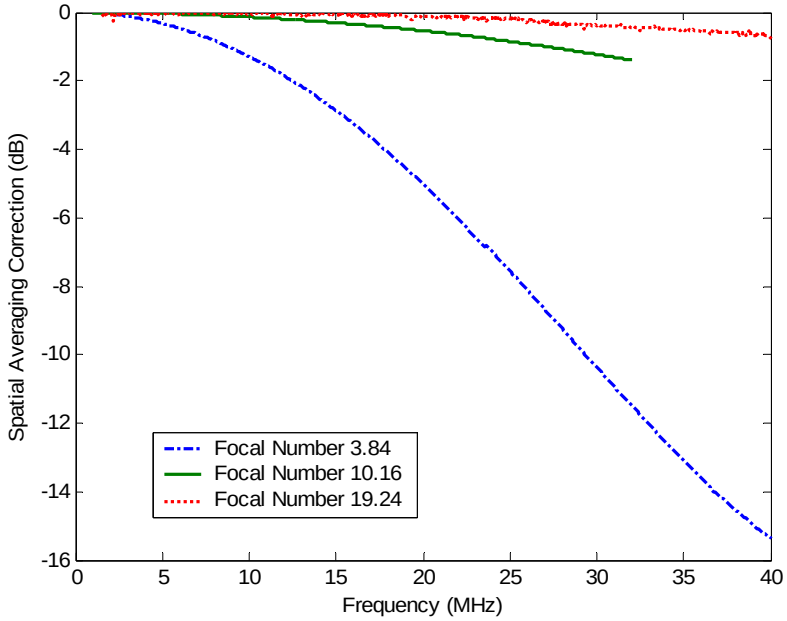

Figure 3.3: The spatial averaging correction factor in dBs for a 150 µm diameter needle hydrophone probe calibrated by substitution method against a 500 µm diameter reference membrane hydrophone in the focal plane of three different acoustic sources.

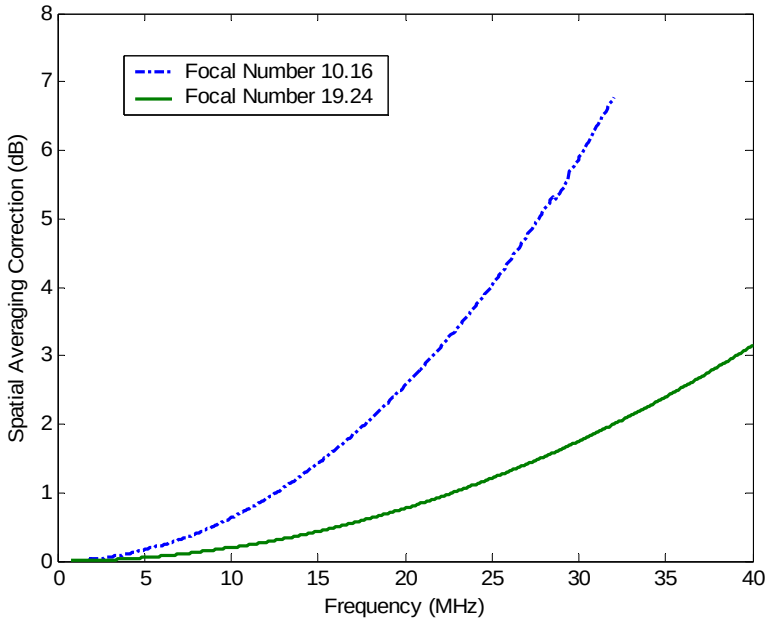

Figure 3.4: The spatial averaging correction factor in dBs for a 1200 µm diameter membrane hydrophone probe calibrated by substitution method against a 500 µm diameter reference membrane hydrophone in the focal plane of two different acoustic sources.

From Figures 3.3 and 3.4, the parameters such as focal numbers and effective diameters were chosen to facilitate experimental verification of the model. The algorithm applied to the hydrophone probes in Figures 3.3 and 3.4 was experimentally validated by performing calibration by substitution using the three focused sources as described in Section 4.1. The 500 μm nominal diameter PVDF membrane hydrophone was used as a reference. The 150 μm nominal diameter needle hydrophone probe and the 1200 μm nominal diameter PVDF membrane hydrophone were calibrated up to 40 MHz using TDS calibration technique (See Section 3.2.1). The measurements were conducted in degassed and deionized water in the focal plane of the sources.

At the frequencies beyond 40 MHz, the correction factors were determined experimentally and then linearly extrapolated from 40 to 100 MHz for hydrophone calibrations using TGFA and nonlinear techniques.

3.2 Hydrophone calibration procedures

This section describes the hydrophone probe calibration techniques in the frequency range up to 100 MHz for the hydrophones listed in Table A1.1. Three calibration methods were used during this work. Two of the methods allowed the hydrophone's sensitivity to be measured as a quasi-continuous function of frequency and one method yielded sensitivity values at discrete frequency intervals; i.e., multiples of 10 MHz. Specifically, the first calibration technique, (see Section 3.2.1) termed Time Delay Spectrometry (TDS), yielded quasi-continuous frequency calibration data up to 40 MHz.

The second calibration technique, (see Section 3.2.2) termed Time-Gating Frequency Analysis (TGFA), provided quasi-continuous calibration data from 20-100 MHz. Finally, the third calibration technique, (see Section 3.2.3) termed semi-empirical nonlinear calibration, delivered discrete frequency response up to 100 MHz.

3.2.1 Time Delay Spectrometry (TDS) calibration

In Figure 3.5, the experimental Time Delay Spectrometry (TDS) setup used is shown. A detailed outline of the TDS calibration technique has been presented in [45, 56, 71, 72]. Briefly, TDS is implemented in the frequency domain. An arbitrary electro-acoustic system comprises a transmitter and receiver separated by a distance d. Since the measurements are performed in a confined space such as a finite-size water tank, there are several signals present, comprised of the desirable direct signal and undesirable echoes. The direct signal has the shortest traveling distance, which corresponds to a propagation time shorter in comparison to that of the reflected signals. In other words, the longer propagation time for the reflected signals translates into a lower frequency than that of the direct signal. With the aid of an appropriate frequency-filtering scheme, the receiver will capture only the direct signal. Therefore, with properly chosen parameters, the TDS technique is capable of eliminating the effects of standing waves and other interferences due to the reflected signals, which means that TDS can create free-field conditions in a highly reverberant environment [56, 71, 72]. In the implementation of TDS shown in Figure 3.5, a spectrum analyzer generated a swept-frequency signal from a tracking generator and had the ability to introduce a shift between the transmitted

frequency and the center frequency of the receiving band-pass filter. The excitation voltage applied to the wideband acoustic source [73] was about 5 V_{pp} (peak-to-peak voltage). The voltage amplitude was sufficiently low to avoid the nonlinearity effects in water yet sufficient to maintain the signal-to-noise ratio (up to 60 dB) during the measurements.

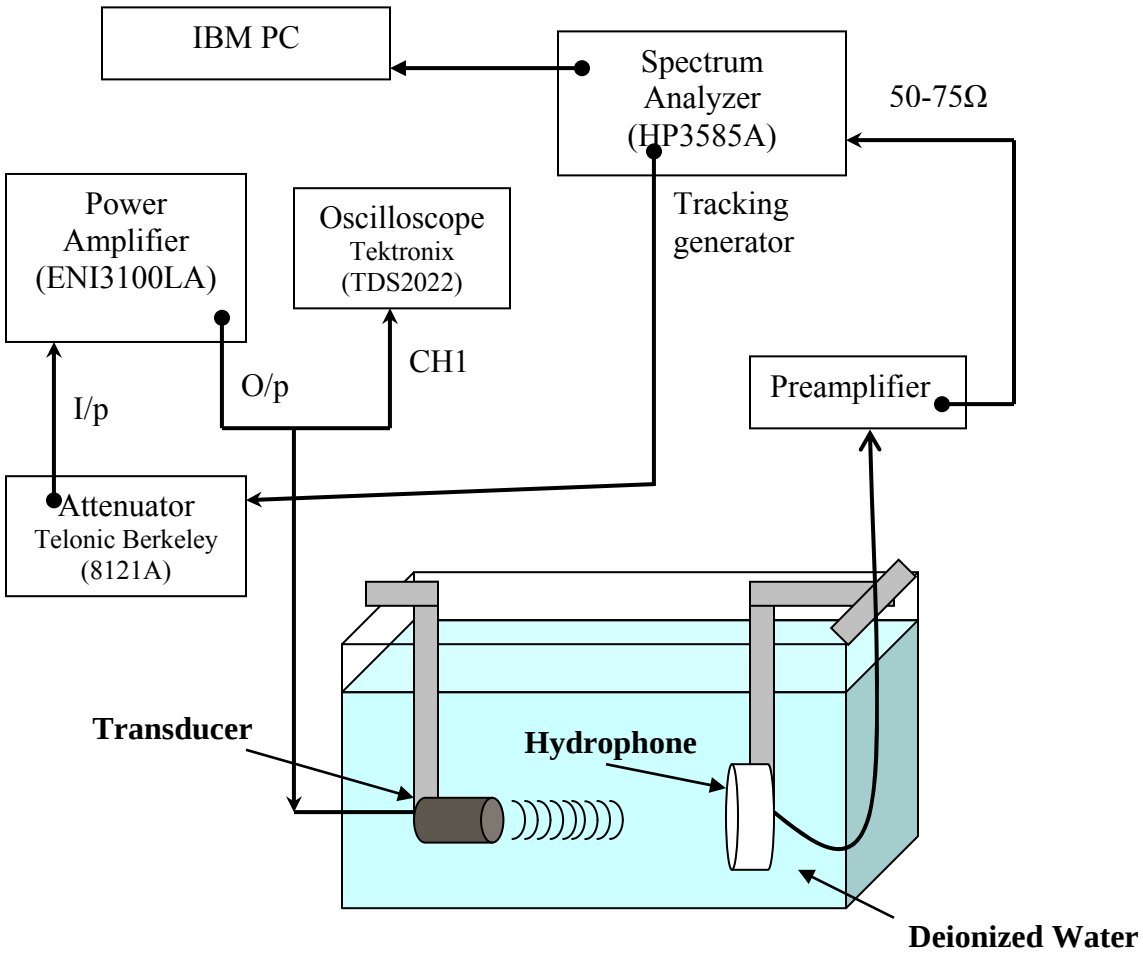

Figure 3.5: The experimental set up for Time Delay Spectrometry (TDS) technique (See Table A3, Appendix 3 for the details of the equipment used).

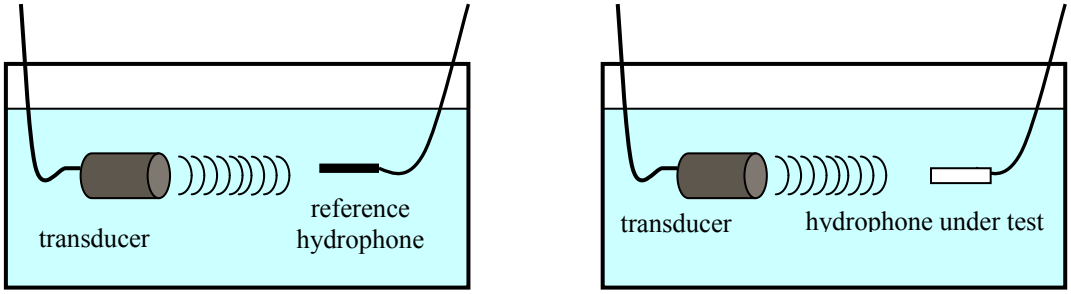

1. Measurement of the voltage response U_{ref} of the reference hydrophone with known sensitivity M_{ref}.

2. Measurement of the voltage response U of the hydrophone to be calibrated.

Figure 3.6: The basic concept of the substitution calibration method using TDS calibration.

Time Delay Spectrometry was used in this work to calibrate hydrophones by substitution technique up to 40 MHz (see Figure 3.6). The calibration was done in the following way: First, the continuous spectrum of previously calibrated reference hydrophone was obtained by placing this hydrophone in the far field or at the focal plane of a wideband ultrasonic transmitter [36]. The reference hydrophone was calibrated by the National Physical Laboratory, NPL, UK. Next, the reference hydrophone was replaced by an unknown one positioned in the very same position in the field. Once again, the amplitude of the signal was maximized and stored for comparison with the reference hydrophone. The sensitivity of the hydrophone being calibrated M was then determined by relating it to the sensitivity of the reference hydrophone M_{ref} and to the measured voltages according to Equation 3.3 [56].

$$M = (U / U_{ref}) M_{ref} \tag{3.3}$$

where U and U_{ref} are the terminal voltages of the tested hydrophone and the reference

hydrophone, respectively.

It should be noted that for all measurements performed here, the speed of sound in water was calculated for each measurement session because it is dependent on the water temperature [74]. Focused wideband transducers were used as sources to maximize signal-to-noise ratio [73]. The focused sources also provided plane wave conditions in the focal plane over a wide frequency range.

The spatial averaging correction was applied to the measured spectrum if the effective aperture of the hydrophone was larger than the incident acoustic beam dimensions. The correction procedure was outlined in Section 3.1. The calibration results obtained using the TDS technique are presented in Section 4.1. The TDS implementation shown in Figure 3.5 allowed hydrophone calibration to be performed up to 40 MHz. Beyond 40 MHz, as mentioned earlier, Time Gated Frequency Analysis (TGFA) technique briefly described in the following was used.

3.2.2 Time Gated Frequency Analysis (TGFA) calibration

Similarly to TDS, TGFA uses a linearly swept frequency excitation signal and establishes reflection-free environment in a bound water tank. However, instead of introducing a frequency shift to account for the wave propagation delay, TGFA requires first transforming the measured signals from the frequency to time domain, and then back to the frequency domain. In other words, TGFA can be considered as a time domain

implementation of the Time Delay Spectrometry (TDS) technique. Figure 3.7 illustrates the principle of TGFA measurement technique. By using the inverse fast Fourier transform (IFFT) the received signal *V(f)* is transferred from the frequency domain into the time domain *V(t)* where a gating window is applied to it. The time domain signal shows a maximum around τ_0, which corresponds to the time delay needed for the wave to travel the axial distance between the acoustic source and the hydrophone probe in water (see Figure 3.7). Next, the time-adjustable gate is positioned in such a way that its center corresponds to τ_0. The width (time span) of the gating window is adjustable (between 300 and 500 ns) and allows maximization of signal-to-noise ratio. The shape of the time gate (see Figure 3.7) was selected to maintain a uniform bandwidth after the gating process. Once the gating has been applied, the time domain signal was Fast Fourier Transformed (FFT-ed) back into the frequency domain. The outcome of these operations provided the combined frequency response of the entire set-up (i.e., hydrophone, transmitter, and associated electronics) [75].

.

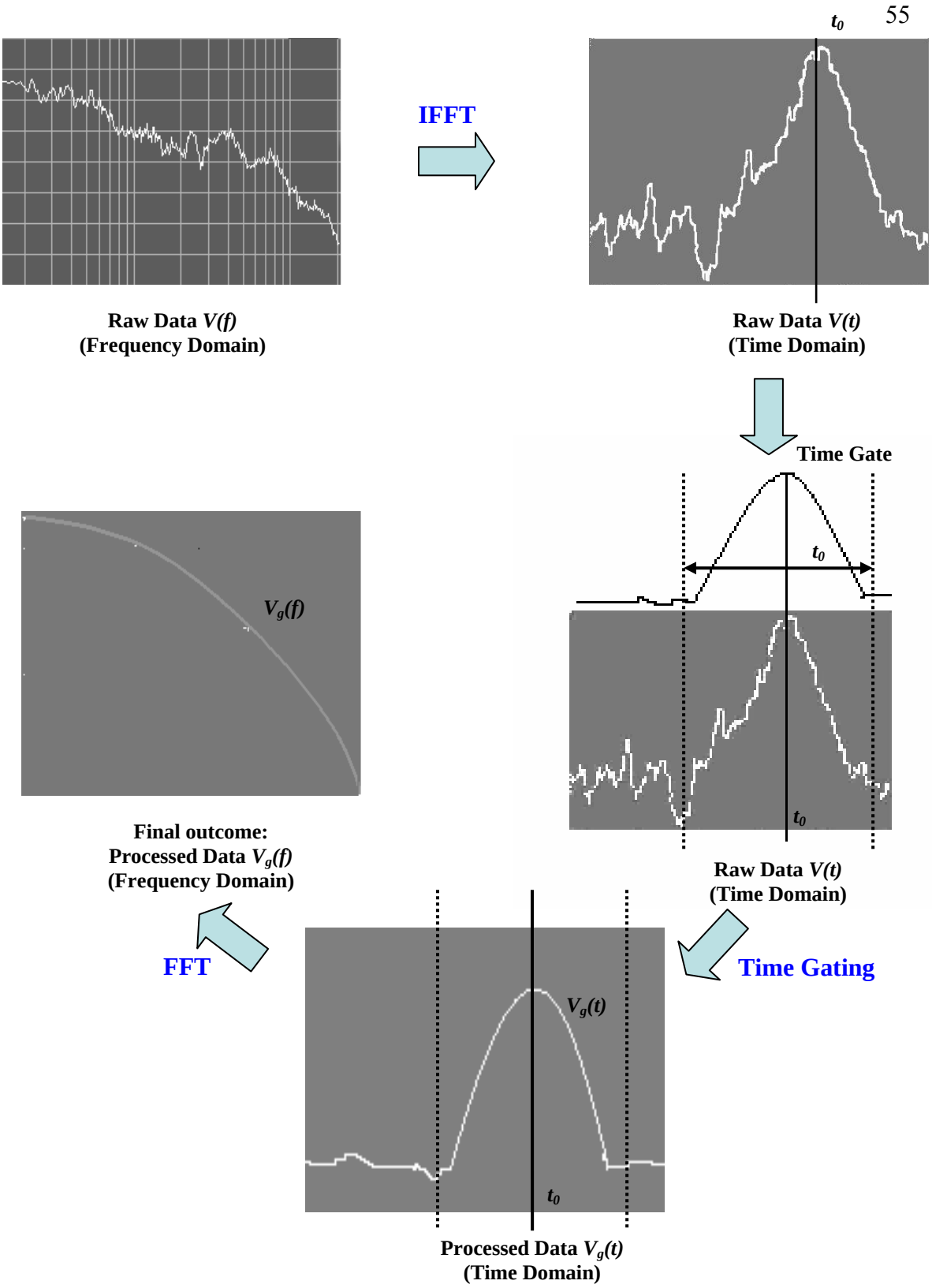

Figure 3.7: The principle of Time Gated Frequency Analysis (TGFA).

The experimental set up for Time Gated Frequency Analysis **(**TGFA) is shown in Figure 3.8. As pointed out earlier, the TGFA method provides a secondary calibration based on the substitution technique (see Figure 3.6). Similarly to TDS, the initial step was to place the reference hydrophone at the focal plane of the ultrasonic source and then store the frequency response of the received signal of the hydrophone in the memory of the network analyzer. The next step was to replace the reference hydrophone with the tested hydrophone and repeat the measurements.

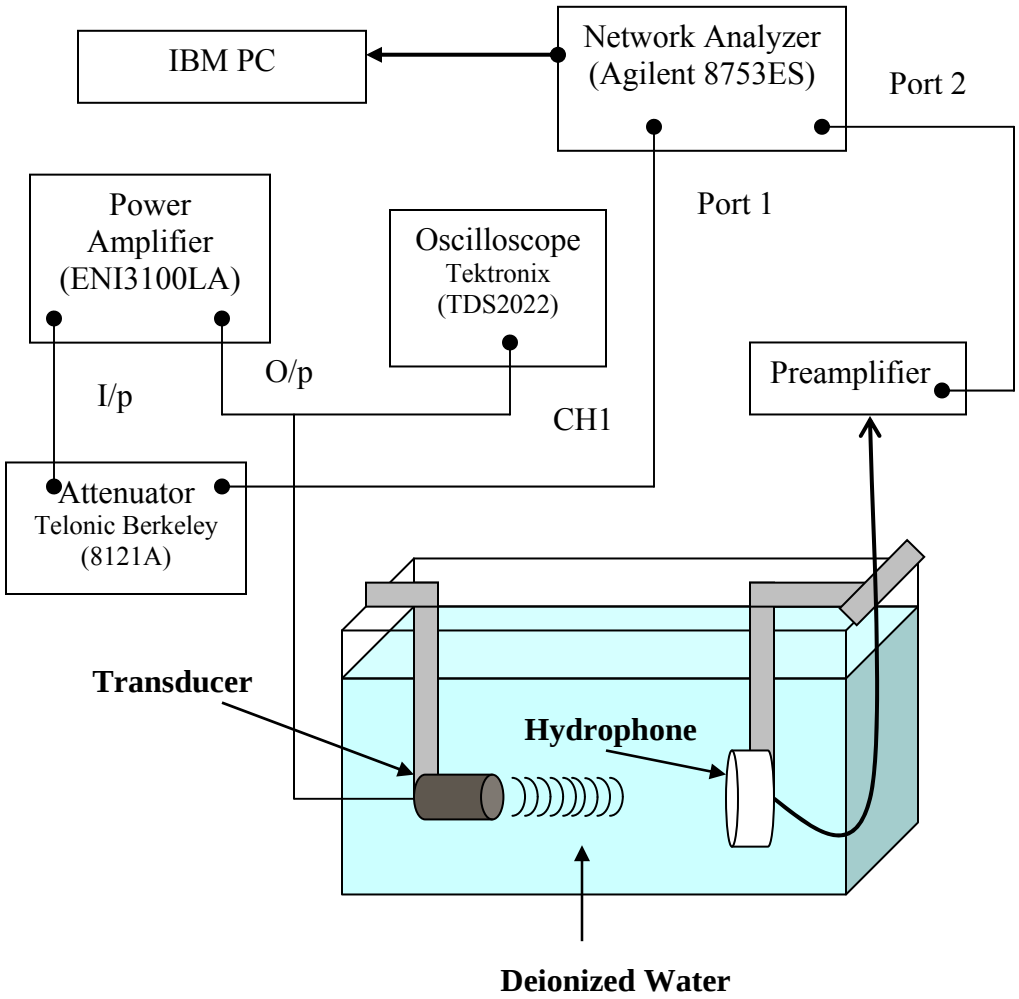

Figure 3.8: The experimental set up for Time Gated Frequency Analysis (TGFA) technique (see Table A3, Appendix 3 for the details of the equipment used).

The absolute sensitivity of the hydrophone being calibrated M was then determined by taking the product of the ratio of two frequency responses; i.e., that of the uncalibrated and the reference hydrophone multiplied by the sensitivity of the reference hydrophone M_{ref} (see Equation 3.3) [56].

The TGFA hydrophone calibration was performed using two wideband focused sources (see Table A2), one having focal number 3.84 (F# 3.84) and another one designed as focal number 2 (F# 2). Both transducers used were circular piston sources with spherical focusing. The F# 3.84 source had an active diameter of 6.6 mm, a focal length of 2.54 cm and a center frequency of about 40 MHz. These two different sources were needed to cover the 100 MHz range and verify the calibration results. The F# 3.84 transducer was used in the frequency range between 20-60 MHz whereas the F# 2 transducer was able to provide an adequate signal in the frequency range 20-100 MHz. The TGFA calibration with F# 3.84 source was limited to 60 MHz because of inadequate signal to noise (S/N) ratio. To overcome this problem, the wideband focused acoustic source operating at the center frequency of 80 MHz with F# 2 was designed by the NIH NCRR, The Resource Center for Medical Ultrasonic Transducer Technology, University of Southern California to maximize the Transmitting Voltage Response (TVR). The behavior of such a source was simulated and involved a computer simulation using PiezoCAD software [76]. The results of the simulation indicated that using either PVDF polymer or Lithium Niobate crystal as an active piezoelectric material would provide 60% fractional bandwidth and generate pressure amplitudes adequate to obtain valid data up to 100 MHz. In its final implementation, the diameter of the F# 2 source was 3 mm and it had the focal distance

of 6 mm.

Similarly to the TDS calibration procedure, the hydrophone spatial averaging correction (see section 3.1) was also applied to all hydrophones calibrated using TGFA technique.

As evidenced in Chapter 4, the combined TDS-TGFA calibration, yielded results in the frequency range of 100 MHz, however, only in the frequency range 1-60 MHz the results could be verified by comparing them with the calibration data obtained from an independent laboratory. The existing standards require calibration traceability to a national laboratory (here National Physical Laboratory (NPL), UK). However, as noted earlier the maximum calibration frequency available from NPL is 60 MHz. Therefore, the absolute sensitivity of the reference hydrophone M_{ref} between 60 MHz and 100 MHz was determined using the semi-empirical nonlinear propagation model. The calibration procedure using the model is summarized below.

3.2.3 Nonlinear hydrophone calibration

This section explains the procedure of the semi-empirical nonlinear hydrophone calibration based on the nonlinear model [61, 75] briefly described in Section 2.2.1.4. The nonlinear hydrophone calibration used during this work provided the sensitivity versus frequency response of the hydrophone probes up to 100 MHz. The calibration was initiated by performing the measurements near the surface of the 10 MHz focal number 4.21 source of circular aperture to determine the boundary conditions, which would be

used as input parameters to the nonlinear propagation model. The boundary conditions, defined in terms of the apodization function, the pressure-time waveform, the focal distance and the acoustic pressure at the surface of the source, are further discussed below. Once the boundary conditions were input, the nonlinear propagation model was used to predict the pressure-time waveforms at the focal plane of the acoustic source as seen by a point receiver. Therefore, the previously introduced spatial averaging correction model (see Section 3.1) was used to account for the effect of the finite aperture of the hydrophone probes that were calibrated. After performing the pressure-time waveform measurement in the focal plane by the hydrophone under test, both the measured pressure-time waveform and the model predicted pressure-time waveform were Fast Fourier Transformed (FFTed). The spectrum of the predicted waveform was compared with the spectrum measured by the hydrophone selected for calibration. The results of the comparison provided the hydrophone sensitivity up to 100 MHz at 10 discrete frequency points corresponding to the harmonic components of the 10 MHz pressure-time waveform. The nonlinear calibration results for several needle and membrane hydrophones are presented in Section 4.1.

Boundary conditions of the nonlinear propagation model

As already mentioned in the previous section, the first step of the nonlinear calibration procedure was to perform the measurements near the surface of the 10 MHz acoustic source (focal number 4.21). These measurements provided input data that were used in the determination of the apodization function, and later in the prediction of the pressure-time waveform. The 150 μm diameter needle hydrophone (NH1) was used to perform the

measurements in the plane that was positioned at the axial distance of 2 mm from the surface of the 10 MHz, 5 mm radius focal number 4.21 acoustic source.

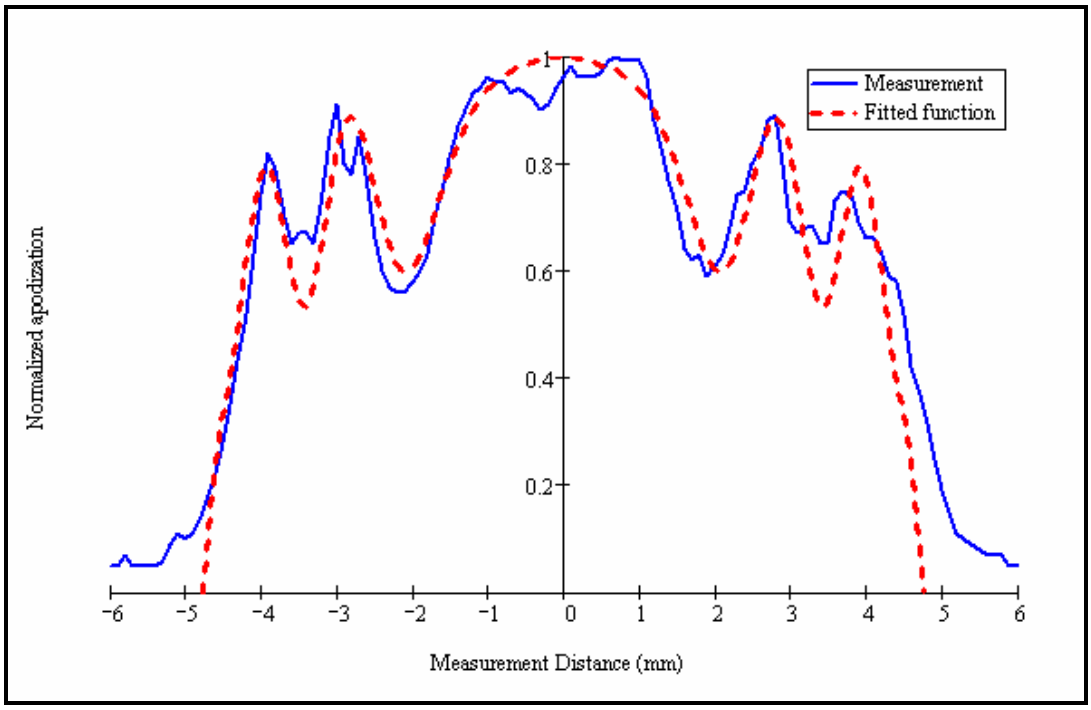

Figure 3.9: Comparison between the calculated normalized apodization function and the one obtained through the measurements performed at 2 mm axial distance from the surface of the 10 MHz focal number 4.21 acoustic source.

The apodization function used in the calibrations reported here is shown in Figure 3.9. The function was determined as a best fit into the experimental. The analytical expression for the apodization function was derived earlier [61, 75]) and is given by Equation 3.4 below:

$$A = 1 - \left(\frac{xx}{r}\right)^{px} - \left[fc\left[\cos\left(fxx\frac{xx}{r}\right)^2\right]^2 - fcf \cdot fc \right] \cdot \left[\left(\frac{xx}{r}\right)^{pxb} - \left(\frac{xx}{r}\right)^{pxa}\right] \qquad (3.4)$$

where *xx/r* is the normalized source radius and the parameters *px, fc, fxx, fcf, pxa* and *pxb* were: 11, 200, 3, 1.3, 2.0 and 2.01, respectively.

The model predicted tone burst waveform on the source's surface was experimentally verified: the 10 MHz; ten cycles normalized pressure-time waveform as measured by the 150 μm diameter needle hydrophone (NH1) is shown in Figure 3.10 along with the normalized simulated pressure-time waveform with an envelope coefficient of 25 (see Figure 2.5).

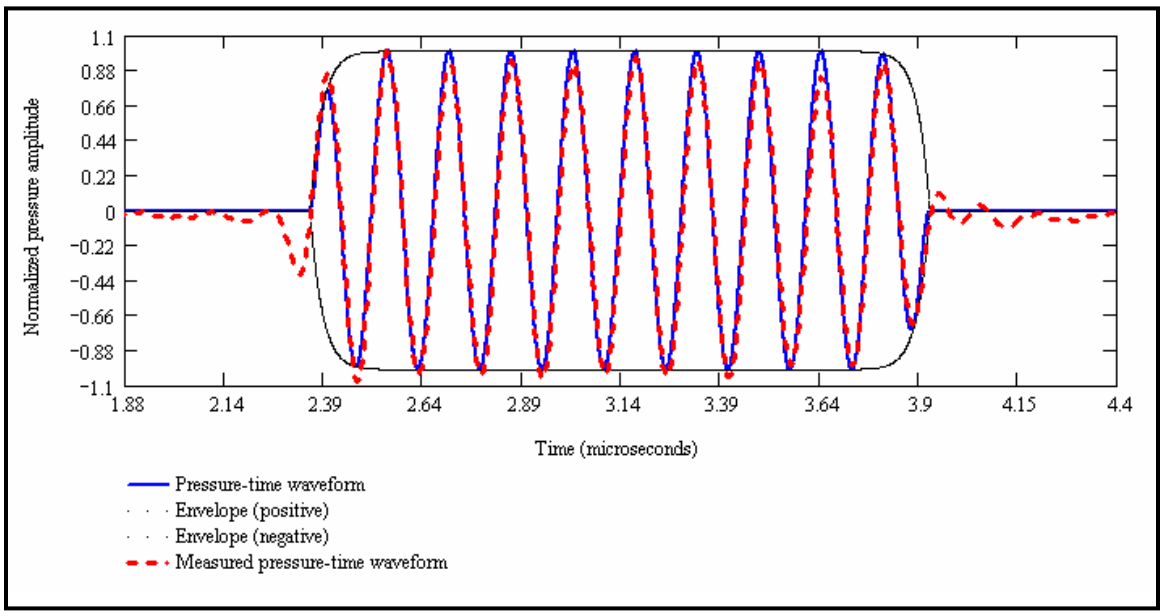

Figure 3.10: Comparison between the normalized measured pressure-time waveform and the simulated pressure-time one. The measurement was performed near the surface (2 mm) of the 10 MHz focal number 4.21 acoustic source by the 150 μm diameter needle hydrophone (NH1).

The steady-state acoustic pressure at the surface of the acoustic source was calculated using the known sensitivity of the needle hydrophone (NH1) and was found to be 270 kPa (see also Figure 4.6).

As noted earlier, once the pressure-time waveform at the focal plane of the 10 MHz acoustic source used here was simulated, the pressure-time waveform measurement was performed in the focal plane by the hydrophone under test as described below.

Nonlinear pressure-time waveform measurement

The experimental set up used for the measurement of the pressure-time waveforms at the focal plane by the hydrophone under test is shown in Figure 3.11.

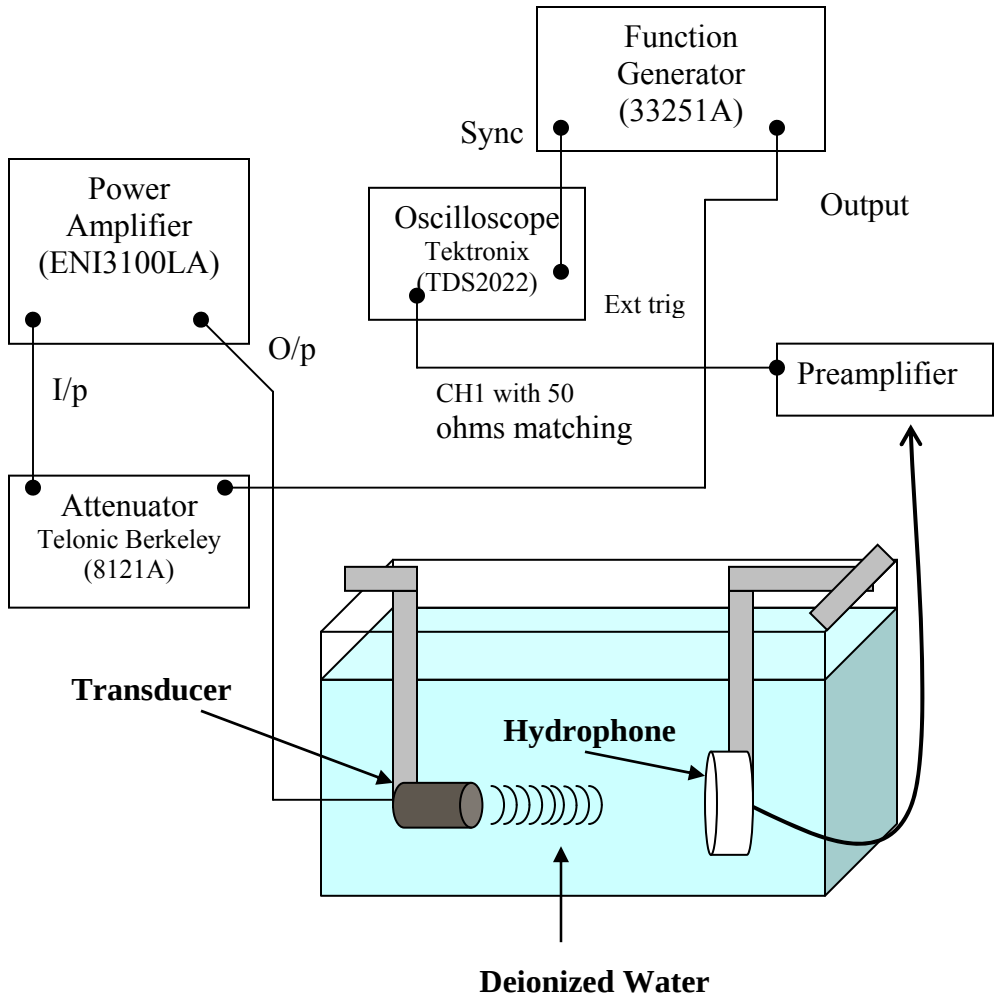

Figure 3.11: The experimental set up used to measure the nonlinear pressure-time waveforms in the focal plane of the 10 MHz focal number 4.21 acoustic source (see Table A3, Appendix 3 for the details of the equipment used).

All positioning was performed under computer control using LabVIEW 6.5 program, which also coordinated data capture by the oscilloscope (Tektronix, TDS 2022). The hydrophone under test was placed in the focal plane the 10 MHz source (see Table A2, Appendix 2). The nonlinear pressure-time waveforms were generated by applying high voltage excitation (approximately 150 V_{pp}) applied to the transducer terminals. With such excitation, the source was able to generate 10 harmonics. The voltage amplitude of about 150 V_{pp} was selected to maximize the long term stability of the source so its Transmitting Voltage Response (TVR) would remain constant. The example of the normalized pressure-time waveform measured by a membrane hydrophone (MH2, see Table A1.1 from Appendix 1) that was to be calibrated using nonlinear approach during this work is shown in Figure 3.12.

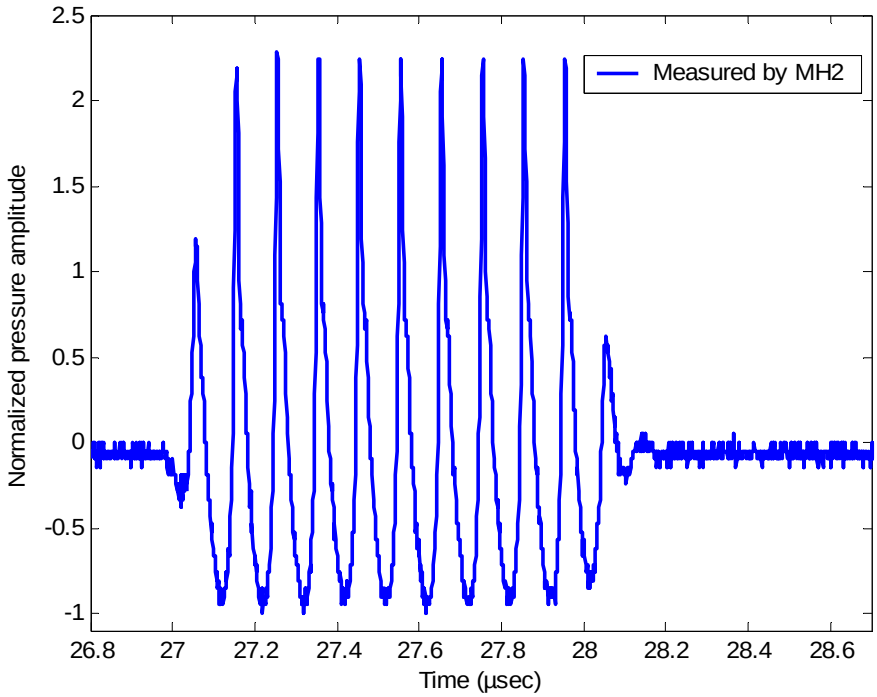

Figure 3.12: The 10 MHz fundamental frequency, 10 cycles, normalized pressure-time waveform as measured by a 400 µm diameter bilaminar membrane hydrophone (MH2).

In addition to the MH2 membrane hydrophone one additional membrane probe (MH1) and two needle probes (NH1 and NH3) were calibrated using the semi-empirical nonlinear propagation technique. The calibration results of these probes are presented in Section 4.1.

3.3 Acousto-optic measurement system

As mentioned earlier, the finite aperture of piezopolymer hydrophones introduces spatial averaging errors. To alleviate this problem, a fiber optic (FO) hydrophone was designed. The fiber optic hydrophone system was constructed using commercially available standard single mode, 10/125 μm cables which were FC/APC connectorized taking advantage of the higher return loss of the APC polish. The sensitive tip of the FO prototype used here was about 10 μm in diameter, so effectively it could be treated as a point receiver up to about 75 MHz. The improved prototype being developed will extend the point receiver behavior up to 100 MHz by reducing the diameter to about 7 μm (as already noted, the active diameter should be smaller than half wavelength to avoid the spatial averaging errors). An experimental set up of the acousto-optic measurement system is shown in Figure 3.13. The specific components of the set-up are briefly described below.

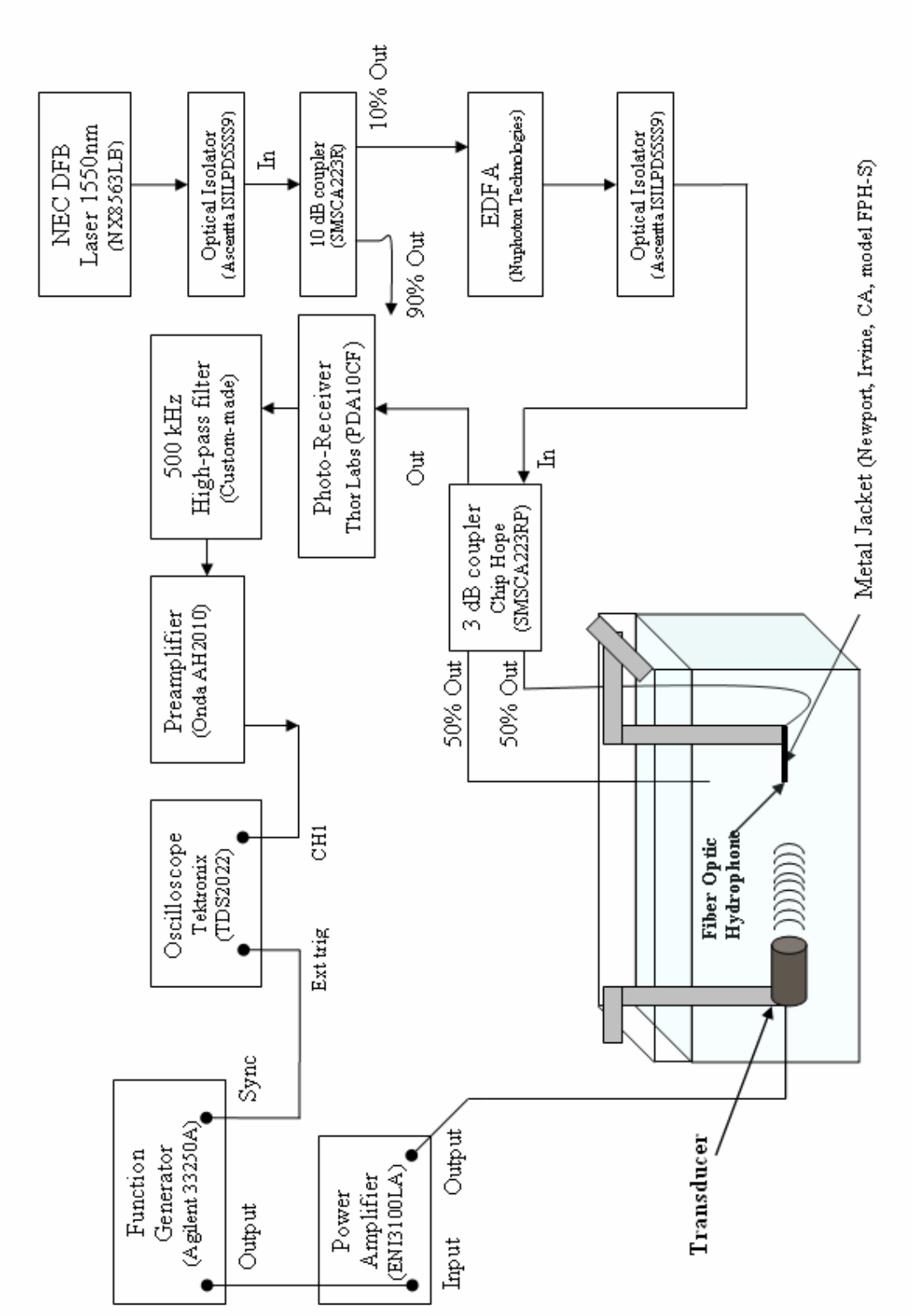

Figure 3.13: The experimental set up of the acousto-optic measurement system (see Table A3, Appendix 3 for the details of the equipment used).

Optical Source and EDFA

As optical source, the 1550 nm distributed feedback (DFB) Laser (NEC Electronics Inc., Japan) producing a minimum output power of 10 mW was used. The laser was "pigtailed" with a polarization maintaining fiber which ensured direct coupling of light and eliminated the need for collimation lenses and other optical instrumentation. The laser was connected to the optical isolator (Ascentta, Somerset, NJ, model ISILPD55SS9) and then coupled to a 10 dB optical coupler (Chip Hope Technology, Lemoyne, PA, model SMSCA223R) and an optical coupler (Ascentta, Somerset, NJ, model ISILPD55SS9). This configuration provided -12 dBm power at the input of the Erbium doped fiber amplifier, EDFA (Nuphoton Technologies, Inc., Murrieta, CA). The EDFA was a RS 232 controlled device with an optical gain block of 40 dB capable of providing up to 30 dBm of optical output power.

Optical sensor

The EDFA output was connected to the optical isolator to ensure unilateral transmission of light. The signal was then divided equally using a 3 dB 2x2 coupler (Chip Hope Technology, Lemoyne, PA, model SMSCA223RP). One of the output leads was immersed in water whereas the other lead acted as the hydrophone probe and was controlled by a precision scanning system (Parker Hannifin Corporation, Compumotor Division, Rohnert Park, CA) that provided precise six-axis positioning. The precision of each axis was repeatable to within 0.1 μm. The fiber optic sensor was inserted through the barrel of a fiber optic metal jacket (Newport, Irvine, CA, model FPH-S) with approximately 1 mm of bare glass protruding beyond the metal jacket to minimize the

ringing effect of the tip. Once the fiber had been inserted into the metal jacket, the jacket was mounted in the calibration tank and the FO hydrophone system was activated by turning on the laser source.

Acoustic source

The acoustic source used was designed as a one element transducer by Sonic Concepts (Woodenville, WA) and allowed operation at two center frequencies, 1.52 MHz and 5 MHz, (see Table A2 of Appendix 2). The bandwidth of the fundamental and 3rd harmonic frequency ranged from 1.41-1.98 MHz and 5-5.7 MHz, respectively. The transducer had an active diameter of 20 mm and a focal length of 38 mm, corresponding to F number of 1.9. It required an impedance matching network and was activated by an (50Ω) ENI power amplifier (ENI3100LA) with a maximum power level of 100 W.

Optical Receiver

The optical receiver used in the measurements was a wide band Indium Gallium Arsenide (InGaAs) detector (Thor Labs, Newton, NJ, model PDA10CF). It had a responsivity of 0.95 A/W at 1500nm with a signal bandwidth of 150 MHz for a trans-impedance gain of 5 kΩ. The noise equivalent power was specified by the manufacturer as 1.2×10^{-11} W/(Hz)$^{1/2}$.

High pass filter, preamplifier and oscilloscope

As already noted light launched into the first input lead from the laser diode module was passed through the optical isolator and then was attenuated by approximately 10dB using a 10 dB optical coupler. The 10% power output of this coupler was fed to EDFA

to boost the signal up to 30 dBm. The output from EDFA was connected to the optical isolator and then split equally using a 3 dB coupler. The output was then directed to both the test lead and the second output lead. The test lead was placed in the acoustic field, and its refractive index at the fiber end face changed according to the pressure exerted by the acoustic source (HIFU transducer, focal number 1.9). This caused the light signals to be directed back through the coupler (again being attenuated by about 3 dB) to each of the two input leads. The photo-receiver (Thor Labs, Newton, NJ, model PDA10CF) was used to convert the light signals to the electrical voltage. The voltage signals representing the acoustic pressure-time waveform were filtered by the custom-made 500 kHz high-pass filter, amplified using a 20 dB voltage preamplifier (Onda Corp., Sunnyvale, CA, model AH-2010) and displayed on an oscilloscope (Tektronix, model TDS 2022).

Sensitivity of the fiber optic hydrophone probe

The sensitivity of the fiber optic hydrophone probe (S) was determined using substitution technique. Briefly, a previously calibrated PVDF needle hydrophone probe (NH5, Table A1.1 from Appendix 1) was used to acquire the pressure-time waveform and determine steady state peak-peak pressure amplitude (p). The needle hydrophone was then replaced by a fiber optic (FO) hydrophone probe and the voltage signal (V_o) produced by the fiber optic hydrophone probe was maximized and recorded. The fiber optic hydrophone's sensitivity was calculated as:

$$S = V_o / p . \tag{3.5}$$

In the next chapter, (Chapter 4) the results of the piezoelectric and fiber optic hydrophone measurements are presented.

CHAPTER 4: Results

This chapter presents the results of the measurements carried out using the experimental setup and methodology outlined in Chapter 3. The chapter is divided into two sections: the first section (4.1) describes the acoustic measurement results obtained by piezoelectric hydrophone probes using three different calibration techniques (TDS, TGFA and nonlinear). The second section includes the results of the acousto-optic measurement obtained from fiber optic hydrophone probe using the 1.52 MHz High Intensity Focused Ultrasound (HIFU) acoustic source (see Table A2, Appendix 2) described in Section 4.2.

All calibration measurements were performed in a tank having dimensions 1 m x 1 m x 60 cm containing deionized water at 22 deg C. A 400 μm diameter bilaminar PVDF membrane hydrophone (Precision Acoustics, UK) calibrated by National Physical Laboratory (NPL), UK up to 60 MHz was used as a primary reference. Also, two in-house calibrated hydrophone probes, a 400 μm diameter bilaminar membrane hydrophone manufactured by Sonora Medical Systems, Inc (Longmont, CO, USA) and a 500 μm diameter bilaminar membrane hydrophone manufactured by GEC-Marconi Research Center, Chelmsford, UK, were used as auxiliary references.

In addition, almost all of the hydrophone probes (see Table A1.1, Appendix 1) tested during this work used preamplifiers that had electrical output impedance of 50 Ohms. Two membrane hydrophones (MH5, MH6) and one needle hydrophone (NH2) were not

equipped with preamplifiers and were calibrated using TDS method up to 40 MHz with 1 Mega-Ohm in parallel with 30 pF as an input impedance. All other hydrophones were connected to a 20 dB gain, 100 MHz bandwidth high input impedance (1 Mega-Ohms || 7 pF) preamplifier with 50 Ohms output impedance and were calibrated using the TDS, TGFA and nonlinear approach.

4.1 Acoustic measurements: piezoelectric hydrophone probes

The calibration results shown in Figures 4.1 and 4.2 were obtained by using the Time Delay Spectrometry (TDS) technique [45]. As noted in Section 3.2, the spatial averaging algorithm was experimentally validated by performing calibration by substitution using three wideband focused sources. Briefly, this calibration was carried out by comparing the output of the unknown hydrophone to the one of the previously calibrated hydrophone probe [45]. The focused sources had focal numbers equal to 3.84, 10.16 and 19.24 (see Table A2 of Appendix 2). A 500 μm diameter bilaminar membrane hydrophone (MH6) was used as a reference and two hydrophones with nominal diameters of 150 and 1200 μm were calibrated (NH2 and MH5, see Table A1.1 from Appendix 1). The results of the calibrations without applying spatial averaging correction are plotted in Figure 4.1 for the 150 μm diameter needle hydrophone probe (NH2) and Figure 4.2 for the 1200 μm diameter membrane hydrophone probe (MH5).

The plots shown in Figures 4.1 and 4.2 were obtained in the frequency range up to 40 MHz. However, the maximum frequency of the focal number 10.16 source was limited to

32 MHz because this transducer source could not provide an adequate signal to noise ratio (20 dB) beyond this frequency.

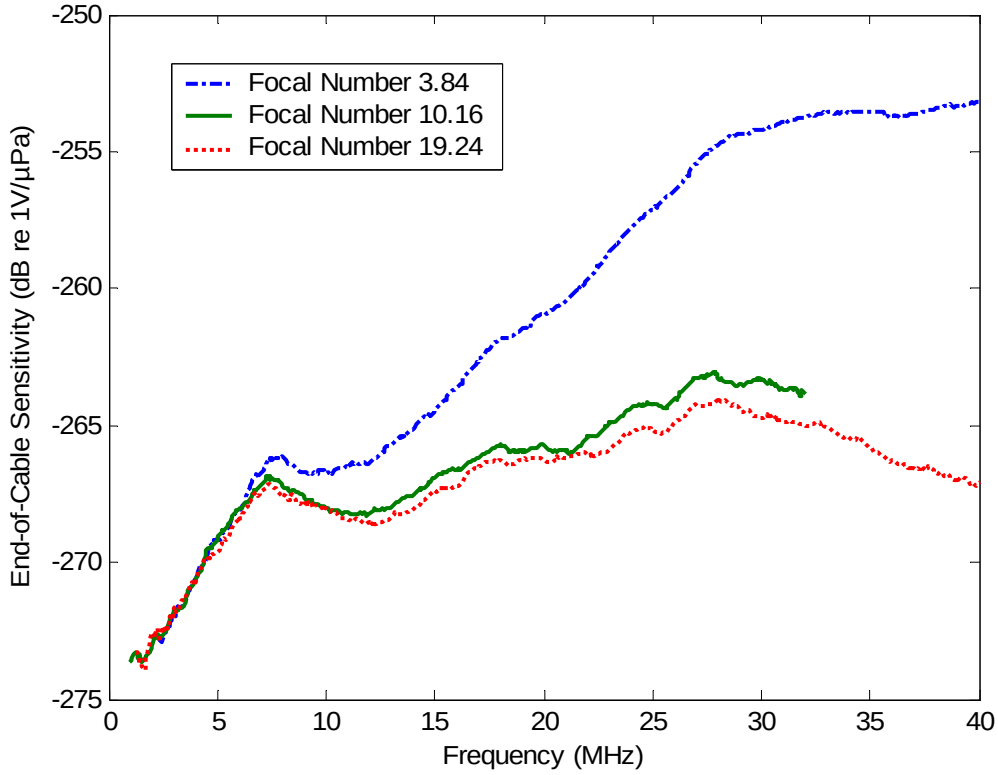

Figure 4.1: End-of-cable sensitivity of a 150 µm diameter needle hydrophone probe (NH2) without the spatial averaging correction obtained using the TDS technique. The probe was calibrated by substitution in the focal planes of different focal number acoustic sources. A 500 µm diameter bilaminar membrane hydrophone (MH6) was used as a reference hydrophone.

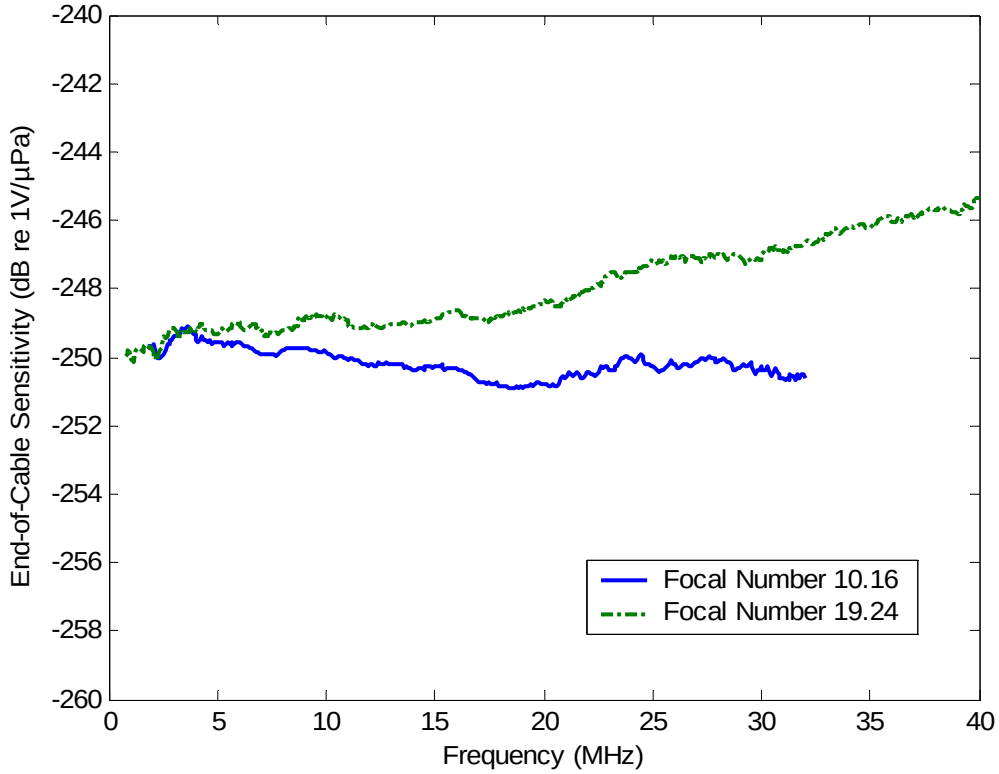

Figure 4.2: End-of-cable sensitivity of a 1200 µm diameter membrane hydrophone probe (MH5) without the spatial averaging correction obtained using the TDS technique. The probe was calibrated by substitution in the focal planes of different focal number acoustic sources. A 500 µm diameter bilaminar membrane hydrophone (MH6) was used as a reference hydrophone.

In order to obtain the true end of cable sensitivities of these two hydrophones (NH2 and MH5), the correction factors shown in Figures 3.3 and 3.4 were added to the uncorrected calibration data presented in Figures 4.1 and 4.2. Figures 4.3 and 4.4 depict the final calibration results of these two hydrophone probes (NH2 and MH5) after applying spatial averaging correction.

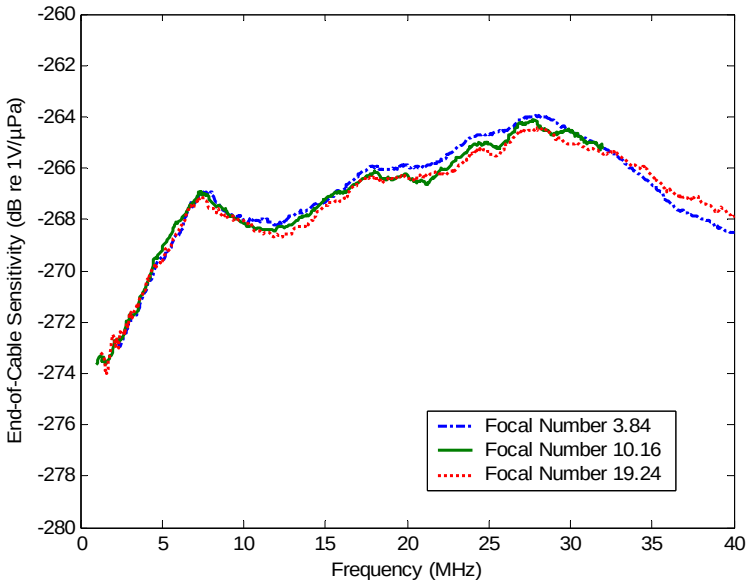

Figure 4.3: End-of-cable sensitivity of a 150 µm diameter needle hydrophone probe (NH2) with the spatial averaging correction obtained using the TDS technique. The probe was calibrated by substitution in the focal planes of different focal number acoustic sources. A 500 µm diameter bilaminar membrane hydrophone (MH6) was used as a reference hydrophone.

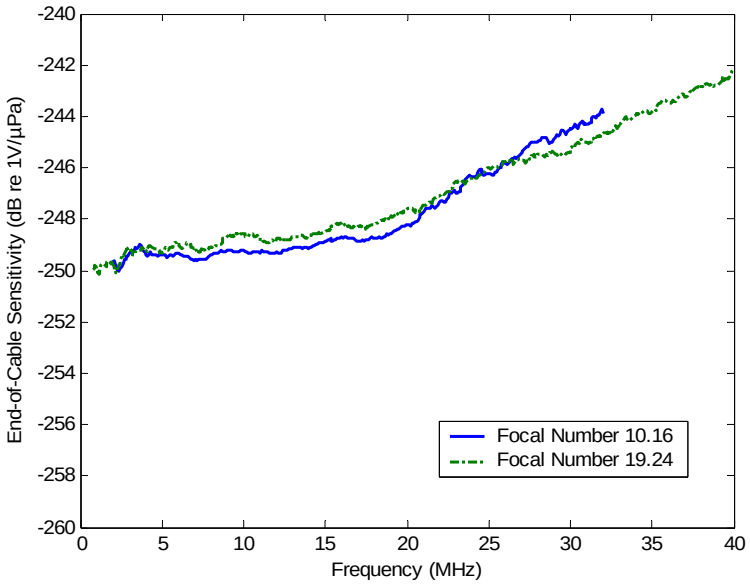

Figure 4.4: End-of-cable sensitivity of a 1200 µm diameter membrane hydrophone probe (MH5) with the spatial averaging correction obtained using the TDS technique. The probe was calibrated by substitution in the focal planes of different focal number acoustic sources. A 500 µm diameter bilaminar membrane hydrophone (MH6) was used as a reference hydrophone.

In Figures 4.5-4.11, the calibration results of ten, both membrane and needle hydrophone probes are shown. These results were also obtained by using Time Delay Spectrometry (TDS) technique and represent the end-of-cable sensitivity in the frequency range up to 40 MHz after applying the spatial averaging correction. The plots in Figures 4.5-4.11 were obtained using a focal number 19.24 source and the MH6 (500 µm diameter bilaminar membrane) hydrophone that served as a reference hydrophone.

The corrected sensitivity against frequency plots for 4 membrane hydrophones (MH1, MH2, MH3 and MH4) are shown in Figure 4.5.

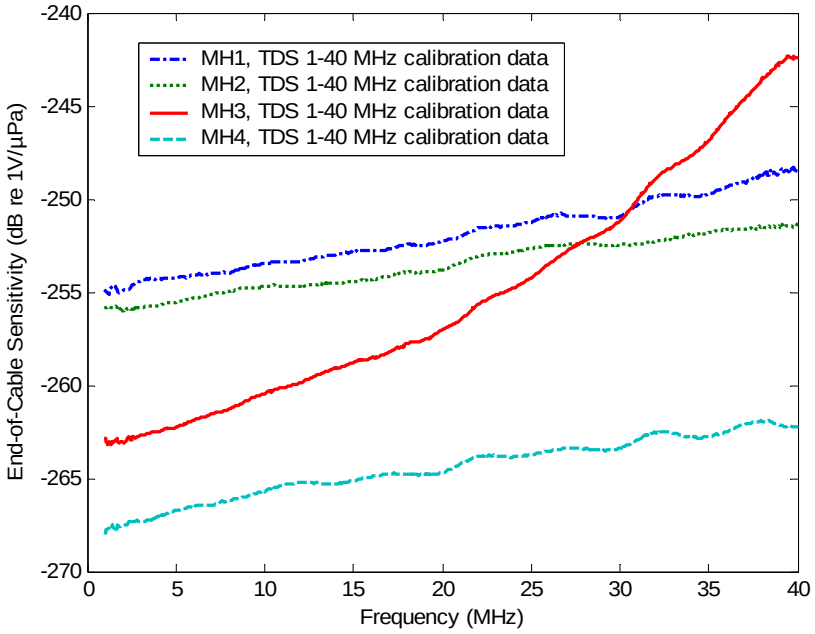

Figure 4.5: End-of-cable sensitivity of a 400 µm diameter membrane hydrophone probe (MH1), 400 µm diameter membrane hydrophone probe (MH2), 400 µm diameter membrane hydrophone probe (MH3), and 500 µm diameter membrane hydrophone probe (MH4) with the spatial averaging correction obtained using the TDS technique. These were calibrated by substitution in the focal plane of a focal number 19.24 acoustic source. A 500 µm diameter bilaminar membrane hydrophone probe (MH6) was used as a reference hydrophone. Overall uncertainty: 1-40 MHz: ±1 dB.

In contrast to membrane hydrophones that exhibited fairly uniform frequency response (positive slope between 0.15 and 0.5 dB/MHz), the needle hydrophone probes' responses showed large variation in sensitivity (about 40 dB/MHz between 1 and 1.5 MHz as evidenced in Figure 4.9). Therefore, the needle hydrophone probes' characteristics are presented separately in Figures 4.6-4.11 and are further discussed in Chapter 5.

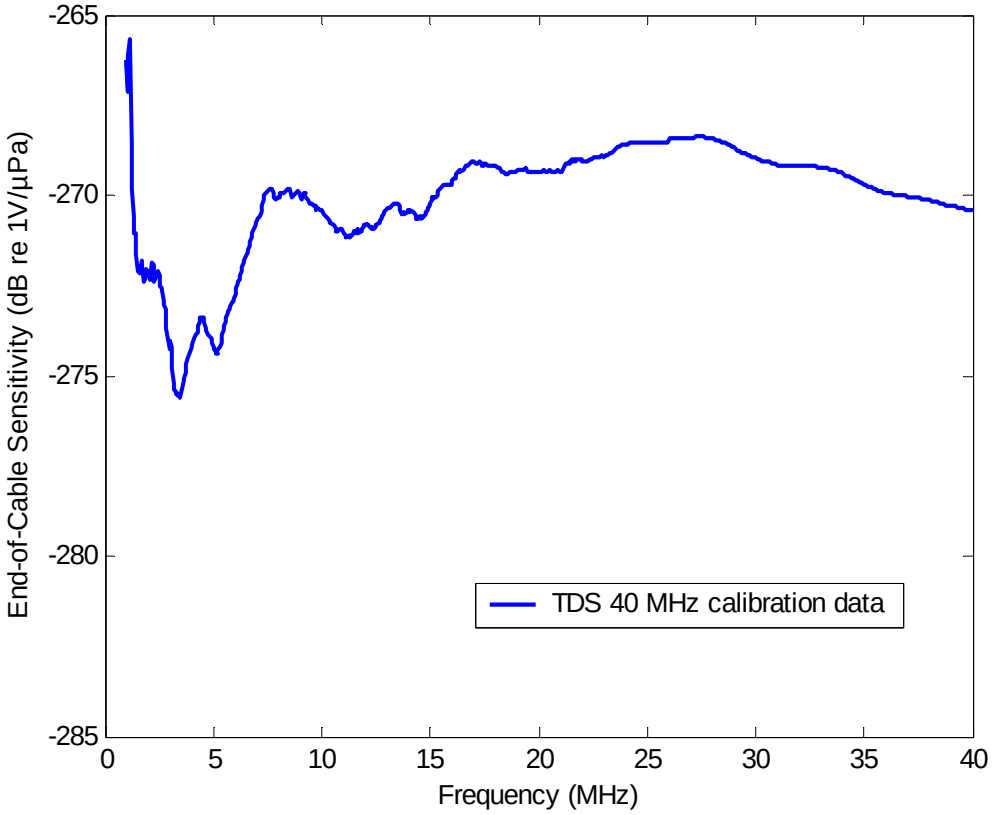

Figure 4.6: End-of-cable sensitivity of a 150 µm diameter needle hydrophone probe (NH1) with the spatial averaging correction obtained using the TDS technique. The probe was calibrated by substitution in the focal plane of a focal number 19.24 acoustic source. A 500 µm diameter bilaminar membrane hydrophone probe (MH6) was used as a reference hydrophone. Overall uncertainty: 1-40 MHz: ±1 dB.

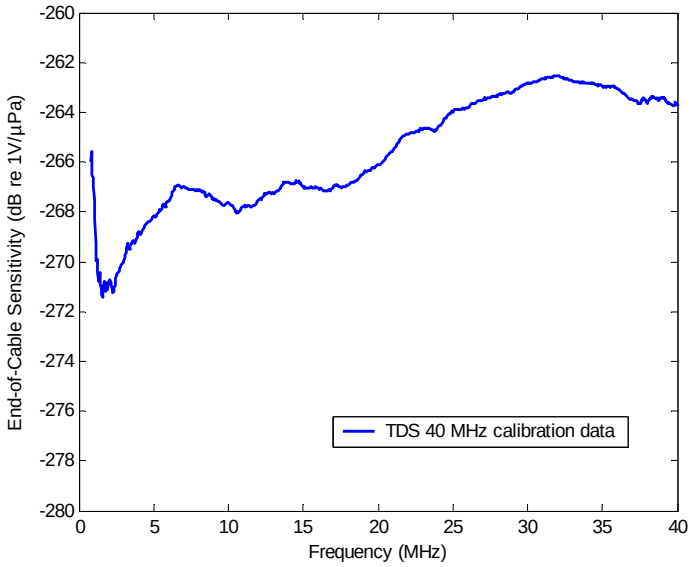

Figure 4.7: End-of-cable sensitivity of a 150 µm diameter needle hydrophone probe (NH3) with the spatial averaging correction obtained using the TDS technique. The probe was calibrated by substitution in the focal plane of a focal number 19.24 acoustic source. A 500 µm diameter bilaminar membrane hydrophone (MH6) was used as a reference hydrophone. Overall uncertainty: 1-40 MHz: ±1 dB.

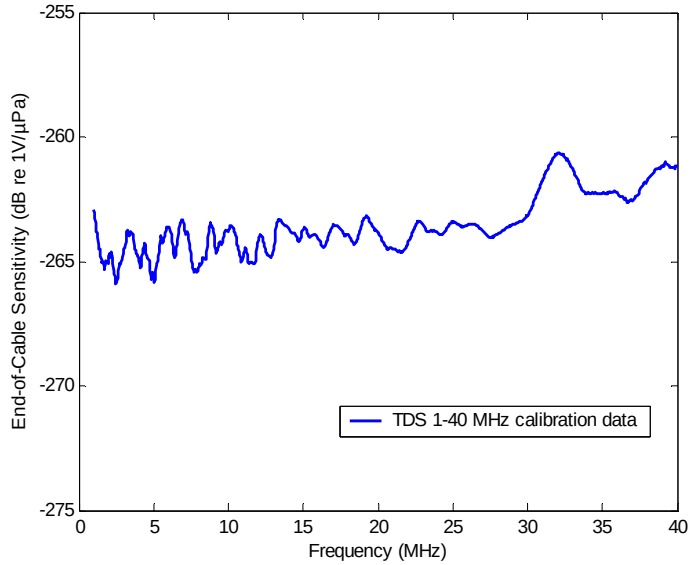

Figure 4.8: End-of-cable sensitivity of a 120 µm diameter needle hydrophone probe (NH4) with the spatial averaging correction obtained using the TDS technique. The probe was calibrated by substitution in the focal plane of a focal number 19.24 acoustic source. A 500 µm diameter bilaminar membrane hydrophone (MH6) was used as a reference hydrophone. Overall uncertainty: 1-40 MHz: ±1 dB.

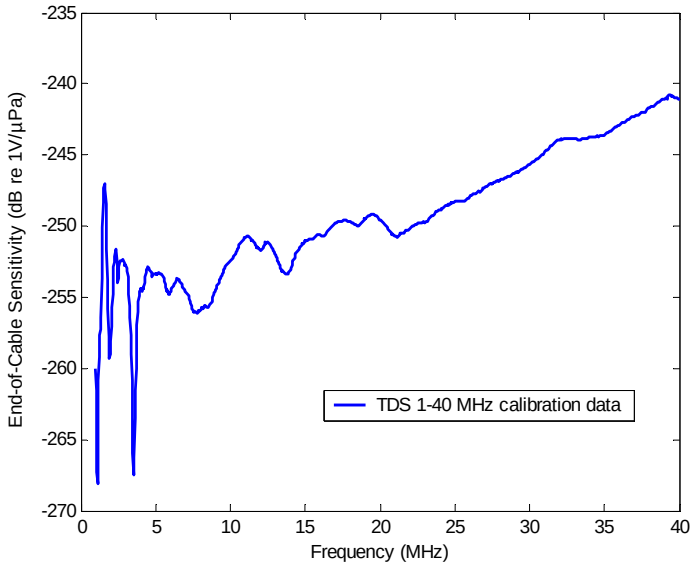

Figure 4.9: End-of-cable sensitivity of a 500 µm diameter needle hydrophone probe (NH5) with the spatial averaging correction obtained using the TDS technique. The probe was calibrated by substitution in the focal plane of a focal number 19.24 acoustic source. A 500 µm diameter bilaminar membrane hydrophone (MH6) was used as a reference hydrophone. Overall uncertainty: 1-40 MHz: ±1 dB.

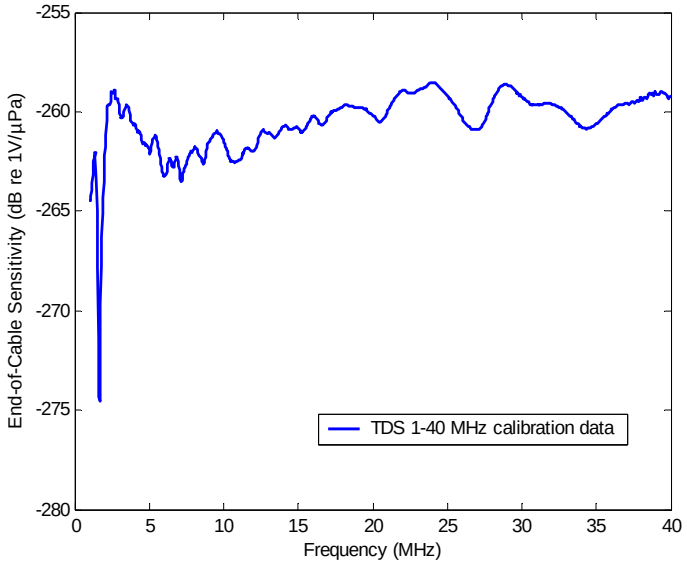

Figure 4.10: End-of-cable sensitivity of a 120 µm diameter needle hydrophone probe (NH6) with the spatial averaging correction obtained using the TDS technique. The probe was calibrated by substitution in the focal plane of a focal number 19.24 acoustic source. A 500 µm diameter bilaminar membrane hydrophone (MH6) was used as a reference hydrophone. Overall uncertainty: 1-40 MHz: ±1 dB.

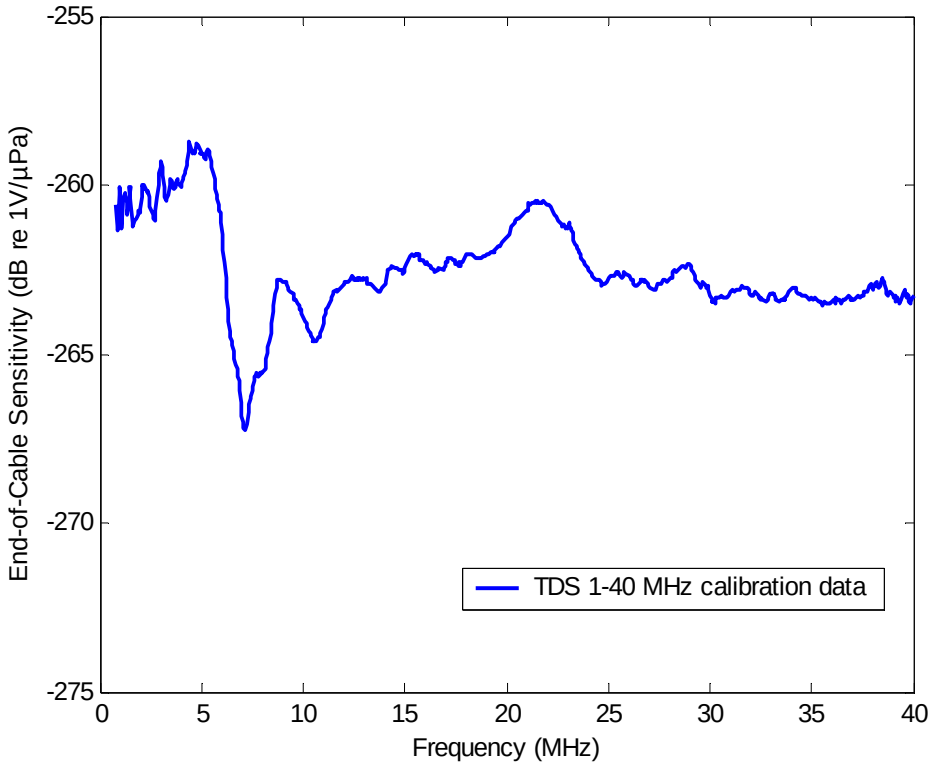

Figure 4.11: End-of-cable sensitivity of a 130 µm diameter needle hydrophone probe (NH7) with the spatial averaging correction obtained using the TDS technique. The probe was calibrated by substitution in the focal plane of a focal number 19.24 acoustic source. A 500 µm diameter bilaminar membrane hydrophone (MH6) was used as a reference hydrophone. Overall uncertainty: 1-40 MHz: ±1 dB.

All plots presented in Figures 4.1-4.11 were obtained using TDS technique. Beyond 40 MHz, the Time-Gated Frequency Analysis (TGFA) technique (see Fig. 3.7) was used and the results are presented in Figure 4.12-4.23. Six of the probes measured were needle hydrophones and four were membrane hydrophones (see Tables A1.1 and A1.2). The sensitivity data were obtained for eight hydrophone probes (five needle and three membrane hydrophones) in the frequency range 20-60 MHz using the acoustic source with the focal number 3.84 (see Table A2 of Appendix 2). In addition, the focal number 2 source was also used to calibrate four hydrophone probes (one needle and three membrane hydrophones) in the frequency range 20-100 MHz. As already noted, beyond

60 MHz the absolute sensitivity of the reference hydrophone (M_{ref}) was determined using the nonlinear technique. In order to assure continuous calibration data from 1-100 MHz, all of the hydrophone probes were also calibrated using the focal number 19.25 source and the TDS technique from 1-40 MHz. In this way, the frequency responses obtained using TDS and TGFA overlapped in the frequency range 20-40 MHz.

Spatial averaging corrections were required for all calibrations performed with the TGFA technique since the beamwidth in the focal plane of the focal numbers 2 and 3.84 sources was smaller than the effective diameter of the PVDF hydrophone probes (see Table A1.1). For convenience and in order to shorten the calibration time, the correction factors were extrapolated from the linear fit of the corrections determined in the 20-40 MHz range.

Figures 4.12-4.14 show the calibration results up to 55 MHz obtained with the TGFA technique using a focal number 3.84 acoustic source whereas Figures 4.15-4.19 represent the calibration results up to 60 MHz using the same technique and acoustic source. The hydrophones (MH2, MH3 and MH4, see Tables A1.1) in Figures 4.12-4.14 were calibrated only up to 55 MHz as they were unable to maintain adequate (20 dB) signal-to-noise ratio (S/N) beyond this frequency. In Figures 4.20-4.23, the TGFA calibration results up to 100 MHz obtained using a focal number 2 acoustic source are presented. All TGFA calibrations were performed using a 400 μm diameter bilaminar membrane hydrophone (MH2), traceable to the NPL, UK as a reference with the exception of the

data plotted in Figs 4.12 and 4.22. There, MH3, in house calibrated hydrophone was used as a reference.

Figures 4.12-4.14 show the end-of-cable sensitivity of a 400 μm bilaminar membrane hydrophone (MH2) calibrated by an independent laboratory (NPL, UK), a 400 μm bilaminar membrane hydrophone (MH3) and a 500 μm bilaminar membrane hydrophone (MH4), respectively. To verify the calibration results, these hydrophones were also calibrated using the TDS technique up to 40 MHz and up to 55 MHz using the TGFA technique with a focal number 3.84 source.

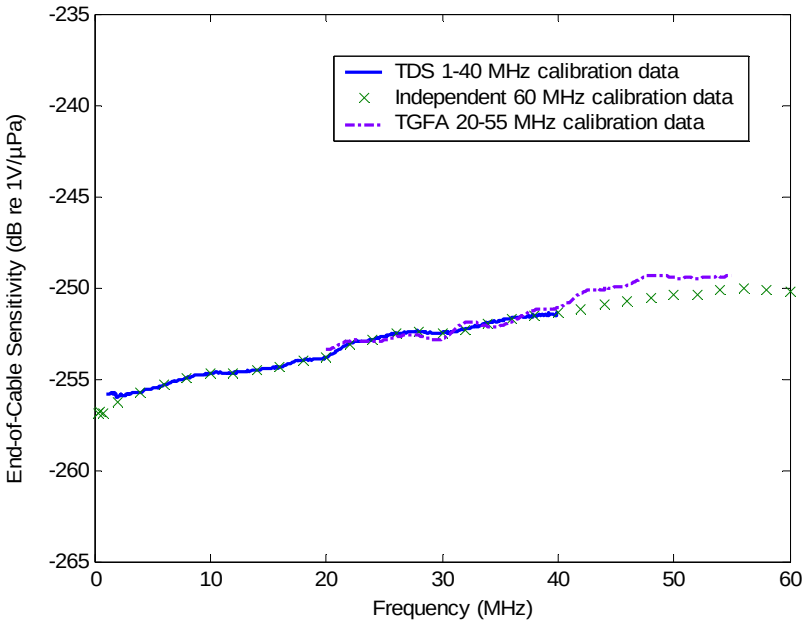

Figure 4.12: End-of-cable sensitivity of a 400 μm diameter bilaminar membrane hydrophone probe (MH2) calibrated up to 40 MHz using the TDS technique and up to 55 MHz using the TGFA technique with a focal number 3.84 acoustic source. A 400 μm diameter bilaminar membrane hydrophone (MH3) was used as a reference hydrophone. Overall uncertainty: 1-40 MHz: ±1 dB, 40-55 MHz: ±1.5 dB.

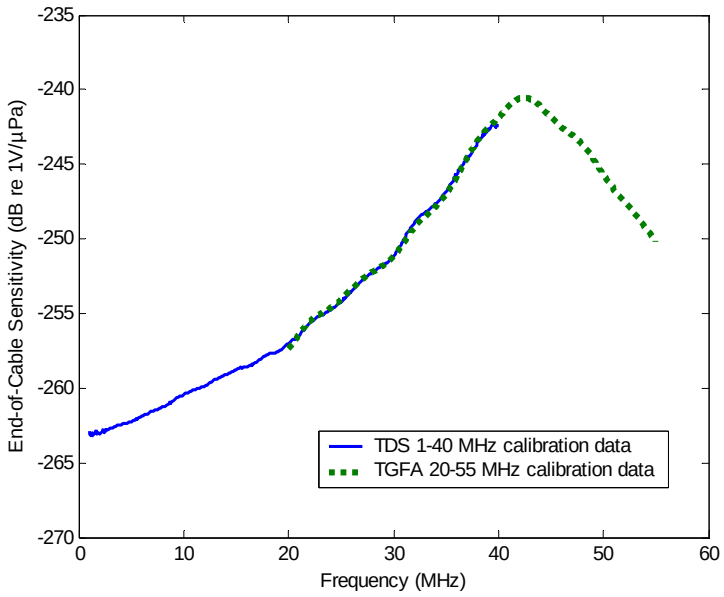

Figure 4.13: End-of-cable sensitivity of a 400 µm diameter bilaminar membrane hydrophone probe (MH3) calibrated up to 40 MHz using the TDS technique and up to 55 MHz using the TGFA technique with a focal number 3.84 acoustic source. A 400 µm diameter bilaminar membrane hydrophone (MH2) was used as a reference hydrophone. Overall uncertainty: 1-40 MHz: ±1 dB, 40-55 MHz: ±1.5 dB.

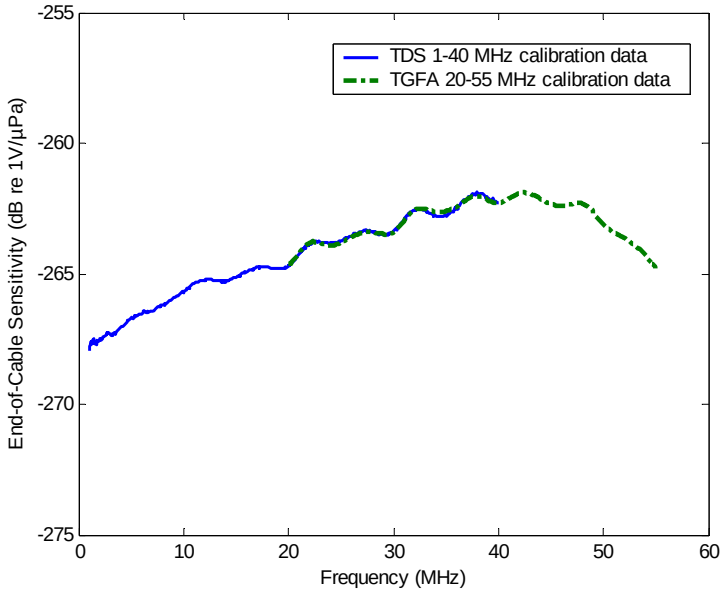

Figure 4.14: End-of-cable sensitivity of a 500 µm diameter bilaminar membrane hydrophone probe (MH4) calibrated up to 40 MHz using the TDS technique and up to 55 MHz using the TGFA technique with a focal number 3.84 acoustic source. A 400 µm diameter bilaminar membrane hydrophone (MH2) was used as a reference hydrophone. Overall uncertainty: 1-40 MHz: ±1 dB, 40-55 MHz: ±1.5 dB.

In Figures 4.15-4.19, frequency responses of needle hydrophones are presented. Figure 4.15 illustrates the end-of-cable sensitivity of a 150 µm diameter needle hydrophone (NH3). Figure 4.16 presents the end-of-cable sensitivity of a 120 µm diameter needle hydrophone (NH4). Figure 4.17 shows the end-of-cable sensitivity of a 500 µm diameter needle hydrophone (NH5). Figure 4.18 shows the end-of-cable sensitivity of yet another 120 µm diameter needle hydrophone (NH6). Finally, Figure 4.19 illustrates the end-of-cable sensitivity of a 130 µm diameter needle hydrophone (NH7). Like previously, the frequency responses shown in Figures 4.15-4.19 were calibrated up to 40 MHz using the TDS technique and up to 60 MHz using the TGFA technique with a focal number 3.84 acoustic source.

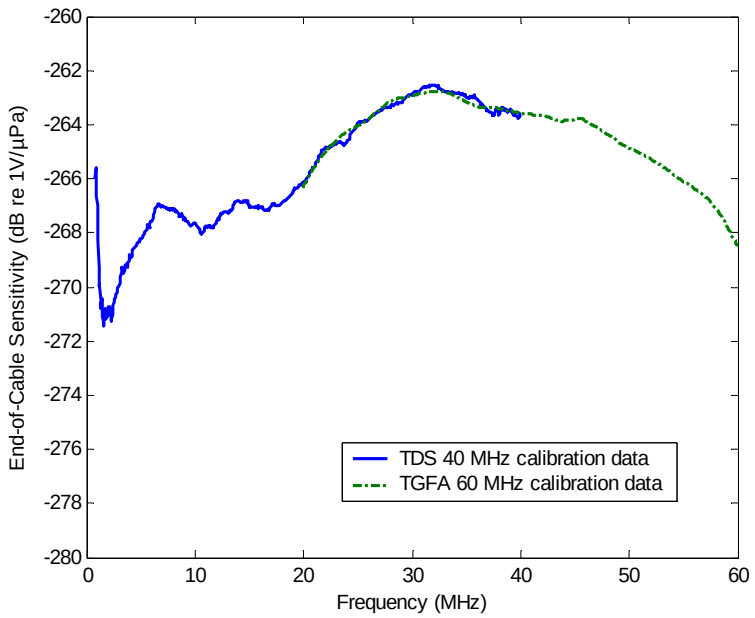

Figure 4.15: End-of-cable sensitivity of a 150 µm diameter needle hydrophone probe (NH3) calibrated up to 40 MHz using the TDS technique and up to 60 MHz using the TGFA technique with a focal number 3.84 acoustic source. A 400 µm diameter bilaminar membrane hydrophone (MH2) was used as a reference hydrophone. Overall uncertainty: 1-40 MHz: ±1 dB, 40-60 MHz: ±1.5 dB.

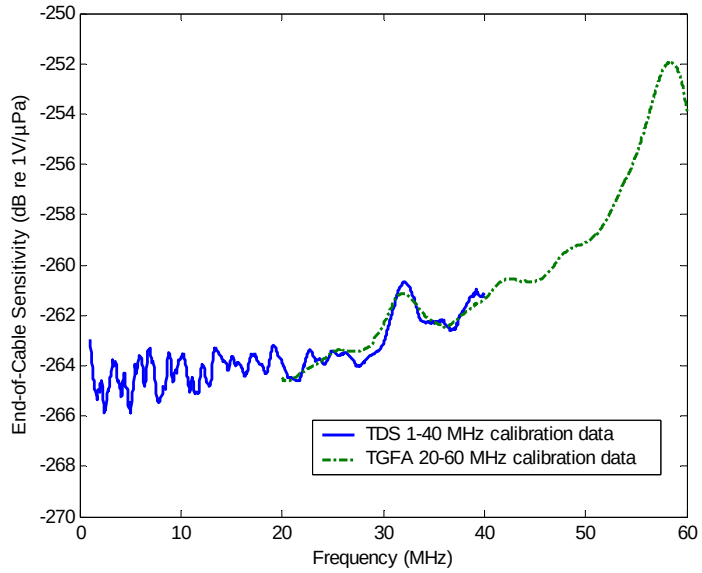

Figure 4.16: End-of-cable sensitivity of a 120 µm diameter needle hydrophone probe (NH4) calibrated up to 40 MHz using the TDS technique and up to 60 MHz using the TGFA technique with a focal number 3.84 acoustic source. A 400 µm diameter bilaminar membrane hydrophone (MH2) was used as a reference hydrophone. Overall uncertainty: 1-40 MHz: ±1 dB, 40-60 MHz: ±1.5 dB.

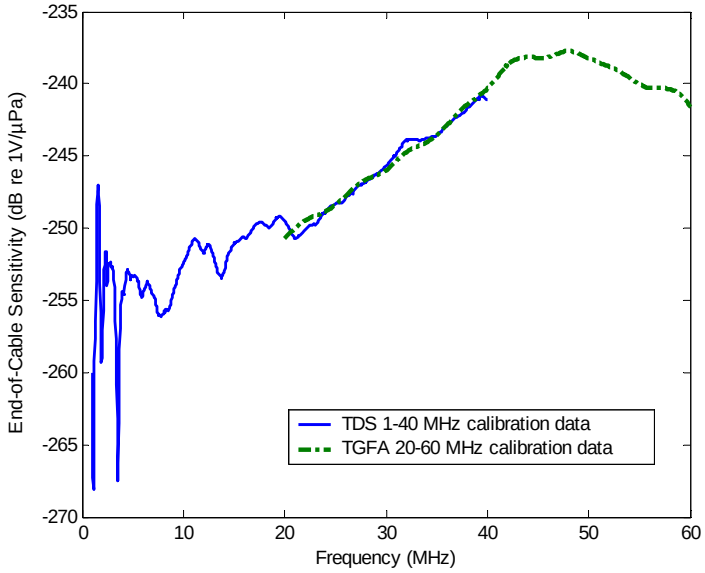

Figure 4.17: End-of-cable sensitivity of a 500 µm diameter needle hydrophone probe (NH5) calibrated up to 40 MHz using the TDS technique and up to 60 MHz using the TGFA technique with a focal number 3.84 acoustic source. A 400 µm diameter bilaminar membrane hydrophone (MH2) was used as a reference hydrophone. Overall uncertainty: 1-40 MHz: ±1 dB, 40-60 MHz: ±1.5 dB.

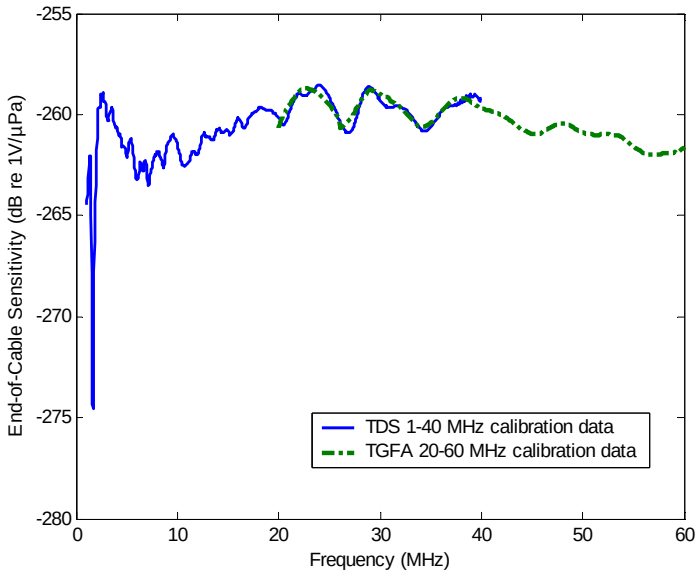

Figure 4.18: End-of-cable sensitivity of a 120 µm diameter needle hydrophone probe (NH6) calibrated up to 40 MHz using the TDS technique and up to 60 MHz using the TGFA technique with a focal number 3.84 acoustic source. A 400 µm diameter bilaminar membrane hydrophone (MH2) was used as a reference hydrophone. Overall uncertainty: 1-40 MHz: ±1 dB, 40-60 MHz: ±1.5 dB.

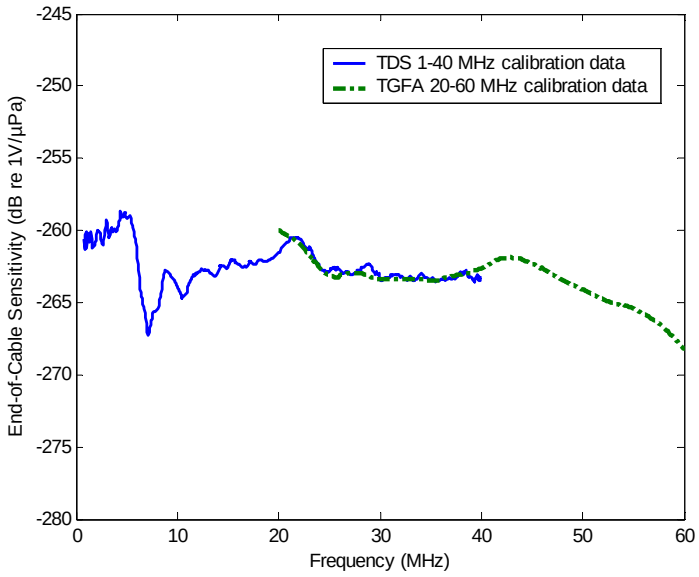

Figure 4.19: End-of-cable sensitivity of a 130 µm diameter needle hydrophone probe (NH7) calibrated up to 40 MHz using the TDS technique and up to 60 MHz using the TGFA technique with a focal number 3.84 acoustic source. A 400 µm diameter bilaminar membrane hydrophone (MH2) was used as a reference hydrophone. Overall uncertainty: 1-40 MHz: ±1 dB, 40-60 MHz: ±1.5 dB.

As mentioned previously a combination of TDS, TGFA and semi-empirical nonlinear technique was utilized to provide calibration data up to 100 MHz. The relevant plots are shown below in Figures 4.20-4.23. Figure 4.20 shows the end-of-cable sensitivity of a 150 μm diameter needle hydrophone (NH1) calibrated up to 40 MHz using the TDS technique with a focal number 19.25 source and up to 100 MHz using the TGFA technique with a focal number 2 source. Figure 4.21 illustrates the end-of-cable sensitivity of a 400 μm diameter bilaminar membrane hydrophone (MH1) calibrated up to 40 MHz using the TDS technique with a focal number 19.25 source and up to 100 MHz using the TGFA technique with a focal number 2 source. For comparison, the calibration by the independent laboratory (NPL, UK) up to 60 MHz is also included. Figure 4.22 presents the end-of-cable sensitivity of a 400 μm diameter bilaminar membrane hydrophone (MH2) calibrated up to 40 MHz using the TDS technique with a focal number 19.25 source, up to 55 MHz using the TGFA technique with a focal number 3.84 source and up to 100 MHz using the TGFA technique with a focal number 2 source. Again, NPL 1-60 MHz calibration is also shown for comparison. Finally, Figure 4.23 illustrates the end-of-cable sensitivity of a 400 μm diameter bilaminar membrane hydrophone (MH3) calibrated up to 40 MHz using the TDS technique with a focal number 19.25 source, up to 55 MHz using the TGFA technique with a focal number 3.84 source and up to 100 MHz using the TGFA technique with a focal number 2 source.

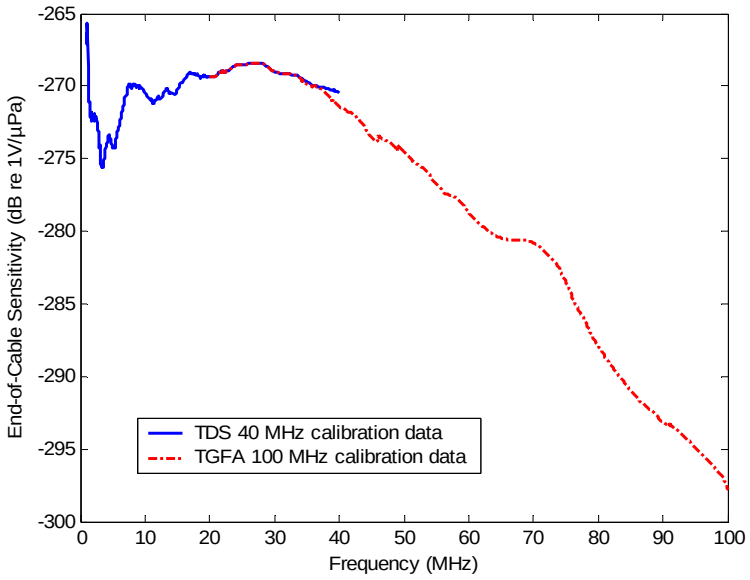

Figure 4.20: End-of-cable sensitivity of a 150 µm diameter needle hydrophone probe (NH1) calibrated up to 40 MHz using the TDS technique and up to 100 MHz using the TGFA technique with a focal number 2 source. A 400 µm diameter bilaminar membrane hydrophone (MH2) was used as a reference hydrophone. Overall uncertainty: 1-40 MHz: ±1 dB, 40-60 MHz: ±1.5 dB, beyond 60 MHz: ±2 dB.

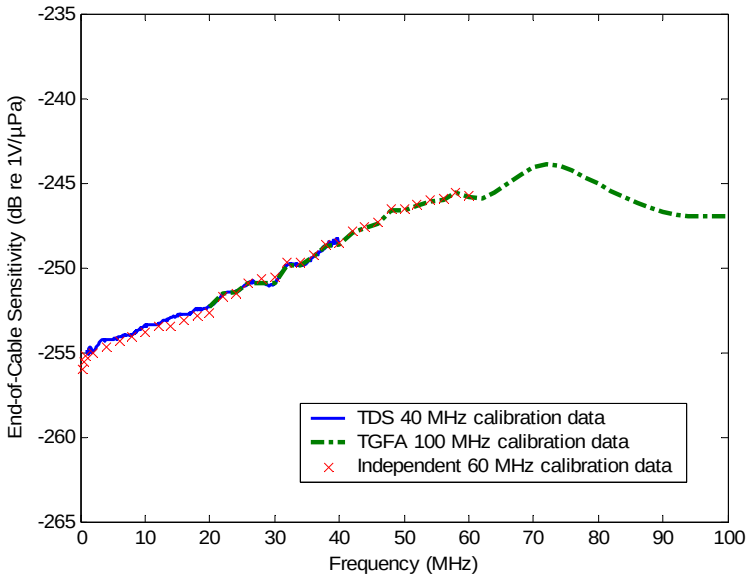

Figure 4.21: End-of-cable sensitivity of a 400 µm diameter bilaminar membrane hydrophone probe (MH1) calibrated up to 40 MHz using the TDS technique and up to 100 MHz using the TGFA technique with a focal number 2 acoustic source. A 400 µm diameter bilaminar membrane hydrophone (MH2) was used as a reference hydrophone. Overall uncertainty: 1-40 MHz: ±1 dB, 40-60 MHz: ±1.5 dB, beyond 60 MHz: ±2 dB.

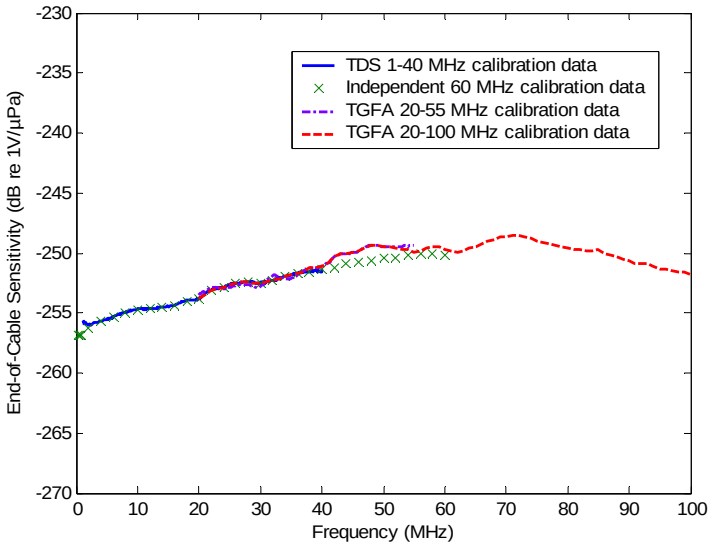

Figure 4.22: End-of-cable sensitivity of a 400 µm diameter bilaminar membrane hydrophone probe (MH2) calibrated up to 40 MHz using the TDS technique, up to 55 MHz using the TGFA technique with a focal number 3.84 acoustic source and up to 100 MHz using the TGFA technique with a focal number 2 acoustic source. A 400 µm diameter bilaminar membrane hydrophone (MH3) was used as a reference hydrophone. Overall uncertainty: 1-40 MHz: ±1 dB, 40-60 MHz: ±1.5 dB, beyond 60 MHz: ±2 dB.

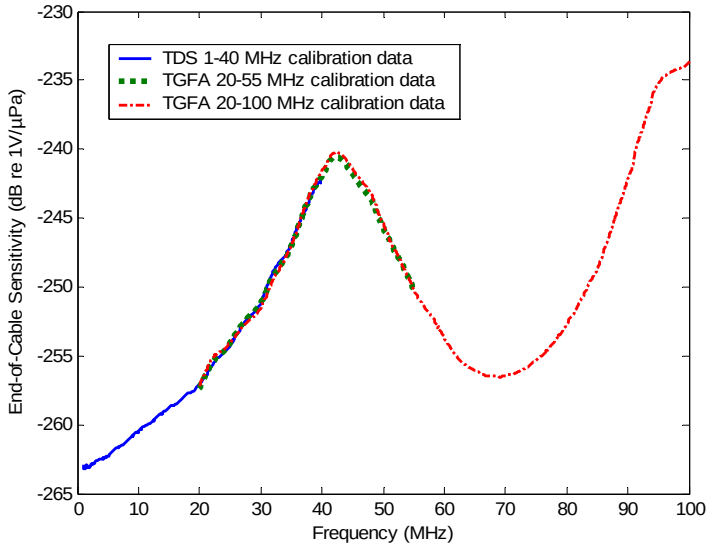

Figure 4.23: End-of-cable sensitivity of a 400 µm diameter bilaminar membrane hydrophone probe (MH3) calibrated up to 40 MHz using the TDS technique, up to 55 MHz using the TGFA technique with a focal number 3.84 acoustic source and up to 100 MHz using the TGFA technique with a focal number 2 acoustic source. A 400 µm diameter bilaminar membrane hydrophone (MH2) was used as a reference hydrophone. Overall uncertainty: 1-40 MHz: ±1 dB, 40-60 MHz: ±1.5 dB, beyond 60 MHz: ±2 dB.

To verify the validity of the TGFA calibration technique, three hydrophone probes (MH1, MH2 and NH1, see Tables A1.1) were also calibrated using the semi-empirical nonlinear propagation technique. As all three calibrations were performed using the same pulsing conditions and the same 10 MHz, focal number 4.21 acoustic source (see Table A2 of Appendix 2) described in Section 3.2.3, only one simulation using the nonlinear propagation model was performed. The simulation predicted pressure-time waveforms in the focal region of the transducer. Once the (point receiver) field prediction was obtained, the pressure-time waveforms were acquired experimentally at the focal plane of the 10 MHz acoustic source by recording the voltage at the hydrophone terminals (see Section 3.2.3, Nonlinear pressure-time waveform measurement in Chapter 3). The spatial averaging correction (see Section 3.1) was applied to account for the hydrophone's finite aperture.

Figure 4.24 shows the normalized spectrum amplitude corresponding to the pressure-time waveform predicted by the nonlinear propagation model in the focal plane of the focal number 4.21 acoustic source with and without applying spatial averaging correction needed for the 400 μm diameter bilaminar membrane hydrophone (MH2).

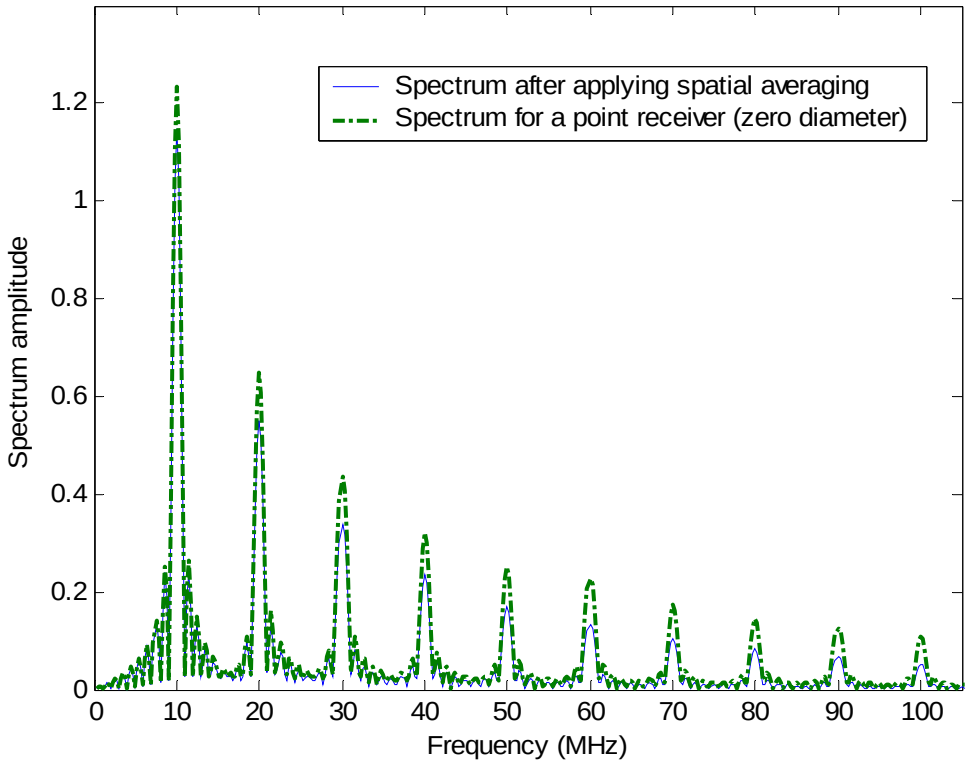

Figure 4.24: Normalized spectrum amplitude corresponding to the pressure-time waveform predicted by the nonlinear propagation model in the focal plane of the 10 MHz focal number 4.21 acoustic source with and without applying spatial averaging correction needed for the 400 μm diameter bilaminar membrane hydrophone (MH2).

Figure 4.25 presents the measured and simulated spectrum amplitudes in dBs for the 400 μm diameter membrane hydrophone (MH2) at 10 MHz intervals. The corresponding discrete sensitivity values resulting from the nonlinear calibration of MH2 and shown in Figure 4.26 (circular dots) were obtained using the data shown in Fig. 4.25. Specifically, the MH2 sensitivity at 10 MHz that was determined previously by the TDS technique (see Fig. 4.5) was used as the main reference point. At each discrete frequency, the corresponding difference between the simulated and measured spectra amplitudes was determined (see Fig. 4.25) and algebraically added to the 10 MHz sensitivity value of

the MH2 hydrophone. In other words, the absolute sensitivity plot shown in Figure 4.26 was obtained by scaling the relative amplitude response at each frequency with respect to the TDS determined sensitivity at the fundamental frequency of the acoustic source, i.e. 10 MHz.

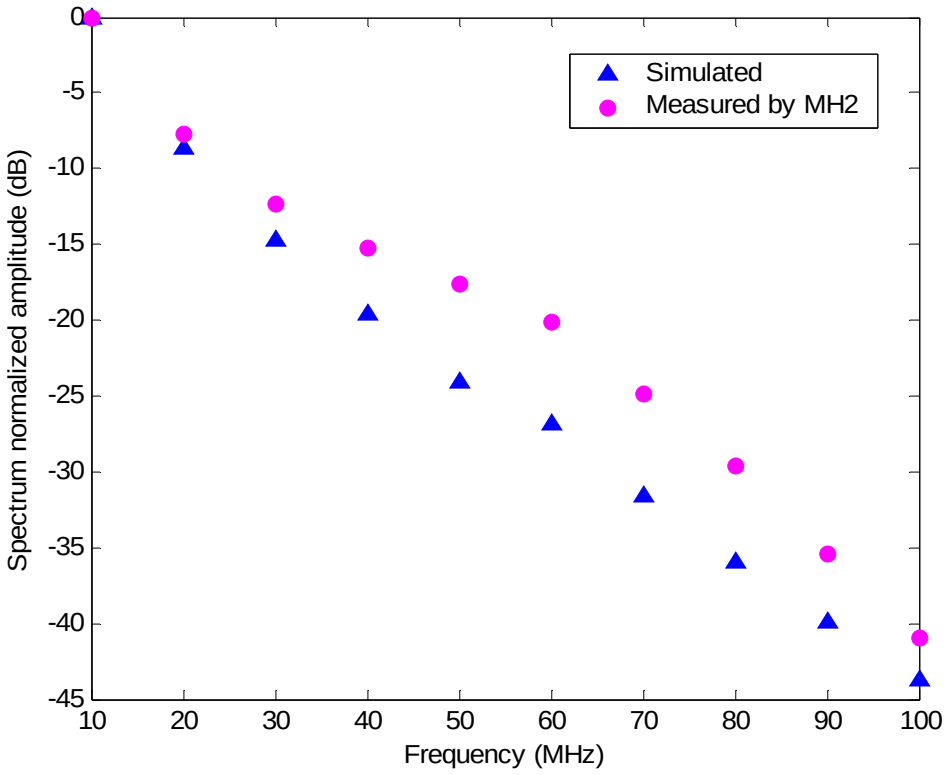

Figure 4.25: Measured and simulated normalized amplitudes for a 400 µm diameter bilaminar membrane hydrophone probe (MH2).

Figures 4.26 through 4.28 present 100 MHz calibration data obtained for hydrophones of different finite apertures and constructions. Figure 4.26 shows the end-of-cable sensitivity of a 400 µm diameter bilaminar membrane hydrophone (MH2) calibrated up to 40 MHz using the TDS technique with a focal number 19.25 source, up to 55 MHz using the TGFA technique with a focal number 3.84 source and up to 100 MHz using both the TGFA technique with a focal number 2 source and the nonlinear calibration method with

a focal number 4.21 source. For comparison, independent laboratory (NPL, UK) data up to 60 MHz are also shown. The frequency response of a similar membrane hydrophone (MH1) is shown in Figure 4.27. Figure 4.28 shows the calibration data obtained using the combined TDS, TGFA and nonlinear calibration methods for a 150 µm diameter needle hydrophone (NH1).

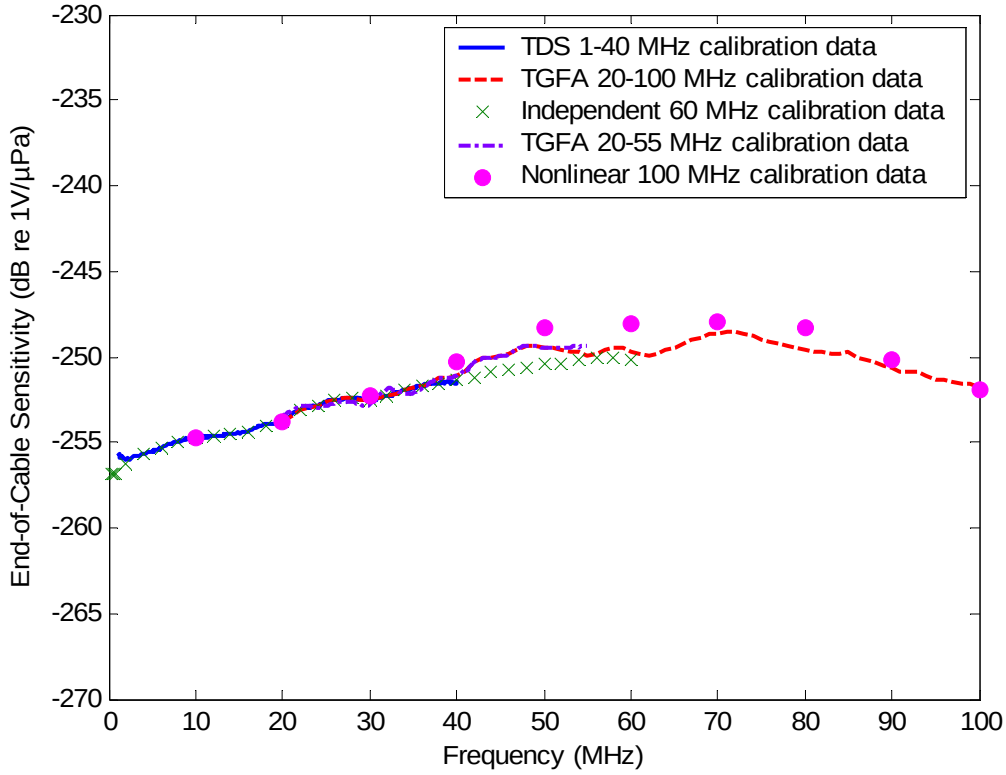

Figure 4.26: End-of-cable sensitivity of a 400 µm diameter bilaminar membrane hydrophone probe (MH2) calibrated up to 40 MHz using the TDS technique with a focal number 19.24 source, up to 55 MHz using the TGFA technique with a focal number 3.84 source and up to 100 MHz using both the TGFA technique with a focal number 2 source and the nonlinear calibration method with a focal number 4.21 source. Overall uncertainty: 1-40 MHz: ±1 dB, 40-60 MHz: ±1.5 dB, beyond 60 MHz: ±2 dB.

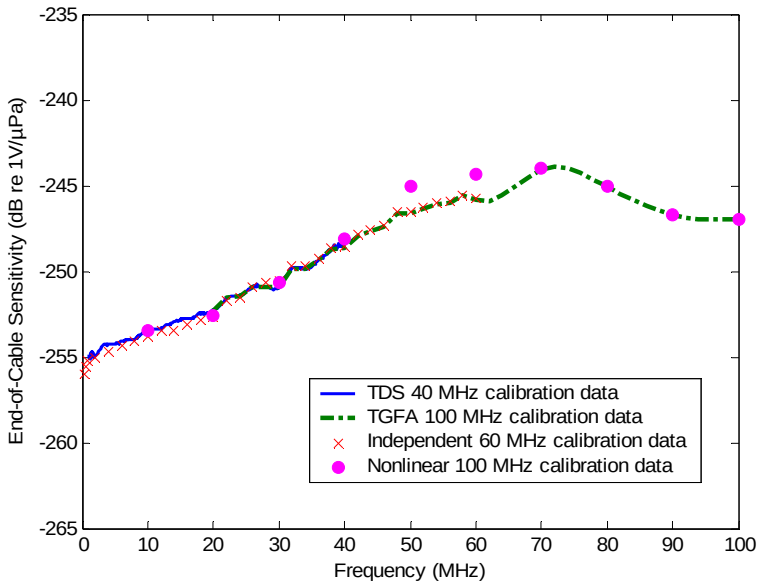

Figure 4.27: End-of-cable sensitivity of a 400 μm diameter bilaminar membrane hydrophone probe (MH1) calibrated up to 40 MHz using the TDS technique and up to 100 MHz using both the TGFA technique and the nonlinear technique. Overall uncertainty: 1-40 MHz: ±1 dB, 40-60 MHz: ±1.5 dB, beyond 60 MHz: ±2 dB.

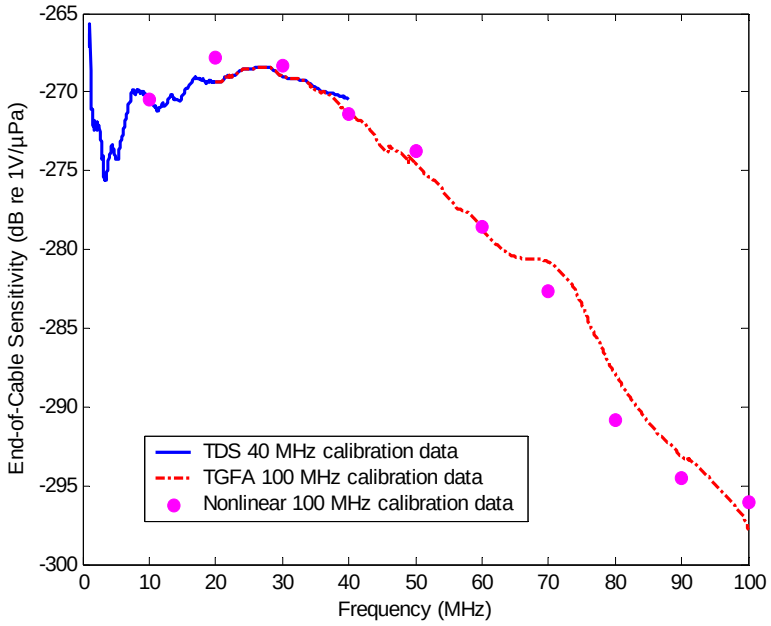

Figure 4.28: End-of-cable sensitivity of a 150 μm diameter needle hydrophone probe (NH1) calibrated up to 40 MHz using the TDS technique and up to 100 MHz using both the TGFA technique and the nonlinear technique. Overall uncertainty: 1-40 MHz: ±1dB, 40-60 MHz: ±1.5dB, beyond 60MHz: ±2 dB.

4.2 Acousto-optic measurements: fiber optic hydrophone probes

The sensitivity of the fiber optic (FO) hydrophone probe was obtained by comparing peak to peak pressure amplitudes of the waveforms generated by a 1.52 MHz HIFU transducer (see Table A2 of Appendix 2) measured first by a previously calibrated needle hydrophone probe (NH5) and then by the fiber optic (FO) hydrophone located in the same position in the acoustic field. The waveforms were sampled at the sampling frequency f_s = 2 GHz using a digital oscilloscope (Tektronix TDS 2022). The calibration performed using this technique yielded the sensitivity of the FO hydrophone probe of 20 mV/MPa (or -274 dB re 1V/μPa). To facilitate comparison of the different hydrophone probes' performance in terms of sensitivity (dB re 1V/μPa) versus frequency (MHz), the frequency responses of the needle (NH1), membrane (MH2) and fiber optic (FO) hydrophones are plotted in Figure 4.29. The data presented in Figure 4.29 indicate that the anticipated FO hydrophone probe's frequency response is indeed uniform in comparison with both needle and membrane designs.

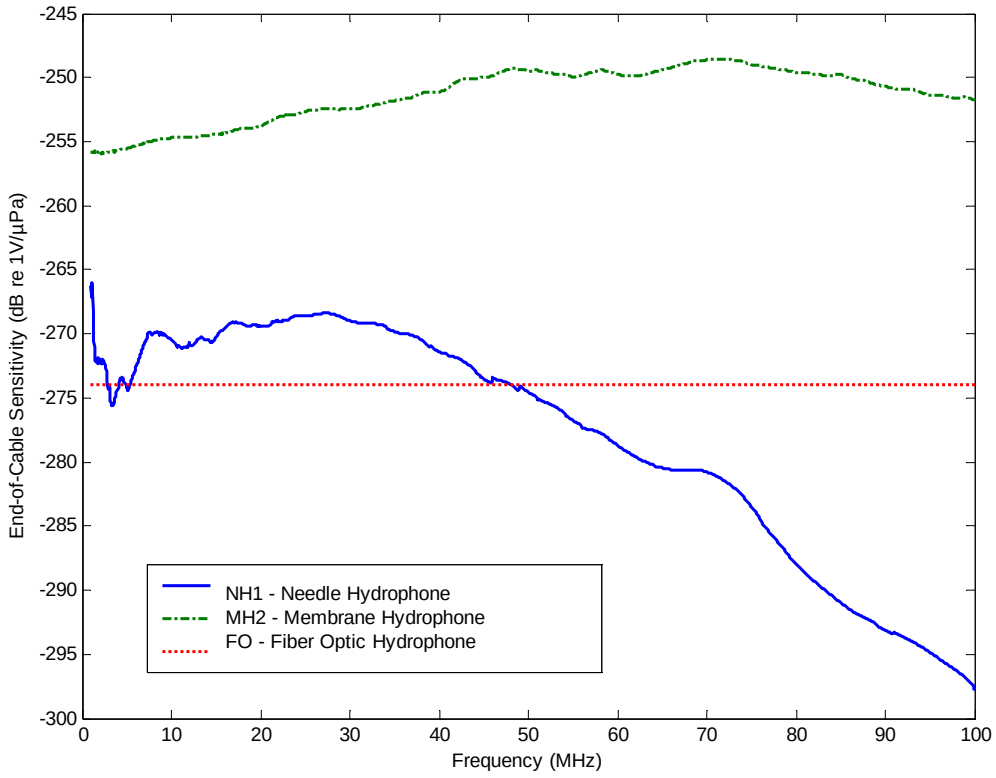

Figure 4.29: End-of-cable sensitivity of a 150 µm diameter needle hydrophone (NH1) and a 400 µm diameter bilaminar membrane hydrophone (MH2) calibrated up to 100 MHz. "Horizontal" line at the -274 dB re 1V/µPa level: preliminary calibration data for 10 micrometers diameter tip, fiber optic (FO) hydrophone. Overall uncertainty: 1-40 MHz: ±1dB, 40-60 MHz: ±1.5dB, beyond 60MHz: ±2 dB.

Figure 4.30 shows a comparison of the pressure-time waveforms measured by the FO hydrophone probe and the PVDF needle hydrophone probe (NH5) under the same excitation conditions. Again, 1.52 MHz HIFU transducer was used as a source. The transducer transmitted a ten-cycle pulse at 5% duty cycle (pulse repetition period of 132 µs). The peak-to-peak pressure was determined to be 5 MPa. The waveform received by the FO hydrophone probe was averaged using 128 point averaging prior to recording to improve the signal-to-noise ratio. In addition, before the waveform of the FO hydrophone probe was displayed on the oscilloscope (Tektronix TDS 2022), it was filtered by the

custom-made 500 kHz high-pass filter and amplified by 20 dB voltage gain preamplifier (Onda Corp., Sunnyvale, CA, model AH-2010). The waveform recorded by the FO hydrophone probe was in general noisier (see Figure 4.30) than the waveforms recorded with the PVDF needle hydrophone (NH5) probe.

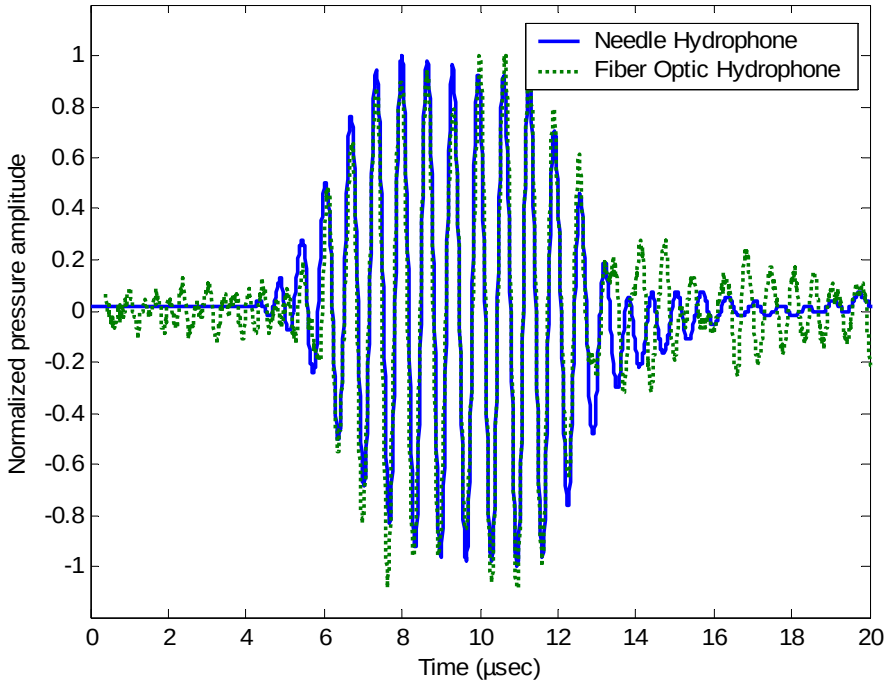

Figure 4.30: Normalized 5 MPa peak-to-peak pressure time waveforms obtained by the needle hydrophone probe (NH5) and the fiber optic (FO) hydrophone probe using a 1.52 MHz HIFU acoustic source (focal number 1.9, see Table A2 of Appendix 2).

CHAPTER 5: Discussion and conclusions

The calibration results of needle (NH2) and membrane (MH5) hydrophone probes presented in Figures 4.1 and 4.2 were obtained by using Time Delay Spectrometry (TDS) technique without the spatial averaging correction. These results indicated that the hydrophones with diameters smaller than that of the reference hydrophone exhibited experimentally determined absolute sensitivity greater than the true one (see Figure 4.1). Conversely, the absolute sensitivity of the hydrophones with diameters larger than that of the reference one was lower (see Figure 4.2). To obtain the correct calibration data, the spatial averaging correction factors shown in Figures 3.3 and 3.4 were used. The correction factors were experimentally validated by performing calibration by substitution using three wideband focused sources (focal numbers 3.84, 10.16 and 19.24). Once the spatial averaging corrections presented in Figures 3.3 and 3.4 were algebraically added to the uncorrected calibration results of Figures 4.1 and 4.2, respectively**,** the resulting hydrophone sensitivities were in excellent agreement, independent on the focal number of the acoustic sources (see Figures 4.3 and 4.4). The discrepancies between the three corrected end-of-cable sensitivities shown in Figures 4.3 and 4.4 were found to be within ±1 dB. Such uncertainty is acceptable in acoustic calibrations. The results presented in Figures 4.3 and 4.4 clearly indicated that the spatial averaging correction developed could be successfully used to obtain true calibration values.

The calibration results shown in Figures 4.5-4.11 were also obtained using Time Delay Spectrometry (TDS) technique in the frequency range 1-40 MHz. The advantages of

using a quasi-continuous calibration technique such as TDS and TGFA are further supported by the calibration results presented. These results show that the TDS technique allowed detailed characterization of the NH5 needle hydrophone probe and revealed its highly nonuniform frequency response. The data presented in Figure 4.5 confirmed that the membrane hydrophones exhibit a uniform frequency response with the sensitivity increasing between 0.15 and 0.5 dB/MHz, whereas the frequency response of the needle hydrophones (see Figures 4.6-4.11) exhibits rapid and relatively large variations in sensitivity (about 40 dB in the frequency range of 1-1.5 MHz as evidenced in Figure 5.1). Such variations are often undetectable when using discrete frequency calibration, which is usually performed at 1 or 2 MHz intervals (see e.g. Figure 4.12, and [77]).

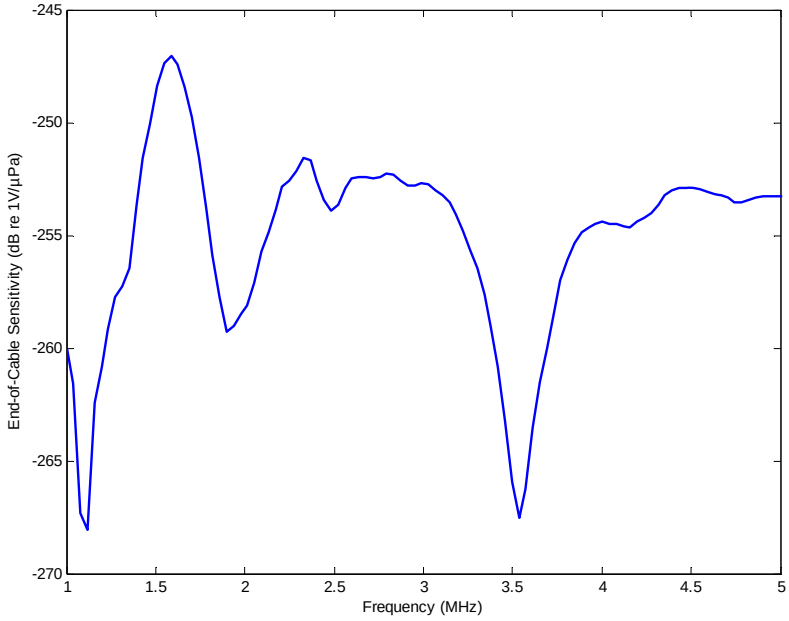

Figure 5.1: Rapid variation in the sensitivity in the frequency range 1-5 MHz of the 500 µm needle hydrophone (NH5).

It is worth noting that in Figure 4.5, MH3 membrane hydrophone probe's response increased at the rate of 0.5 dB/MHz that was higher than the slope exhibited by MH1,

MH2 and MH4 probes. This is because MH3 was loaded with a 1.2 meter coaxial cable before the signal was amplified by a preamplifier, whereas other hydrophones' construction involved a shorter, about 20 centimeter cable followed by a preamplifier. The frequency response of the MH3 probe up to 100 MHz is shown in Figure 4.23. There, the first resonance peak at about 40 MHz is followed by the 2^{nd} one at approximately 100 MHz. The 100 MHz resonance is due to the transmission line phenomenon and is caused by the cable length (1.2 meters) connecting the hydrophone probe and a preamplifier. This cable length corresponds to about half wavelength ($\lambda/2$) at 100 MHz.

As already noted the TDS technique allows a relatively quick hydrophone calibration by substitution and ensures a high (typically 50 dB) signal-to-noise ratio [56, 71, 72]. However, as mentioned earlier because of the limitation of the hardware in the set up developed, the TDS technique could only be used up to 40 MHz. To extend the quasi-continuous calibration of hydrophones beyond 40 MHz, the time gated frequency analysis (TGFA) calibration technique was developed. The technique was successfully applied to calibrate ten PVDF hydrophone probes, including both membrane and needle designs as shown in Figures 4.12-4.23. Although the data presented here correspond to four membranes and six needle hydrophones, both TDS and TGFA techniques were successfully employed to calibrate over 20 different hydrophones available (see Appendix A)

.

Figures 4.12-4.19 show the sensitivity data obtained for eight hydrophone probes (five needle and three membrane hydrophones) in the frequency range 20-60 MHz using the acoustic source with the focal number 3.84. These results are in good agreement (to within ±1.5 dB) with the sensitivities obtained using the TDS technique. In addition, the focal number 2 acoustic source was also used to calibrate four hydrophone probes (one needle and three membrane hydrophones) in the frequency range 20-100 MHz with the TGFA technique (see Figs. 4.20-4.23). As shown in Figures 4.21 and 4.22, the calibrations yielded results that were consistent with those provided by the independent laboratory (NPL, UK). The agreement between the three calibration results (TDS, TGFA and the independent one) presented in Figs. 4.20-4.23 was determined to be within ±2 dB. Overall, the TGFA technique exhibited similar advantages as the TDS one, and in addition offered an extended, 100 MHz calibration bandwidth.

Since the maximum calibration frequency provided by the National Physical Laboratory (NPL) was 60 MHz, the absolute sensitivity of the reference hydrophone (M_{ref}) at frequencies beyond 60 MHz was determined using the semi-empirical nonlinear propagation model (see Section 2.2.1.4 and [61, 75]). The semi-empirical nonlinear calibration technique allowed calibration at discrete harmonic frequencies from 10-100 MHz and was also used to verify the TGFA measurement results from 40 to 100 MHz. Three hydrophone probes (Figs 4.26-4.28) were calibrated using a combination of the TDS, TGFA and the semi-empirical nonlinear technique to obtain the frequency response up to 100 MHz. The agreement between the different calibration methods varied depending on frequency. The membrane hydrophone calibrations (MH2 and MH1, see

Table A1.1) shown in Figures 4.26 and 4.27 indicated that in the frequency range up to 40 MHz this agreement was within ±0.5 dB. The discrepancy between the TGFA and nonlinear calibration increased slightly beyond 40 MHz and exhibited a maximum of about 2.5 dB in the range between 50 and 60 MHz. The reason for this discrepancy is currently being investigated. For the 150 μm needle hydrophone (NH1) calibration shown in Figure 4.28, the agreement between the data obtained using the nonlinear method and the quasi-continuous one was less favorable with the discrepancies reaching 2 dB at 20 MHz, 2.5 dB at 70 MHz and almost 3 dB at 80 MHz. Again, the cause for these disagreements is being examined as there is no apparent reason for their existence. As pointed out earlier, in the frequency range between 60-100 MHz no independent confirmation is available, but the consistency obtained up to 60 MHz with the NPL results and the agreement between the nonlinear discrete data and the virtually continuous TGFA ones indicate that the values of the sensitivity beyond 60 MHz as determined here are correct (to within the overall uncertainty as discussed above). Additional support for this notion comes from the theoretical modeling of the hydrophone responses using PiezoCAD (Sonic Concepts, Woodenville, WA).

Overall, the results of Figures 4.26-4.28 confirm that quasi-continuous calibration of hydrophones in the frequency range up to 100 MHz is possible using a combination of TDS, TGFA and nonlinear methods. Also, these data (see Figures 4.26-4.28) corroborate the consistency of the calibration in the four frequency spans, i.e. 1-40 MHz, 20-60 MHz, 20-100 MHz and 10-100 MHz using TDS, TGFA and semi-empirical nonlinear approaches.

The frequency response of the 10μm diameter fiber optic (FO) prototype probe shown in Figure 4.29 was obtained by the substitution technique using the PVDF needle hydrophone (NH5) as a reference. The FO probe sensitivity was determined to be 20 mV/MPa (or -274 dB re 1V/μPa). Based on the data presented in [42, 44], the uniformity of the FO probe response can be anticipated in the whole frequency range considered. It is worth noting that such a uniform behavior would make the FO hydrophone useful in determining phase response of piezoelectric hydrophones. Although the phase can also be determined using the nonlinear propagation model [61] the phase measurement would be simplified by using a uniform response hydrophone [44]. The phase measurement issue is further discussed in the following.

In Figure 4.30, the normalized pressure time waveforms measured by the needle hydrophone (NH5) and the fiber optic hydrophone probe using the 1.52 MHz HIFU acoustic source (focal number 1.9, see Table A2 of Appendix 2) at 5 MPa peak-to-peak pressure amplitude are presented. Overall, the measurement results show very good agreement in terms of pulse repetition period, pulse duration and the number of pulse cycles. However, as mentioned earlier, the noise level of the FO hydrophone probe was higher in comparison with that produced by the needle hydrophone (see Figure 4.30). This was because the sensitivity of the FO probe was about 10 dB lower in comparison with that of the NH5 needle hydrophone and also the experimental set up of the FO probe was more susceptible to the extraneous noise than the measurement arrangement used to record the needle hydrophone signal. The methods suggested to improve the sensitivity of the FO hydrophone system are discussed in the following section, Chapter 6.

The availability of a hydrophone probe that would perform as a point receiver in the frequency range considered (here, 100 MHz) and exhibit uniform frequency response is highly desirable. As noted earlier, such probe would be able to reproduce the pressure-time waveforms faithfully without the necessity of applying spatial averaging corrections and also be useful as a reference in determining phase characteristics of finite aperture and limited bandwidth hydrophone probes [42, 44]. In contrast to the optic measurement systems discussed in [42, 44], which employ a fairly complex and expensive interferometric approach, the goal of this work was to examine a feasibility of using a less expensive option based on the designs described in [66] and [39]. Similar designs were proved to be useful in HIFU measurements [78, 79]**,** in practice, however, the voltage sensitivity of the FO probes described in [78, 79] was inadequate for acoustic output measurements. Also, the probes' aperture was on the order of 100 μm, which would prevent point receiver behavior at frequencies beyond 7.5 MHz. The sensitivity of the 10 μm diameter quasi-point receiver prototype tested here was determined to be about -274 dB re 1 V/μPa (see Figure 4.29), which is approximately 6-8 dB closer to the desirable sensitivity value of -266 to -268 dB (see Figure 4.29). Such sensitivity level is considered to be adequate in ultrasound diagnostic imaging applications [2-4]. Hence, the fiber optic (FO) measurement system developed – once its sensitivity is boosted up by additional – say 10 dB – will constitute a universal reference tool in the 100 MHz bandwidth.

From the results presented in Chapter 4, it can be inferred that both fiber optic and piezoelectric probes have their advantages and disadvantages depending upon the specific

task. With the calibration approach presented, the PVDF probes in connection with an oscilloscope offer 100 MHz measurement assembly that is less complex and less expensive than the FO probe's one. However, their finite aperture and limited bandwidth gradually introduce a phase shift that may have to be accounted for [42, 44]. It was noted earlier that this phase shift could be determined using a nonlinear propagation theory, however, now and then it may be more convenient to use FO hydrophone probes. The FO probes exhibit bandwidth readily exceeding 100 MHz and limited only by the associated electronics. As their sensitivity is frequency independent and they do not suffer from intrinsic mechanical resonances their phase shift will be zero. Hence, although their measurement arrangement in more complex than that of the PVDF probes, once calibrated using e.g. the combined approach presented in this work, the FO probes could be conveniently used to determine phase characteristics of finite aperture piezoelectric polymer hydrophones. The only equipment that could limit the bandwidth of the acousto-optic probe assembly used here was the photo-receiver (Thor Labs, Newton, NJ, model PDA10CF) and preamplifier (Onda Corp., Sunnyvale, CA, model AH-2010). Both the photo-receiver and preamplifier exhibited the bandwidth of 150 MHz, which is well beyond 100 MHz considered here.

In conclusion, two swept frequency techniques together with a semi-empirical nonlinear propagation model were combined to form a consistent 100 MHz calibration tool. As the calibration techniques developed do not suffer from any intrinsic limitations, they can be easily extended to frequencies beyond 100 MHz. Up to 60 MHz, the calibration results were in agreement (see previous section) with the ones obtained from a national

laboratory (NPL, UK). As already noted, beyond 60 MHz no independent verification of the data was available but the consistency obtained up to 60 MHz with the NPL results and the agreement between the nonlinear discrete data and the virtually continuous TGFA ones indicate that the values of the sensitivity beyond 60 MHz are correct (to within the overall uncertainty less than ±2 dB). In addition, the results of the calibration of the FO probe indicate that its sensitivity should be uniform (to within the uncertainty of the measurements, ±1 dB). However, the currently obtained sensitivity is equal to approximately 20 mV/MPa or −274 dB re 1 V/μPa. This may be too low to ensure signal-to-noise ratio needed for the measurement of acoustic output of modern diagnostic imaging devices and ideally should be increased by approximately 8 dB. The methods to enhance the sensitivity of the FO hydrophone probes are discussed in the next Chapter, along with the suggestions for future work.

CHAPTER 6: Suggestions for future work

As evidenced above, the results of this work have been very encouraging. Below a few research topics that require further attention and development are discussed.

Nonlinear calibration: The nonlinear calibration method provided calibration data at discrete intervals, multiple of the fundamental frequency of the acoustic source. The 10 MHz transducer source (Table A2 of Appendix 2) used to perform the nonlinear calibration provided only 10 discrete calibration points. Therefore, to increase the number of calibration points presented in Figures 4.26-4.28, in addition to using the 10 MHz source, the lower fundamental frequency sources should be used. The 1.52 MHz HIFU transducer (focal number 1.9, see Table A2 of Appendix 2) could be conveniently employed, however, it is unlikely that it would produce 60 harmonics needed to cover 100 MHz bandwidth. On the other hand it can also operate at the third harmonic frequency (approximately 5 MHz), and it is likely that it would be capable of generating 20 harmonics. Hence, operation at 5 MHz would double the number of discrete calibration frequencies in comparison with those reported here. The use of the HIFU source would also improve S/N ratio in comparison with the 10 MHz source used in this work.

Improvement of the sensitivity of the FO hydrophone probe: As noted earlier for the measurement of acoustic output produced by diagnostic imaging machines of a variety of diagnostic fields, the current sensitivity of the FO probes should be increased by

approximately 8 dB. The immediate improvements of the FO hydrophone probe sensitivity can be achieved by using a low Relative Intensity Noise (RIN) high power (1 Watt) laser to boost the light signal and reduce noise level [80], and by using a differential optical receiver for common-mode rejection of RIN [80]. This receiver noise reduction will enhance the signal-to-noise ratio by about 26 dB and thus improve sensitivity of the fiber-optic hydrophone by an order of magnitude, so it will become comparable with the currently used PVDF hydrophones. Further improvement in the FO probe sensitivity can be achieved by using abs appropriate metal coating of the fiber optic tip. Recently, Gopinath et al [80] reported that the gold coated fiber would provide about 15 dB improvement in sensitivity in comparison with the uncoated one.

Calibration of the FO hydrophone probes up to 100 MHz: A novel wideband measurement technique developed during this work should be used to calibrate the FO hydrophone up to 100 MHz. This will provide the sensitivity of the fiber optic hydrophone probes as a virtually continuous function of frequency and allow the verification of the uniformity of the FO sensor frequency response in the 100 MHz frequency range.

Phase calibration of piezoelectric finite aperture hydrophones using the FO hydrophone as a reference: Fiber optic sensors bandwidth is governed by that of the photodetectors used. As the photodetectors are available with a bandwidth that is well beyond 100 MHz, the FO hydrophone measurement set up is expected to have a uniform frequency response and exhibit a zero phase shift in the 100 MHz bandwidth. These

features will be very useful in complex calibration i.e. determining both magnitude and phase response [42, 44] of finite aperture PVDF hydrophones making use of substitution method and using the FO probe as a reference hydrophone.

Optimization of the semi-empirical nonlinear method calibration time: In this work the simulation of the nonlinear field generated by the 10 MHz source required about 3 hours**.** To shorten this time, in future work a newly developed algorithm should be employed. The implementation of this algorithm was recently described [62]. The algorithm makes use of Time-Averaged Wave Envelopes (hence termed TAWE) and the results of the initial testings indicate that the use of TAWE can reduce the computational time to about 10-15 minutes depending on the frequency and geometry of the source [62].

List of references

1. Patton, C., G.R. Harris, and R.A. Philips, *Output levels and bioeffects indices from diagnostic ultrasound exposure data reports o the FDA.* IEEE Trans. Ultrason. Ferroelec. Freq. Contr., 1994. **41**(3): p. 353-359.

2. *Acoustic output measurement standard for diagnostic ultrasound equipment*. in *AIUM, Laurel, MD*; *National Electrical Manufacturers Association (NEMA)*. 1998. Rosslyn, VA.

3. FDA. *Revised FDA 510(k) Information for Manufacturers Seeking Marketing Clearance of Diagnostic Ultrasound Systems and Transducers*. September 30, 1997.

4. *Standard for Real-Time Display of Thermal and Mechanical Acoustic Output Indices on Diagnostic Ultrasound Equipment, Rev. 1*. in *American Institute of Ultrasound in Medicine (AIUM), Laurel, MD*; *National Electrical Manufacturers Association (NEMA)*. 1998. Rosslyn, VA.

5. Cherin, E., A. Saed, P. Laugier, P. Netter and G. Berger, *Evaluation of Acoustical Parameter Sensitivity to Age-Related and Osteoarthritic Changes in Articular Cartilage Using 50-MHz Ultrasound.* Ultrasound in Medicine & Biology, 1998. **24**(3): p. 341-354.

6. Dneg, C.X., F.C. Lizzi, R.H. Silverman, R. Ursea and D.J. Coleman, *Imaging and spectrum analysis of contrast agents in the in-vivo rabbit eye using very-high-frequency ultrasound.* Ultras. Med. Biol. , 1998. **24**: p. 383-394.

7. Fleischer, A.C., *Sonographic depiction of tumor vascularity and flow: from in vivo models to clinical applications.* J Ultrasound Med, 2000. **19**(1): p. 55-61.

8. Lockwood, G.R., L. R. Ryan, A. I. Gotlieb, E. Lonn, J.W. Hunt, P. Liu, and F.S. Foster, *In vitro high resolution intravascular imaging in muscular and elastic arteries.* J. Am. Coll. Cardiol., 1992. **20**: p. 153.

9. Reinstein, D.Z., R.H. Silverman, M.J. Rondeau, D.J. Coleman, *Epithelial corneal thickness measurements by high frequency ultrasound digital signal processing.* Ophthalmology, 1994. **101**: p. 140.

10. Turnbull, D.H., B.G. Starkoski, K.A. Harasiewicz, J.L. Semple, L. From, A.K. Gupta, D.N. Sauder and F.S. Foster, *A 40-100 MHz B-scan ultrasound backscatter microscope for skin imaging.* Ultrasound in Medicine & Biology, 1995. **21**(1): p. 79-88.

11. Foster, F.S., C. J. Pavlin, G.R. Lockwood, L.K. Ryan, L.B. Harasiewicz and A.M. Rauth, *Principles and applications of ultrasound backscatter microscopy.* Ultrasonics, Ferroelectrics and Frequency Control, IEEE Transactions on, 1993. **40**(5): p. 608-617.

12. Passmann, C. and H. Ermert, *A 100-MHz ultrasound imaging system for dermatologic and ophthalmologic diagnostics.* Ultrasonics, Ferroelectrics and Frequency Control, IEEE Transactions on, 1996. **43**(4): p. 545-552.

13. Lizzi, F.L., M.C. Rorke, J.B. Sokil-Melgar, A. Kalisz, and J. Driller, *Interfacing very high frequency transducers to digital-acquisition scanning systems*. in *New Developments in Ultrasonic Transducers and Transducer Systems*. 1992. San Diego, CA, USA: SPIE.

14. Pavlin, C.J., K.A. Harasiewicz, M.D. Sherar and F.S. Foster, *Clinical use of ultrasound biomicroscopy.* Ophthalmology, 1993. **100**: p. 1351.

15. Ferrara, K.W., B.G. Zagar, R.H. Silverman, J.B. Sokil-Melgar, and I.M. Aslanidis, *Estimation of blood velocity with high frequency ultrasound.* Ultrasonics, Ferroelectrics and Frequency Control, IEEE Transactions on, 1996. **43**(1): p. 149-157.

16. Goertz, D.E., J.L. Yu, R.S. Kerbel, P.N. Burns, and F.S. Foster, *High-frequency 3-D color-flow imaging of the microcirculation.* Ultrasound in Medicine & Biology, 2003. **29**(1): p. 39-51.

17. Foster, F.S., M.Y. Zhang, Y.Q. Zhou, G. Liu, J. Mehi, K.A. Harasiewicz, B.G. Starkoski, L. Zan, D.A. Knapik, and S.L. Adamson, *A new ultrasound instrument for in vivo microimaging of mice.* Ultrasound in Medicine & Biology, 2002. **28**(9): p. 1165-1172.

18. Zhou, Y.Q., F.S. Foster, D.W. Qu, M. Zhang, K.A. Harasiewicz, and S.L. Adamson, *Applications for multifrequency ultrasound biomicroscopy in mice from implantation to adulthood.* Physiol. Genomics, 2002. **10**(2): p. 113-126.

19. Preston, R.C., A.J. Livett, and D.R. Bacon, *Absolute calibration of the hydrophones in the frequency range 0.5 MHz to 15 MHz.* Proc. Inst. Acoustics, 1984. **6**(5): p. 60-67.

20. Harris, G.R., *Pressure pulse distortion by hydrophones due to diminished lowfrequency response.* IEEE Transactions UFFC 1995. **42**(6): p. 989-992.

21. Bleeker, H.J. and P.A. Lewin, *A novel method for determining calibration and behavior of PVDF ultrasonic hydrophone probes in the frequency range up to 100 MHz.* Ultrasonics, Ferroelectrics and Frequency Control, IEEE Transactions on, 2000. **47**(6): p. 1354-1362.

22. Bacon, D.R., *Characteristics of a PVDF membrane hydrophone for use in the range of 1-100 MHz.* IEEE Trans. UFFC 1982. **SU-29**: p. 18-25.

23. Bacon, D.R., *Nonlinear acoustics in ultrasound calibration and standard*, in *In: Frontiers of Nonlinear Acoustics, Proc. of 12th ISNA*. 1990: Austin.

24. Filipczynski, L., *Nonlinear and linear propagation of diagnostic ultrasound pulses.* Ultras. Med. Biol. , 1999. **25**(2): p. 285-299.

25. Baker, A.C. and V.F. Humphrey, *Distortion and high frequency generation due to nonlinear propagation of short ultrasonic pulses from a plane circular piston.* J. Acoust. Soc. Am., 1992. **92**(3): p. 1699-1705.

26. Lum, P., M. Greenstein, E.D. Verdonk, C. Grossman, Jr., and T.L. Szabo, *A 150 MHz Bandwidth Membrane Hydrophone for Acoustic Field Characterization.* The Hewlett-Packard Journal, 1998(February 1998).

27. Lum, P., *High frequency membrane hydrophone.* IEEEE UFFC, 1996. **43**(4): p. 536-544.

28. *Ultrasonics: Focusing transducers definitions and measurement methods for the transmitted fields*. in *IEC Draft 87/155/CD TC87/WG6*. 1991.

29. Esward, T.J. and S.P. Robinson, *Extending the frequency range of the National Physical Laboratory primary standard laser interferometer for hydrophone calibrations to 60 MHz.* IEEE UFFC, 1999. **46**(3): p. 737-744.

30. Bleeker, H.J. and P.A. Lewin, *A new method of hydrophone calibration using the KZK wave modeling.* J. Acoust. Soc. Am., 1998. **103**(5): p. 2952

31. Clement, G.T., *Perspectives in clinical uses of high-intensity focused ultrasound.* Ultrasonics, 2004. **42**(10): p. 1087-93.

32. Rivens, I.H. and G.terHaar, *HIFU calibration status and challenges.* J. of Physics, CS, 2004: p. 180.

33. Szabo, T., *Diagnostic Ultrasound Inside Out*. 2004: Elsevier. p.491 and p.422-427.

34. Yang, X., R.A. Roy, and R.G. Holt, *Bubble dynamics and size distributions during focused ultrasound insonation.* J. Acoust. Soc. Am. , 2004. **116**(6): p. 3423-3431.

35. Bjorno, L. and P.A. Lewin, *measurement of nonlinear acoustic parameters in tissue, Ultrasonic Tissue Characterization.* J. Greenleaf, ed. CRC Press, 1986: p. 141-146.

36. Lewin, P.A. and M.E. Schafer, *Wide-band piezoelectric polymer acoustic sources.* IEEE Transactions UFFC, 1988. **35**(2): p. 175-185.

37. Schafer, M.E., T. Kraynak, and P.A. Lewin, *Miniature in-vivo hydrophones for lithotripter use.* Proc. IEEE Ultrasonics Symposium 1990, 1991.

38. Witte, R.S., R. Olafsson, and M. O'Donnell. *Acoustoelectric Detection of Current Flow in a Neural Recording Chamber*. in *IEEE Ultrasonics Symposium.* 2006.

39. Staudenraus, J. and W. Eisenmenger, *Fibre-optic probe hydrophone for ultrasonic and shock-wave measurements in water.* Ultrasonics, 1993. **31**(4): p. 267-273.

40. Beard, P.C., A.M. Hurrel, and T.N. Mills, *Characterization of a Polymer Film Optical Fiber Optic Hydrophone for Use in the Range 1 to 20 MHz; A Comparison with PVDF Needle and Membrane Hydrophones.* IEEE Transactions UFFC 2000. **47**(1): p. 256-264.

41. Schneider, B. and K.K. Shung, *Quantitative analysis of pulsed ultrasonic beam patterns using Schlieren systems.* IEEE UFFC, 1996. **43**: p. 1181.

42. Koch, C. and W. Molkenstruck, *Primary calibration of hydrophones with extended frequency range 1 to 70 MHz using optical interferometry.* Ultrasonics, Ferroelectrics and Frequency Control, IEEE Transactions on, 1999. **46**(5): p. 1303-1314.

43. Wilkens, V. and C. Koch, *Amplitude and phase calibration of hydrophones up to 70 MHz using broadband pulse excitation and an optical reference hydrophone.* J. Acoust. Soc. Amer., 2004. **115**(6): p. 2892–2903.

44. Wilkens, V. and W. Moltenstruck, *Broadband PVDF Membrane hydrophone for comparisons of hydrophone calibration methods up to 140 MHz.* IEEE Trans, UFFC, 2007. **54**(9): p. 1784-1791.

45. Ziskin, M.C. and P.A. Lewin (eds), *Ultrasonic Exposimetry*. 1993, Boca Raton, Florida: CRC Press.

46. Lewin, P.A., *Miniature piezoelectric polymer ultrasonic hydrophone probes.* Ultrasonics, 1981. **19**: p. 213-16.

47. Harris, G.R., *Sensitivity considerations for PVDF hydrophones using the spot-poles membrane design.* IEEE Trans. Ultrason. Ferroelec. Freq. Contr., 1982. **SU-29** (6): p. 370-77.

48. Lewin, P.A., *Miniature piezoelectric polymer hydrophones in biomedical ultrasonics.* Ferroelectrics, 1984. **60**: p. 127-39.

49. Harris, G.R., *Hydrophone measurements in diagnostic ultrasound fields.* IEEE Trans. Ultrason. Ferroelec. Freq. Contr., 1988. **35**(2): p. 87-101.

50. Smith, R.A., *The importance of the frequency response of a hydrophone when characterizing medical ultrasonic fields.* Proc. Inst. Acoustics, 1986. **8**(2): p. 119-28.

51. Lewin, P.A., M.E. Schafer, and R.C. Chivers, *Integrated Preamplifiers for Ultrasound Transducers.* Ultrasonics Symposium, 1985. 0090-9607/85/0000-0503: p. 503-506.

52. Harris, G.R., *A model of the effects of the hydrophone and amplifier frequency response on ultrasound exposure measurements.* IEEE Trans. Ultrason. Ferroelec. Freq. Contr., 1991. **38**(5): p. 413-17.

53. Meeks, S.W. and K.Y. Ting, *Effects of static & dynamic stress on piezoelectric and dielectric properties of PVF2.* Acoustical society of America Journal, 1984. **74**(6): p. 1681-1686.

54. Beljaev, P.A., V.D. Bochkov, V.M. Djagilev, V.N. Zakharov and V.G. Ushich, P*seudospark Switch in the generator of Shock-Wave pulses for lithotripter*. in *Proc. 17th Intern. Symp. on Discharges and Electr. Insulat. in Vacuum Eindhoven*. 1998. The Netherlands.

55. Shombert, D.G. and G.R. Harris, *Use of miniature hydrophones to determine peak intensities typical of medical ultrasound devices.* IEEE Trans. Ultrason. Ferroelec. Freq. Contr., 1986. **33**(3): p. 287-93.

56. Ludwig, G. and K. Brendel, *Calibration of hydrophones based on reciprocity and time delay spectrometry.* Ultrasonics, Ferroelectrics and Frequency Control, IEEE Transactions on, 1988. **35**(2): p. 168-174.

57. Radulescu, E.G., P.A. Lewin, A. Nowicki and W.A. Berger, *Hydrophones' effective diameter measurements as a quasi-continuous function of frequency.* Ultrasonics. , 2003. **41**(8): p. 635-41.

58. Bacon, D.R., *Primary calibration of ultrasonic hydrophones using optical interferometry.* IEEE Trans. on Ultrason. Ferroelec. Freq. Contr., 1988. **35**(2): p. 152-161.

59. Bacon, D.R., *Finite amplitude distortion of the pulsed fields used in diagnostic ultrasound.* Ultrasound in Med. & Biol., 1984. **10**(2): p. 189-195.

60. Wojcik, J., *Conservation of energy and absorption in acoustic fields for linear and nonlinear propagation.* The Journal of the Acoustical Society of America, 1998. **104**(5): p. 2654-2663.

61. Radulescu, E.G., J. Wojcik, P.A. Lewin and A. Nowicki, *Nonlinear propagation model for ultrasound hydrophones calibration in the frequency range up to 100 MHz.* Ultrasonics, 2003. **41**(4): p. 239-245.

62. Wojcik, J., A. Nowicki, P.A. Lewin, P.E. Bloomfield, T. Kujawska and L. Filipczyński, *Wave envelopes method for description of nonlinear acoustic wave propagation.* Ultrasonics, 2006. **44**(3): p. 310-329.

63. Herman, B.A. and G.R. Harris, *Calibration of miniature ultrasonic receivers using a planar scanning technique* J. Acoust Soc. Am., 1982. **72**(5): p. 1356-1363.

64. Yadav, H.S., D.S. Murty, S.N. Verma, K.H.C. Sinha, B.M. Gupta, and D. Chand, *Measurement of refractive index of water under high dynamic pressures.* Journal of Applied Physics, 1973. **44**(5): p. 2197-2200.

65. Barker, L.M. and R.E. Hollenbach, *Shock-Wave Studies of PMMA, Fused Silica, and Sapphire.* Journal of Applied Physics, 1970. **41**(10): p. 4208-4226.

66. Lewin, P.A., C. Mu, S. Umchid, A. Daryoush and M. El-Sherif, *Acousto-optic, point receiver hydrophone probe for operation up to 100 MHz.* Ultrasonics, 2005. **43**(10): p. 815-821.

67. Radulescu, E.G., P.A. Lewin, A. Goldstein and A. Nowicki, *Hydrophone spatial averaging corrections from 1 to 40 MHz.* Ultrasonics, Ferroelectrics and Frequency Control, IEEE Transactions on, 2001. **48**(6): p. 1575-1580.

68. O'Neill, H.T., *Theory of Focusing Radiators.* J. Acoust. Soc. Am., 1949. **21**(5): p. 516.

69. Lucas, B.G. and T.G. Muir, *The Field of a Focusing Source.* J. Acoust SOC. Am., 1982. **72**(4): p. 1289.

70. Zequiri, B. and A. D. Bond, *The Influence of Waveform Distortion on Hydrophone Spatial - Averaging correction - Theory and Measurement.* J. Acoust Soc. Am., 1992. **92**(4): p. 1809.

71. Lewin, P.A. *Calibration and performance evaluation of miniature ultrasonic hydrophones using Time Delay Spectrometry*. in *Proc. IEEE Ultrasonics Symposium*. 1981.

72. Pederson, P.C., P.A. Lewin, and L. Bjorno, *Application of time-delay spectrometry for calibration of ultrasonic transducers.* Ultrasonics, Ferroelectrics and Frequency Control, IEEE Transactions on, 1988. **35**(2): p. 185-205.

73. Selfridge, A. and P.A. Lewin, *Wideband Spherically Focused PVDF Acoustic Sources for Calibration of Ultrasound Hydrophone Probes.* IEEE Transactions UFFC 2000. **47**(6): p. 1354-1362.

74. Bilaniuk, N. and G.S.K. Wong, *Speed of sound in water as a function of temperature.* J. Acoust Soc. Am., 1993. **93**(3): p. 1609-1612.

75. Radulescu, E.G., P.A. Lewin, J. Wojcik, and A. Nowicki, *Calibration of ultrasonic hydrophone probes up to 100 MHz using time gating frequency analysis and finite amplitude waves.* Ultrasonics, 2003. **41**(4): p. 247-254.

76. *PiezoCAD software*. 2003, Sonic Concepts: Woodinville, Washington.

77. Umchid, S., R. Gopinath, K. Srinivasan, L. Bansal, P.A. Lewin, A.S. Daryoush, and M. El-Sherif, *100 MHz sub-millimeter size fiber optic pressure sensors: luxury or necessity?* in *IEEE International Ultrasonics Symposium*. 2007. New York, NY, USA.

78. Zhou, Y., L. Zhai, R. Simmons, and P. Zhonga, *Measurement of high intensity focused ultrasound fields by a fiber optic probe hydrophone.* J. Acoust. Soc. Am., 2006. **120**(2): p. 676-685.

79. Parsons, J.E., C.A. Cain, and J.B. Fowlkes, *Cost-effective assembly of a basic fiber-optic hydrophone for measurement of high-amplitude therapeutic ultrasound fields.* J. Acoust. Soc. Am., 2006. **119**(3): p. 1432-1440.

80. Gopinath, R., K. Srinivasan, S. Umchid, L. Bansal, A.S. Daryoush, P.A. Lewin, and M. El-Sherif, *Sensitivity Improvements in Fiber Optic Hydrophone*. in *IEEE International Ultrasonics Symposium*. 2007. New York, NY, USA.

81. Preston, R.C., D.R. Bacon, and R.A. Smith, *Calibration of medical ultrasonic equipment-procedures and accuracy assessment.* Ultrasonics, Ferroelectrics and Frequency Control, IEEE Transactions on, 1988. **35**(2): p. 110-121.

APPENDIX 1: List of ultrasonic hydrophone probes used

Table A1.1 shows the list of hydrophone probes used during this work. Furthermore, Table A1.2 illustrates the list of measurements carried out with each hydrophone probe.

Table A1.1: List of ultrasonic hydrophone probes with circular active elements used in this work.

Hydrophone ID	Serial Number	Preamp.	Type	Nominal diameter	Manufacturer
MH1	PA-C-117	AH-2010-100	Bilaminar membrane	400 μm	Precision Acoustics
MH2	PA-UC-099	AH-2010-100	Bilaminar membrane	400 μm	Precision Acoustics
MH3	S5-165	Custom 100MHz	Bilaminar membrane	400 μm	Sonora Medical
MH4	S5-173	Custom 100MHz	Bilaminar membrane	500 μm	Sonora Medical
MH5	ST01	N/A	Bilaminar membrane	1200 μm	Sonora Medical
MH6	IP26	N/A	Bilaminar membrane	500 μm	GEC Marconi
NH1	H291	Custom 100MHz	Needle	150 μm	SEA / Onda
NH2	H291	N/A	Needle	150 μm	SEA / Onda
NH3	H294	AH-2020-DCBSW	Needle	150 μm	SEA / Onda
NH4	HGL-1040	AH-2020-100	Needle Lipstick	120 μm	SEA / Onda
NH5	NTR-07050589	Custom 100MHz	Needle	500 μm	NTR
NH6	HGP-1003	AH-2010-100	Needle Lipstick	120 μm	SEA / Onda
NH7	GL-G693	Custom 100MHz	Needle Lipstick	130 μm	SEA / Onda
FO	N/A	AH-2010-100	Fiber Optic	10 μm	Corning Glass

In the Table A1.2, ***TDS using 3 focal numbers*** refers to the measurements performed using the TDS calibration method up to 40 MHz using 3 different circular, spherically focused acoustic sources (focal numbers 3.84, 10.16 and 19.24) as described in Section 3.2.1. ***TDS using 1 focal number*** refers to the measurements performed using the TDS calibration method up to 40 MHz using only one circular, spherically focused acoustic sources (focal number 19.24). ***60MHz - TGFA*** refers to the measurements performed using the TGFA calibration technique up to 60 MHz using the focal number 3.84 source (see Section 3.2.2). ***100MHz - TGFA*** refers to the measurements performed using the TGFA calibration technique up to 100 MHz using the focal number 2 source (see Section 3.2.2). ***100MHz – Nonlinear*** refers to the 100 MHz nonlinear propagation hydrophone calibration technique presented in Section 3.2.3. Finally, ***HIFU*** refers to the High Intensity Focused Ultrasound (HIFU) field measurement using the HIFU transducer operating either at its fundamental (1.52 MHz) or third harmonic (5 MHz) frequency (see Section 3.3).

Table A1.2: List of measurements carried out with each hydrophone probe.

Hydro. ID	**MH 1**	**MH 2**	**MH 3**	**MH 4**	**MH 5**	**NH 1**	**NH 2**	**NH 3**	**NH 4**	**NH 5**	**NH 6**	**NH 7**	**FO**
TDS using 3 focal numbers					X		X						
TDS using 1 focal number	X	X	X	X		X		X	X	X	X	X	
60MHz - TGFA		X	X	X				X	X	X	X	X	
100MHz – TGFA	X	X	X			X							
100MHz – Nonlinear	X	X				X							
HIFU										X			X

APPENDIX 2: List of acoustic sources used

Table A2 shows the list of (one-element) circular, spherically focused acoustic sources used during this work.

Table A2: List of circular, spherically focused acoustic sources used in this work.

Focal number	Frequency	Manufacturer
Focal number 19.24	Wideband 40 MHz	SEA / Onda
Focal number 10.16	Wideband 35 MHz	SEA / Onda
Focal number 3.84	Wideband 60 MHz	SEA / Onda
Focal number 2	Wideband 100 MHz	NIH NCRR
Focal number 4.21	Center frequency = 10 MHz	Olympus / Panametrics
Focal number 1.9	Center frequency = 1.52 MHz Third harmonic frequency = 5 MHz	Sonic Concepts

APPENDIX 3: List of measurement equipment used

Table A3 shows the list of the measurement equipment used during this work.

Table A3: List of measurement equipment used in this work.

Equipment	Manufacturer	Model	Specifications
Function Generator	Agilent	33250A	80 MHz Function/Arbitrary Waveform Generator
Power Amplifier	ENI	3100LA	250 kHz – 150 MHz Gain 55 dB
Digital Oscilloscope	Tektronix	TDS2022	200 MHz Bandwidths, 2 GS/s Sample Rates
Attenuator	Telonic Berkeley	8121A	Attenuator 0-60 dB 50 ohms
Spectrum Analyzer	HP	3585A	20 Hz – 40 MHz
Network Analyzer	Agilent	8753ES	30 kHz – 6 GHz
Laser	NEC	NX 8563LB	1550 nm InGaAsP Distributed feedback (DFB) laser diode
EDFA	Nuphoton Technologies	NP2000CORSV303500FCA1	Optical gain of 40 dB and output power of up to 30 dBm
10 dB coupler	Chip Hope	SMSCA223R	2x2 coupler with 10/90 coupling ratio
3 dB coupler	Chip Hope	SMSCA223RP	2x2 coupler with 50/50 coupling ratio
Photo-Receiver	Thor Labs	PDA10CF	Sensor InGaAs, Bandwidth 150MHz, Peak Response 0.95 A/W @ 1550nm
High-pass filter	In-house (custom-made)	N/A	500 kHz high-pass filter
Optical isolator	Ascentta	ISILPD55SS9	Single mode, 1550 nm isolators
Metal jacket	Newport	FPH-S	Hold 80-200 micron diameter fibers using a stressless spring-leaf assembly

APPENDIX 4: Characterization of the 1.52 MHz HIFU source

The 500 μm diameter needle hydrophone, NH5 (see Table A1.1 from Appendix 1), was used to obtain the isobar scans at the focal plane located at the axial distance of 38 mm from the 1.52 MHz HIFU transducer's surface. The scan shown in Figure A4.1 was performed using AIMS system (Onda, Sunnyvale). The corresponding color and three-dimensional reconstruction (wire frame) plots are shown in Figures A4.2 and A4.3, respectively. In addition, the same needle hydrophone (NH5) was used to measure the axial response of the HIFU acoustic source as shown in Figure A4.4.

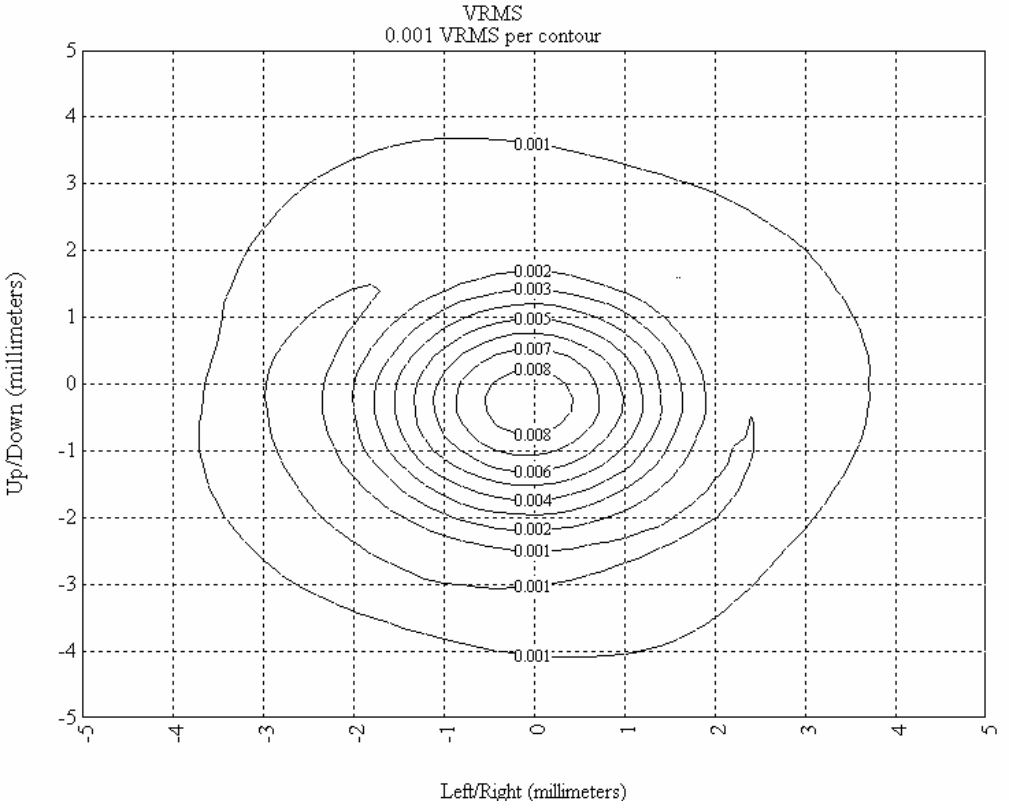

Figure A4.1: Contour plot of the isobars generated by 1.52 MHz HIFU transducer. The plot was obtained using needle hydrophone (NH5) at the focal plane (38 mm axial distance from the transducer's surface).

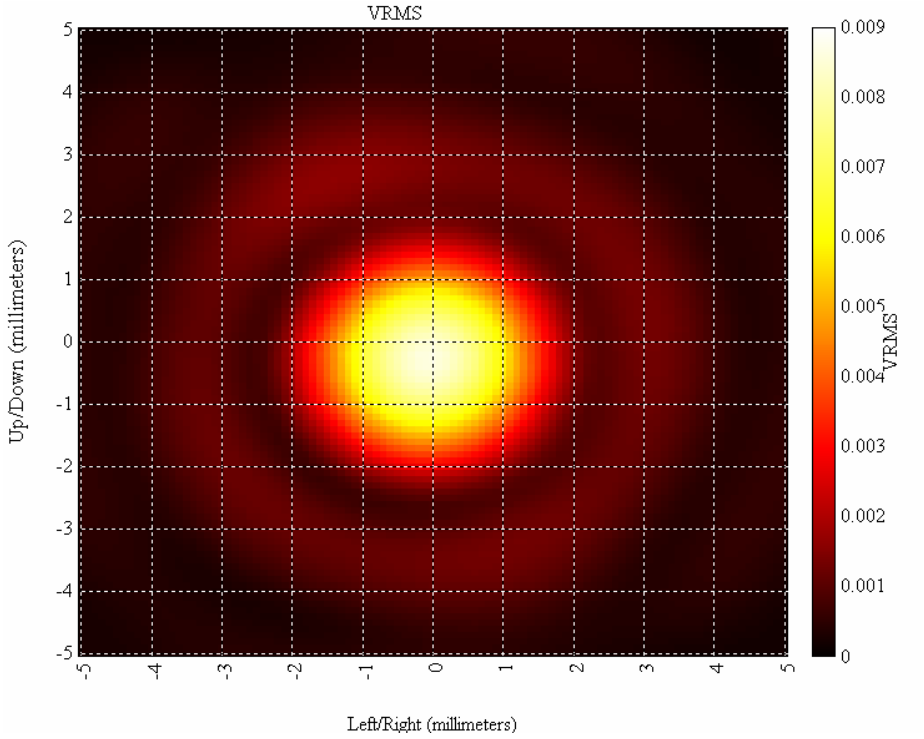

Figure A4.2: Color representation of the data shown in Fig. A4.1.

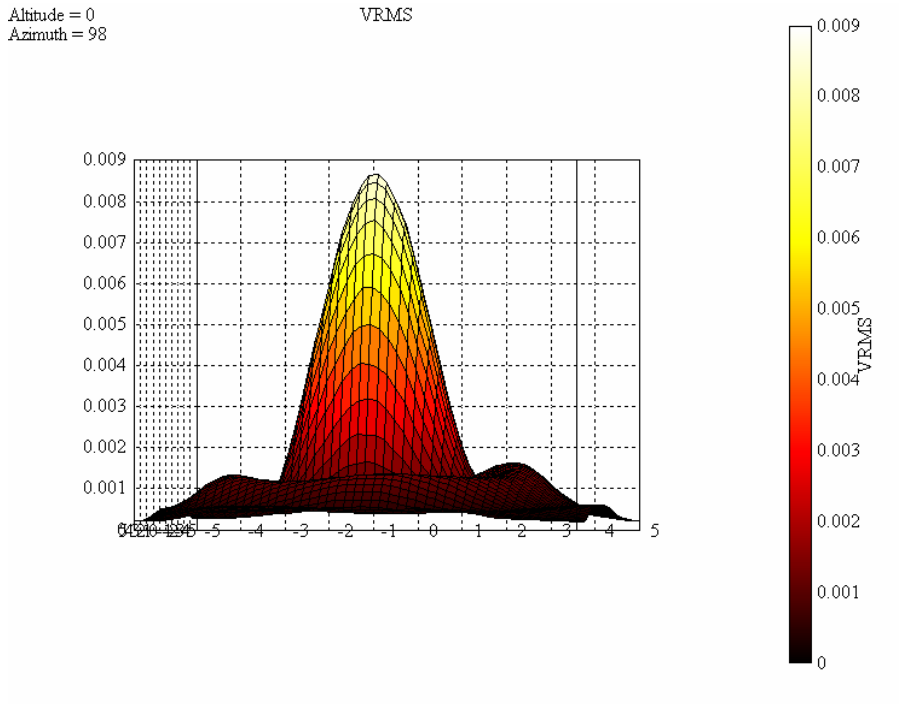

Figure A4.3: Three-dimensional reconstruction of the isobars of Fig. A4.1.

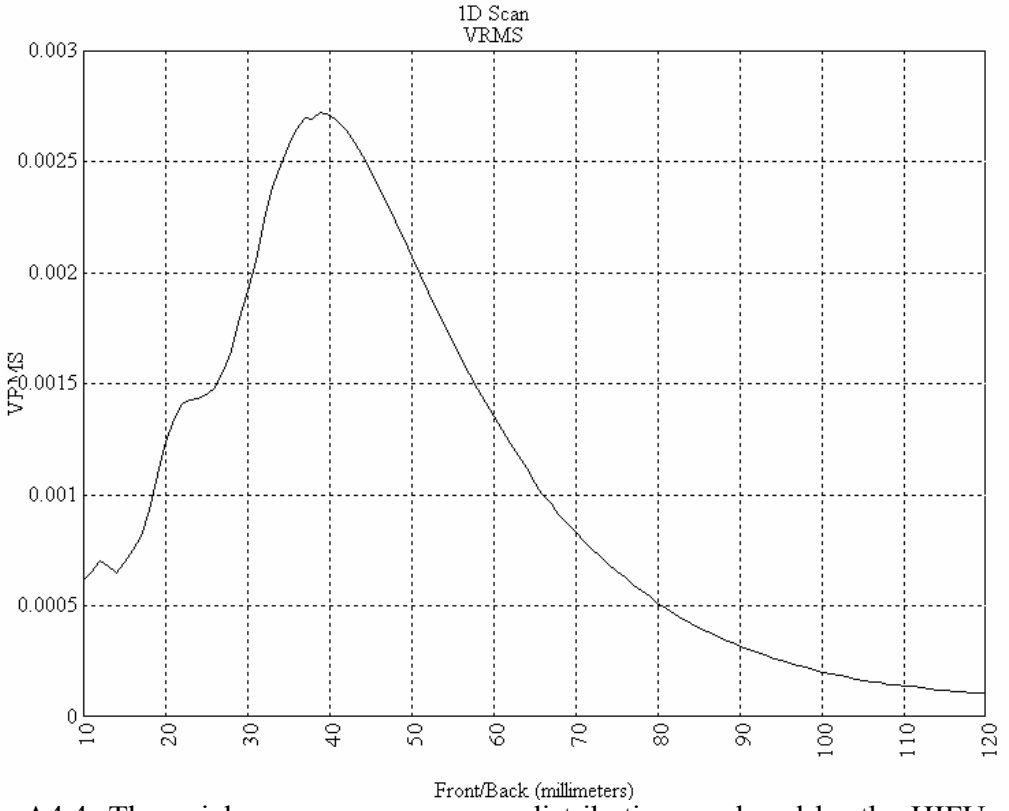

Figure A4.4: The axial response or pressure distribution produced by the HIFU source and measured by the needle hydrophone (NH5).

From the results shown in Figures A4.1-A4.3, the focal plane beam dimensions of the HIFU transducer were calculated as:

2D Scan Beam Dimensions

-3	dB Width:	2.029	x	2.01	millimeters	Area:	3.2	millimeters²
-6	dB Width:	2.802	x	2.788	millimeters	Area:	6.12	millimeters²
-10	dB Width:	3.539	x	3.5	millimeters	Area:	9.64	millimeters²
-12	dB Width:	3.806	x	3.773	millimeters	Area:	11.24	millimeters²
-13	dB Width:	3.938	x	3.9	millimeters	Area:	11.96	millimeters²
-20	dB Width:	6.255	x	6.318	millimeters	Area:	46.96	millimeters²

The results indicated that the focal plane area as determined by – 3dB isobar of the HIFU source was 3.2 mm^2 (about 2 mm in diameter).

APPENDIX 5: Assessment of the overall uncertainty of hydrophone calibrations

In any measurements, including those of acoustic or ultrasound field, the overall uncertainty should be evaluated and minimized. As the existing standards and guidance [2-4, 81] require absolute hydrophone sensitivity calibration to be referred to that determined by a national laboratory, in this work the primary calibration was the one provided by the National Physical Laboratory (NPL), UK. The overall uncertainty of the primary calibration depends on the frequency and the NPL uncertainties were specified as ±7% (±0.6 dB) in the frequency range 1 to 10 MHz, ±12% (±1dB) in the frequency range up to 40 MHz and ±20% (±1.5dB) in the frequency range up to 60 MHz. The discussion below provides a brief definition of the uncertainties encountered in this work and establishes the overall uncertainty pertaining to the hydrophone measurement results presented in Chapter 4.

The overall uncertainty of the hydrophone calibrations was assessed by determining both the random and systematic (non-random) uncertainties. The details are explained below; briefly, random uncertainties are unpredictable errors varying in each measurement and are determined by repeating the measurements several times and calculating the standard deviation. Systematic uncertainties result from an intrinsic fault in the measurement process. They affect each and every measurement in the same way and are determined by analyzing the various sources of possible bias in the measurements.

Random uncertainties

The random uncertainties (U_r) were calculated at the 95% confidence level (Chapter 14 in [45]) from five repeated measurements. Usually, the uncertainty measurement increases with increasing frequency. The potential sources of the random uncertainties include: spatial misalignment between the hydrophone probe and the acoustic source, signal-to-noise (S/N) ratio of the measurement equipment, local temperature variations, averaging errors, instability of the acoustic and laser (fiber optic) sources, intrinsic noise levels of the hydrophone and the fiber optic sensors assembly, and environmental uncertainties such as those associated with time varying adherent air bubbles on the acoustic source or hydrophone. As it was difficult to quantify the contributions from individual factors listed above, only the total amount of noise was considered here by examining the total random uncertainties in a typical voltage amplitude measurement on the acoustic sources.

The random uncertainties, U_r, at the 95% confidence interval were calculated as [81]:

$$U_r = t_{0.95} \frac{S_x}{\sqrt{n}}. \tag{A5.1}$$

where n was the number of measurements, t was the appropriate Student's t factor, and S_x was the standard deviation of the measurements.

Table A5 lists five voltage amplitudes measured at an axial distance of 4 cm and the frequency of 10 MHz by a 400 μm diameter bilaminar membrane hydrophone (MH2).

The pressure wave was generated by the 10 MHz focal number 4.21 transducer (see Table A2 of Appendix 2). The five values listed were obtained by repositioning the MH2 membrane hydrophone and the acoustic source, re-aligning them, and re-recording the responses during a 2 hours period. The mean and the standard deviation were calculated based on the equations given in the table.

Table A5: Overall random uncertainties in the beam profile measurement of the focal numbers 4.21 transducer.

Measurements (x_i)	1.54	1.49	1.43	1.42	1.36
Mean $\bar{x} = \frac{\sum_{i=1}^{5} x_i}{5}$	1.45				
Standard deviation $S_x = \sqrt{\frac{\sum_{i=1}^{5} (x_i - \bar{x})^2}{4}}$	0.069				
Random uncertainty $U_r = t_{0.95} \frac{S_x}{\sqrt{n}}$	0.086				

Systematic uncertainties

The systematic uncertainties (U_s) were determined by first considering all the sources of nonrandom uncertainty and assessing their probability distributions and magnitudes. It was assumed that the systematic uncertainty's contributions were similar, with each

factor (of contributions) having a rectangular probability distribution. When combined, these gave rise to a resultant probability distribution that approximated the normal distribution. Denoting the semi-ranges (one-half the total spread) of the contributions as a_1, a_2, etc., the variance of the resultant distribution (σ_S^2) was determined as [81]:

$$\sigma_S^2 = \frac{\left\{a_1^2 + a_2^2 + \ldots + a_n^2\right\}}{3} . \qquad \text{(A5.2)}$$

The overall systematic uncertainty (U_s) in a measurement at the 95% confidence level was then determined as [81]:

$$U_S = 1.96\sigma_S . \qquad \text{(A5.3)}$$

Several parameters contributed to the systematic uncertainty in the measurement, including the repeatability of the function generator, Agilent 33250A (±1%, based on the manufacturer's specification), reproducibility of the hydrophone calibration measurement (typically ±2%, [28]**),** and recording uncertainty of the Tektronix oscilloscope TDS2022 (±2%, provided by the manufacturer). As already noted, because the occurrence of the systematic errors had the same probability, it was assumed that they exhibited a rectangular distribution [81]. Therefore, with the assumption that each of the above errors was independent, the overall systematic uncertainty in the measurement at 95% confidence level could be calculated from Equations A5.2 and A5.3, and expressed as:

$$U_s = 1.96\sqrt{\frac{1\%^2 + 2\%^2 + 2\%^2}{3}} = 0.034 \quad \text{(A5.4)}$$

Once the random uncertainties (U_r) and systematic uncertainties (U_s) were quantified, the overall uncertainty (U_T) was calculated as the square root of the quadratic sums of the random and systematic uncertainties as shown in Equation A5.5 [81]:

$$U_T = \sqrt{U_r^2 + U_s^2} \quad \text{(A5.5)}$$

By inserting the appropriate value of the random uncertainty (U_r) listed in Table A5 and that of the systematic uncertainty (U_s) calculated using Equation A5.4, the overall uncertainty (U_T) was calculated from Equation A5.5 and determined to be 0.175. Therefore, the percentage of the total uncertainties can be determined as 12% (0.175/1.45 = 0.12, where 0.175 is the overall uncertainty and 1.45 is the mean value listed in Table A5).

Accordingly, the overall uncertainty of the calibrations performed during this work was determined to be ±12% (±1 dB) in the frequency range up to 40 MHz, ±20% (±1.5 dB) in the frequency range up to 60 MHz and ±25% (±2 dB) in the frequency range up to 100 MHz. These values of uncertainties are also marked in respective captions of each figure of Chapter 4. As the hydrophone sensitivity values presented in Chapter 4 are displayed using a logarithmic scale (y axis), the uncertainties are given in decibels (dBs).

APPENDIX 6: List of symbols

λ	Wavelength
μm	Micron
C	Capacitance
C_a	Internal capacitance of the hydrophone
C_c	Parallel capacitance of hydrophone's output connection cable
C_p	Parallel capacitance
C_{pre}	Input capacitance of the preamplifier
DFB	Distributed feedback
EDFA	Erbium Doped Fiber Amplifier
FFT	Fast Fourier Transform
FO	Fiber Optic
HIFU	High Frequency Focused Ultrasound
InGaAs	Indium gallium arsenide
Im(Z)	Imaginary portions of the hydrophone's complex impedance
$Im(Z_{el})$	Imaginary components of the complex impedance of the measuring device
L_c	Inductance of the output connection cable
M	Sensitivity of the hydrophone being calibrated
MI	Mechanical Index
M_{ref}	Sensitivity of the reference hydrophone
$M_c(f)$	End-of-cable open-circuit sensitivity
$M_L(f)$	End-of-cable loaded sensitivity of a hydrophone

NA	Network Analyzer
NPL	National Physical Laboratory
PVDF	Polyvinylidene Fluoride
PZT	Lead Zirconate Titanate
Q_a	Charge produced by a hydrophone when received acoustic pressure
R	Resistance
R_a	Internal resistance of the hydrophone
Re(Z)	Real portions of the hydrophone's complex impedance
$Re(Z_{el})$	Real components of the complex impedance of the measuring device
RF	Radio frequency
RIN	Relative Intensity Noise
SA	Spectrum Analyzer
S_q	Hydrophone's charge sensitivity
S_v	Hydrophone's voltage sensitivity
TDS	Time Delay Spectrometry
TGFA	Time Gated Frequency Analysis
TI	Thermal Index
TIB	Bone at Focus Thermal Index
TIC	Bone at Surface Thermal Index
TIS	Soft Tissue Thermal Index
TrFE	Trifluoroethylene
U	Terminal voltages of the uncalibrated hydrophone
U_{ref}	Terminal voltages of the standard hydrophone

V_a	Voltage produced by a hydrophone when exposed to acoustic pressure
V_{ao}	Voltage appears at the impedance which includes the hydrophone impedances and the parallel capacitance (C_c) of the output connection cable
V_{pp}	Peak-to-peak Voltage
Z_a	Internal impedance of the hydrophone
Z_{ao}	Impedance includes the hydrophone impedances and the parallel capacitance (C_c) of the output connection cable

Vita

Sumet Umchid was born in Bangkok, Thailand, on September 15, 1978. After completing his high school degree at Suankularb Wittayalai School in Bangkok, he enrolled at the College of Engineering, Mahidol University, Thailand in 1995 where he received the degree of Bachelor of Science in Electrical Engineering in 1999. A year later, he has received the prestigious Royal Thai Government Scholarship to continue his graduate study in USA. In 2001, he was admitted into the Graduate School at Drexel University. In 2003, he received his degree of Master of Science in Biomedical Engineering. Sumet's research interests include high frequency ultrasound imaging, imaging transducers and acousto-optic measurements. Once he has defended his Ph.D. dissertation, he intends to join the Department of Industrial Physics and Medical Instrumentation, King Mongkut's Institute of Technology North Bangkok, Thailand as a lecturer.

Listed below are publications, which were published during Sumet's graduate career at Drexel University:

C. Mu, **S. Umchid**, L. Bansal, A. Daryoush, P. Lewin, M. El-Sherif, "Broadband fiber optic ultrasound hydrophone probe," IEEE Lightwave Technologies in Instrumentation & Measurement Conference, Palisades NY, Page 149-152, October 2004.

P. A. Lewin, **S. Umchid**, A. Sutin and A. Sarvazyan, "Beyond 40 MHz frontier: The future technologies for calibration and sensing of acoustic fields," Journal of Physics CS 1: 38-43, 2004.

P. A. Lewin, **S. Umchid**, W. Andrew Berger, C. Mu, A. Daryoush, M. El-Sherif, “Toward 100 MHz Frontier: Acousto-Optic Methods and Fiber Optic Sensors in Ultrasound Metrology,” The 2005 Congress and Exposition on Noise control engineering, Rio de Janeiro, Brazil, August 2005.

P. A. Lewin, C. Mu, **S. Umchid**, A. Daryoush, M. A. El-Sherif, “Acousto-optic, point receiver hydrophone probe for operation up to 100 MHz,” Ultrasonics, 43(10): 815-821, 2005.

M. Pong, **S. Umchid**, A. J. Guarino, P. A. Lewin, J. Litniewski, A. Nowicki and S. P. Wrenn, "In vitro ultrasound-mediated leakage from phospholipid vesicles," Ultrasonics, 45(1):133-145,2006.

A. S. Daryoush, C. Mu, **S. Umchid**, and P. A. Lewin, "RF and microwave photonics in biomedical applications," in Photonics North 2006, Quebec City, Quebec, Canada 2006.

R. Gopinath, K.Srinivasan, **S. Umchid**, L. Bansal, A. S. Daryoush, P. A. Lewin, and M. El-Sherif, " Improved fiber optic hydrophone Sensors," in *IEEE International Ultrasonics Symposium*, New York, NY, USA, 2007.

S. Umchid, R. Gopinath, K.Srinivasan, L. Bansal, P. A. Lewin, A. S. Daryoush, and M. El-Sherif, " 100 MHz sub-millimeter size fiber optic pressure sensors: luxury or necessity?," in *IEEE International Ultrasonics Symposium*, New York, NY, USA, 2007.